Sustainable Materials and Technologies 46 (2025) e01683

Contents lists available at ScienceDirect

Sustainable Materials and Technologies

journal homepage: www.elsevier.com/locate/susmat

# MXenes as sustainable functional nanomaterials for photocatalytic degradation of dye pollutants: Performance, effect of process parameters, stability and re-useability evaluation – A critical review

Stephen Sunday Emmanuel [a], Ademidun Adeola Adesibikan [b], Shepherd M. Tichapondwa [a], Manoj P. Rayaroth [c], Francisco Bosca [d], Maria Luisa Marin [d], Bakhtiar Ali Samejo [e], Grzegorz Boczkaj [e,f,*]

[a] Department of Chemical Engineering, Sustainable Environmental and Water Utilisation Processes Division, University of Pretoria, Pretoria 0002, South Africa Private Bag X20, Hatfield 0028, South Africa
[b] Department of Industrial Chemistry, Faculty of Physical Sciences, University of Ilorin, P. M. B. 1515, Ilorin, Nigeria
[c] Department of Life Sciences, School of Science, GITAM (Deemed to be) University, Visakhapatnam, 530045, India
[d] Instituto de Tecnología Química, Universitat Politècnica de València-Consejo Superior de Investigaciones Científicas, Avda. de los Naranjos s/n, Valencia E-46022, Spain
[e] Department of Sanitary Engineering, Faculty of Civil and Environmental Engineering, Gdansk University of Technology, Gdansk, G. Narutowicza St. 11/12, Poland
[f] School of Civil, Environmental, and Architectural Engineering, College of Engineering, Korea University, 145 Anam-ro, Seongbuk-gu, Seoul 02841, Republic of Korea

ARTICLE INFO

*Keywords:*
Mxene
Water pollution
Photocatalyst
Advanced oxidation processes (AOPs)
Dye waste
Hybrid materials
Heterojunction
Radicals
2D materials
Functional materials

ABSTRACT

MXene, an emerging cutting-edge functional material with unique properties like high electron conductivity, improved surface functionality, efficient charge separation, good optical properties, and lower Schottky barrier for photocatalytic applications, has gained a high interest of the scientific community in the recent decade. This work aimed to critically review the advances in the application of MXENE-based materials (MXBM) for photocatalytic degradation of various hazardous dye contaminants for water and wastewater treatment applications. Specifically, the effect of various technical operating parameters that are of high importance for the evaluation of MXBM's real applicational value was analyzed. Mechanisms of photocatalytic degradation in MXBM were rationally discussed. Usefulness of MXenes in photocatalytic materials include enhancement of photo-generated charge carrier separation, serving as stable support, limitation of photocatalyst size, improving reactant adsorption. $Ti_3C_2$ ($Ti_3C_2T_x$) is the most popular MXene for this application, while few attempts have been made also for $Nb_2CT_x$. Effective nanocomposites were synthesized with $TiO_2$, MOFs, g-$C_3N_4$, chitosan, cellulose, BiOBr, CdS. Other attempts included hybrid materials containing $Ag_3PO_4$, CuO, $MoS_2$, $NiCo_2S_4$, Nd-$NiCo_2O_4$, ZnO. Coating the MXenes with Ag and Pd nanoparticles (NPs) was another effective method. Several effective applications were developed for degradation of Congo Red (CR), Crystal violet (CV), Direct Red 31 (DR31), Malachite Green (MG), Methylene Blue (MB), Methyl Orange (MO), Orange G, Rhodamine B (RhB). Based on the performed review, it was found that for many applications, the photocatalytic degradation efficiency exceeds 90 % for 60–80 min treatment. Typically, the optimal dose of MXBM photocatalyst is in the range of 10–100 mg/L, and the optimal pH is in the range 2–7.5. The major reactive species in the photocatalytic reaction catalysed by MXBM were hydroxyl radicals ($^{\bullet}OH$) and superoxide radical anions ($^{\bullet}O_2^-$), which are accountable for the degradation of the dye contaminants via Advanced Oxidation Processes (AOPs). The reusability of the materials is an important advantage of MXBM, as it can be treated mostly employing pure water or with addition of ethanol and can be reused up to 3–8 cycles while still maintaining degradation efficiency of >75 %. In the end, the knowledge gap and problematic issues that can help to improve the MXBM, as well as provide future research directions for investigators, were highlighted. Future studies should focus, beside the degradation effectiveness, on intermediate products (by-products) formation, cost analysis, sustainable scale-up strategies under real-case scenario conditions. Importantly, a long-term toxicity assessments of MXBMs should be studied along with research on particle size-dependent toxicity of different types of photocatalytic MXene-based materials. Due to

* Corresponding author at: Department of Sanitary Engineering, Faculty of Civil and Environmental Engineering, Gdansk University of Technology, Gdansk, G. Narutowicza St. 11/12, Poland.
*E-mail addresses:* grzegorz.boczkaj@pg.edu.pl, grzegorz_boczkaj@korea.ac.kr (G. Boczkaj).

https://doi.org/10.1016/j.susmat.2025.e01683
Received 16 June 2025; Received in revised form 9 September 2025; Accepted 21 September 2025
Available online 22 September 2025

utilisation of hydrated electrons in specific conditions MXBMs could find applicability also in Advanced Reduction Processes (ARPs). Photocatalyzed reactions could utilize sulphite, dithionate or gaseous hydrogen as reductans and sources of reductive radicals. This application of MXBMs seems to be overlooked by scientific community.

## 1. Introduction

Dyes are among the major contributors to environmental pollution, often discharged in untreated or inadequately treated form from industries such as pharmaceuticals, plastics, leather, food, and textiles into the water bodies, especially [1,2]. Therefore, sustainable solutions are needed to reduce dye concentrations to an acceptable level [3].

Notably, adsorption [4–6], coagulation [7], membrane filtration [8,9], bioremediation, chemical oxidation, and electrochemical methods [10,11] have been used as some of the approaches for the treatment of wastewater containing dyes. However, it is worth mentioning that the majority of these strategies (excluding electrochemical and biodegradation) move contaminants from one medium to another or generate extra sludge, which needs additional treatments and disposal [12]. Also, some of the adsorbents and catalysts employed for the aforementioned methods are linked to diverse drawbacks, such as low adsorption capacity, slow adsorption kinetics, a small number of reactive sites, low physical and chemical stability, and relatively low-moderate reusability [13].

To overcome these issues, a very effective, ecofriendly, and economically feasible process called advanced oxidation processes (AOPs) which is focused on the in-situ generation of highly oxidizing reactive oxygen species (especially, $^{\bullet}OH$ radicals) are used to degrade the toxic organic contaminants into less toxic molecules and finally to $CO_2$, water and inorganic ions (sulfate, nitrate, etc.) [14–16]. There are various AOPs, such as photolysis, Fenton process, photocatalysis, cavitation, and electrochemical methods, reported in the removal of dye waste from water matrices. The main advantages of these AOPs are that they don't produce any sludge, can be operated with very less or without toxic chemicals, and have a rapid and high mineralization efficiency. Among them, photocatalysis has advantages such as efficiency in natural reaction conditions, low operational cost, reusability, and eco-friendliness. Semiconductors like $TiO_2$, $Fe_2O_3$, ZnO, ZnS, and CdS are widely used in photocatalytic applications. [1,17]. However, photocatalytic materials employed also have several limitations. The recombination reaction of the electron-hole pair and the subsequent processes affect the degradation efficiency in many of the semiconductor-based photocatalysts. As a result, several modifications or photocatalysts of different morphologies have been developed for environmental remediation applications. Two-dimensional (2D) photocatalysts have emerged as important materials for water purification due to their unique physicochemical properties. Their planar structure allows for functionalization with various co-catalysts and surface atoms, providing numerous active sites for catalytic reactions [18,19].

MXenes are 2D materials produced by etching their ternary layered nitride or carbide precursors having a common formula of $M_{n+1}X_nT_x$, and are composed of stacked two-dimensional sheets, where M denotes an early transition metal, X is C and/or N, and T represents surface functional groups/terminators such as O, OH, and F, as color-coded in Fig. 1 [20,21].

These materials are very effective in photocatalytic degradation of pollutants owing to their numerous unique properties such as outstanding electron conductivity, exceptional crystal structure, large specific surface area (SSA), good conductivity, good hydrophilicity, high catalytic performance, efficient separation [22–24], excellent biocompatibility [25], good optical properties, and a lower Schottky barrier for photocatalytic applications [26]. Therefore, MXene-based materials are explored for various environmental applications, including wastewater treatment. Many studies have reported the removal of antibiotics and heavy metals using MXenes [27,28]. Meanwhile, some reviews have been published focusing on MXenes for the adsorption and photocatalytic degradation of organic pollutants [29–31]. For example, Illahi's team [29] review study focused on the photocatalytic degradation efficiency of only metal oxide/semiconductor doped MXene for azo dyes, while Mathew et al. [30] work provides an overview of $Ti_3C_2$ MXene fabrication and their performance, as well as mechanisms for dye photocatalytic degradation. Recently, another review study by Seling et al. also concentrated solely on the synthesis of $Ti_3C_2T_x$ MXene-based hybrid photocatalysts and their efficiency for the degradation of organic dye and other water pollutants like pharmaceuticals. The study also

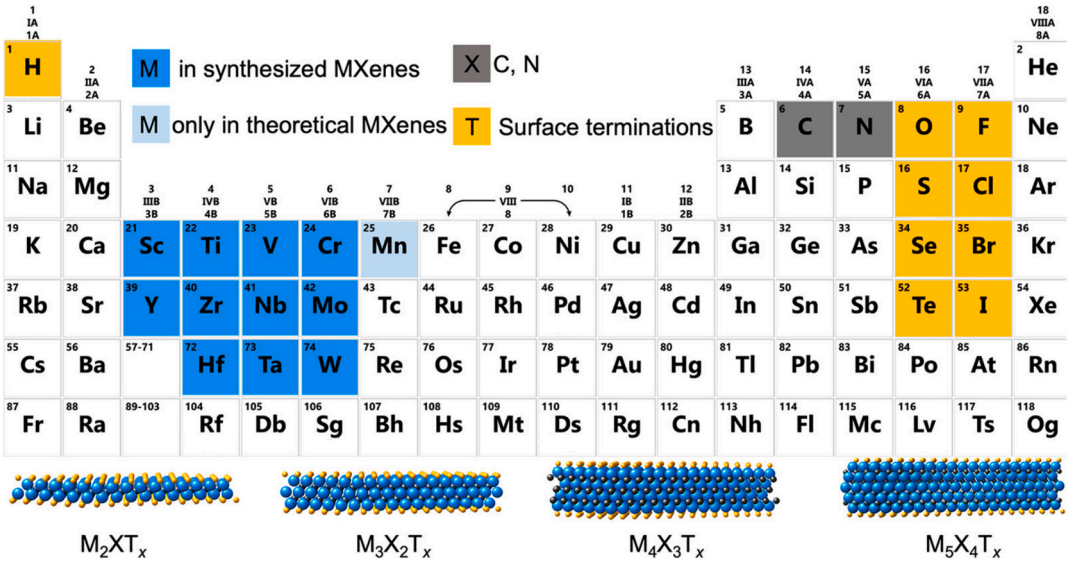


**Fig. 1.** Periodic table displaying the chemical makeup of MXenes. MXenes' building blocks are color-coded. At the bottom, four schematics of MXenes' quintessential frameworks are shown [20]. Reused with approval from the American Chemical Society (Copyright 2021).

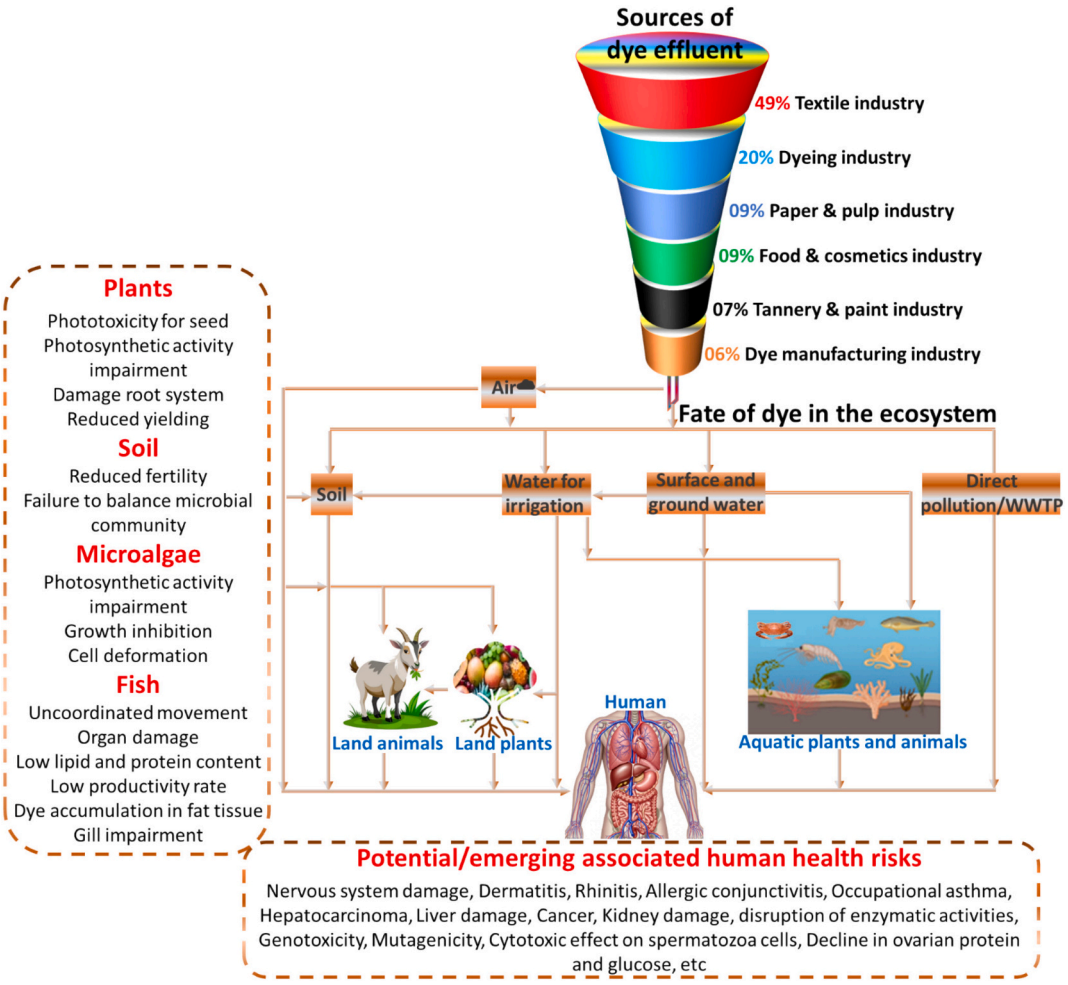


**Fig. 2.** Fate of dye pollutants within the ecosystem and associated ecotoxicities/health risks.

underscores computational methods for evaluating and improving the performance of $Ti_3C_2T_x$ MXene-based hybrid photocatalysts [31].

However, for a thorough grasp of the MXenes photocatalytic degradation process for dye pollutants, these existing review papers lack in-depth elucidative analysis of the effect of various technical operating parameters on photocatalytic degradation performance, which is crucial for process and cost effectiveness optimization in any of the sustainable remediation approaches. Moreover, these reviews lack empirical analysis on the identification of reactive species in various MXene-based materials and do not critically evaluate the formation of dominant radical species facilitating dye degradation. A thorough investigation of the effect of co-existing ions in MXene materials has not been reviewed. The reusability studies were also not covered in the previous reviews.

Therefore, this review covers all the aspects of the studies related to dye remediation using MXene-based materials, including their economic benefits and real-world/pilot-scale application potential. This review furthermore discussed various challenges in the full implementation of MXenes-based materials for the photocatalytic degradation of dye pollutants, while identifying emerging future research directions. Therefore, the review will be beneficial for industries, engineers, investors, and various stakeholders to pragmatically establish MXenes' scalability, sustainability, fiscal feasibility, and industrial applicability, particularly in wastewater treatment applications.

## 2. Sources, fate, toxicities, and environmental impact of dyes

Dyes are colouring substances that are employed to impart color to or polish substrates like clothes, polyethylene bags/plastics, cosmetics, papers, paints, drugs, food, etc. [32–34]. Thus, they have found applications in various industries that are very important to humanity. These industries serve as the major sources of dye effluent within the environment, with the textile industry leading the chart, followed by the dyeing industry, as presented in Fig. 2 [35,36]. Specifically, approximately 280,000 tons of dyes are wasted every year and released into the environment without proper treatment [3,37]. Another direct potential source of dyes in water environments could be aquaculture, where dyes like methylene blue, crystal violet, malachite green, etc., are used unlawfully to treat or manage parasitic, bacterial, or fungal infections in fish [38]. Household wastewater is another source of dye pollutants in the water because people throw away old or unused dye-based products, hair dyeing, use cosmetics or household chemicals that contain dyes, which are released into the sewer and then end up in a sewage treatment plant or are released directly into the environment [38,39]. These dye effluents mainly consist of aromatic and heterocyclic dyes with complex and stable structures and are often persistent in the environment owing to their thermal and photo-stable properties. Thus, when these effluent is emitted from various sources presented in Fig. 2, they migrate through different places of the ecosystem [38,40]. For example, they can reach surface water like rivers and lakes, which normally serve as a source of drinking water and irrigation water in drought zones or during the dry season [40,41]. Once dyes get to these surface water systems, they remain dissolved or adsorb onto suspended solids or degrade partially to form toxic aromatic amines and thus affect water quality, including color and taste. Furthermore, when dye-contaminated water is used for

irrigation, dye pollutants enter the soil, plants, and get to animals within the food chain [40]. Moreover, dyes can enter groundwater from surface water, through leaching from contaminated soils, or infiltration of dye wastewater from unlined disposal sites or landfills where dye-containing wastes are stored [38,42]. This makes dye-contaminated groundwater used for drinking, irrigation, or livestock a potential route of exposure to humans. Also, soil can be polluted by dyes through sludge application and airborne [36,38]. Specifically, even though dyes are not typically volatile, they can enter the air as fine/powder dust, aerosol droplets, particulates, and toxic vapors during manufacturing, spray applications, handling, textile printing, or incineration of dye-containing waste. The airborne dye pollutants then later settle onto land or aquatic systems through wet or dry deposition to continue their migration within the ecosystem. Notably, numerous toxicological and environmental impacts have been associated with the presence of dye pollutants in the ecosystem [36,38,42]. For instance, they can negatively affect soil chemistry by inhibiting soil microbial activity, altering nutrient cycling, and reducing soil fertility, which later affects plants and animals, including human beings [36,43]. In aquatic systems, the presence of dye pollutants can hinder the penetration of sunlight, which affects photosynthesis and therefore affects aquatic flora and fauna [36,44,45]. The presence of dyes in the water increases the chemical oxygen demand, biological demand, and changes the dissolved oxygen level of wastewater. In addition, the intake of dyes by plants can ultimately affect their growth as well as affect human health [36,37]. The dye contamination in water affects the growth and reproduction, development, and behavior of aquatic organisms. Ingestion is the major exposure pathway for humans. The biotransformation of dyes into reactive intermediates or toxic metabolites like aromatic amines was reported in the human body [3]. In particular, when humans are exposed to these reactive intermediates or toxic metabolites by eating plants and meat that have been impacted by dye pollutants within the food chain, or by occupational exposure, or through drinking, bathing, or swimming, it can cause many health-related issues. In particular, human exposure to dye pollutants has been linked to cancer, DNA damage, oxidative stress, nervous system damage, skin problems, asthma, liver damage, disruption of enzymatic activities, genotoxicity, and kidney damage, among others, as highlighted in Fig. 2 [3,36,46,47]. Reproductive issues such as cytotoxic effect on spermatozoa cells, decline in ovarian protein, and glucose have also been linked to dye pollutant exposure [37,48].

Understanding these fates is critical for mitigating the ecological and health concerns linked with dye pollutants, and this may require a combination of source reduction measures as well as the use of advanced remediation techniques. The photocatalytic degradation of dyes with MXenes-based materials, with their advantages, is underscored in the following sections.

## 3. Review methodology

A systematic literature search was performed on various reputable scientific databases such as Scopus, Google Scholar, Science Direct, and PubMed (up to January 2025) related to the theme of the proposed review, following the PRISMA protocol (Preferred Reporting Items for Systematic Reviews and Meta-Analyses) used by Bayode et al. [49] with slight modifications. MXene/metal carbonitrides /$Ti_3C_2T_x$/$Ti_3C_2$, photocatalytic degradation, dye, electron trapping, effect of pH, effect of dose, effect of initial concentration, effect of ionic species, effect of time, effect of radical scavengers, regenerability, and recyclability/reusability were a few of the keywords. These were organized in different combinations using the Boolean "AND" and "OR" to refine the search results.

Numerous articles were collected and subsequently sorted and filtered based on various predetermined inclusion and exclusion criteria. Only peer-reviewed articles published in English were selected. The results of opinions, corrigenda, retracted articles, abstracts, encyclopedias, and seminars were not considered. In addition, the core analysis did not take into account experimental articles that did not examine

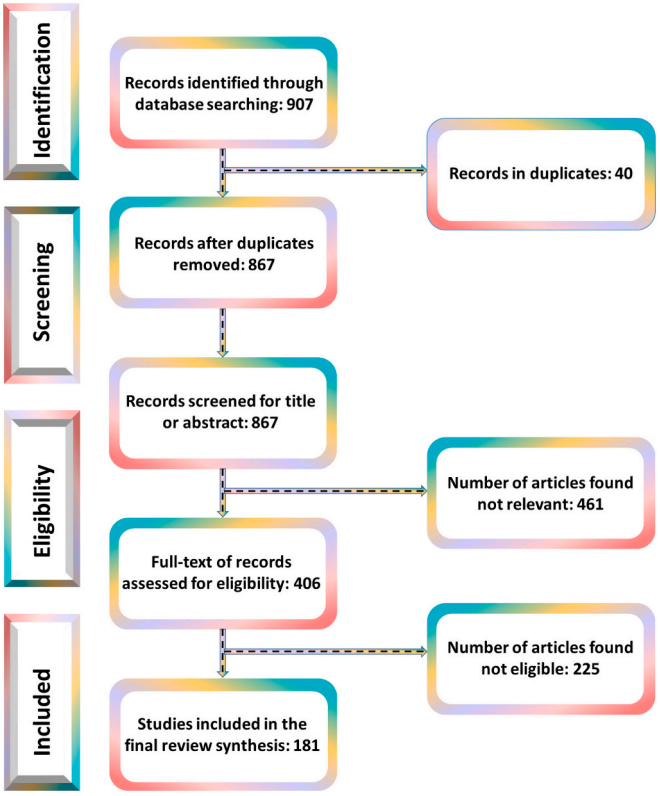


**Fig. 3.** Review methodology process.

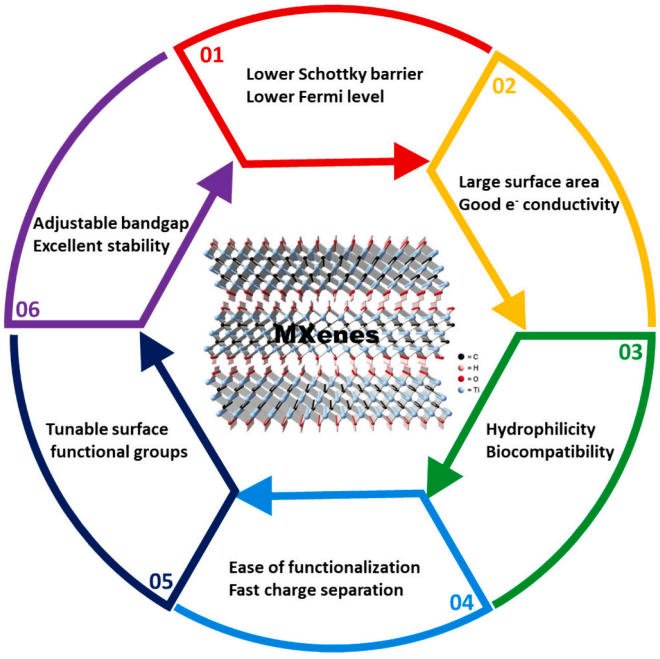


**Fig. 4.** Major unique properties of MXenes.

MXenes for the photocatalytic degradation of dye. Then, a collaborative article evaluation and discussion were done by the authors. After that, articles that satisfied the above criteria were deemed appropriate for the review work, and a total of 181 papers were finally used for the preparation of this review paper. A schematic overview of the review methodology is presented in Fig. 3.

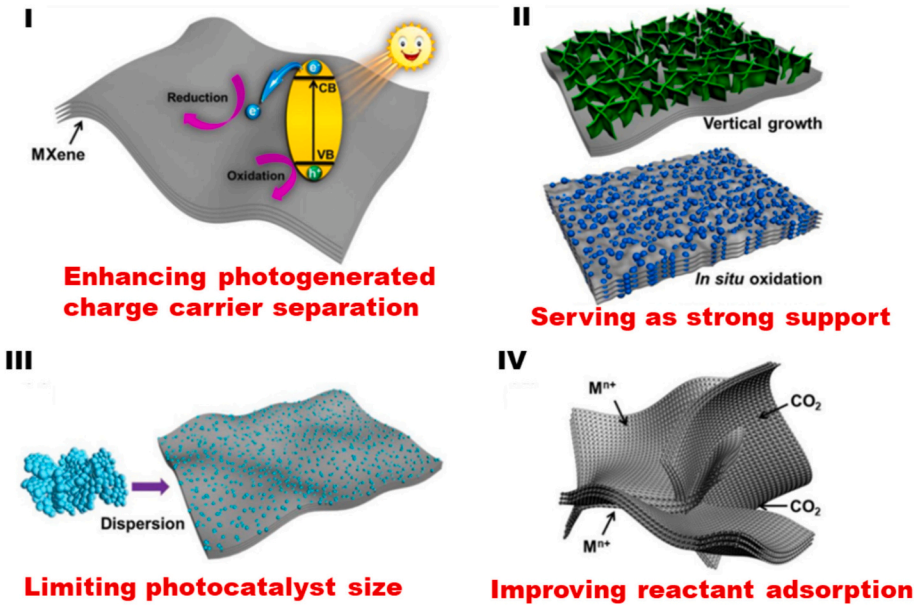


**Fig. 5.** Major advantageous functions of MXene in photocatalytic degradation [50]. Reprinted with approval from Elsevier (License code: 5612020177935).

## 4. Advantages of MXene in chemical reactions

MXene, owing to its lower Fermi level, is often named as a very good material for photocatalysis [50]. However, considering MXenes' uniqueness (Fig. 4), such as the possibility to modify the surface functional groups and large SSA, the true functions of MXene in boosting the photocatalytic activity are far beyond the photo-generated electron ($e^-$) acceptor [50]. Moreover, in general chemical reactions, high and tunable surface area and excellent chemical stability allow MXenes optimization for the degradation of specific chemical pollutants and ensure their reliability in diverse chemical environments while facilitating stable performance. The exclusive advantages of MXene are shown in Fig. 5 and briefly highlighted below.

I. ***Enhancing photo-generated charge carrier separation:*** The recombination of $e^-$ and holes ($h^+$) in a photocatalyst can somewhat reduce the separation efficiency of charge carriers. As a result, one of the best methods for enhancing photocatalytic activity is to provide a conjunction of the photocatalyst with a co-catalyst for separating the photo-generated charge carriers [50,51]. Furthermore, MXenes show metallic conductivity characteristics, and compared to most n-type nanosemiconductors, their relatively low Fermi energy level is more positive, suggesting that they may be used as a co-catalyst for exchange and accumulation of photo-generated $e^-$ [50,52]. More specifically, by utilizing MXenes as co-catalysts, a Schottky junction could be created to speed up the photo-generated charge carrier separation [50,53]. Likewise, due to their lower Fermi level during the photocatalytic reaction, $e^-$ on the CB might move to $Ti_3C_2$. Additionally, $H^+$ may be effectively reduced to create $H_2$ due to $Ti_3C_2$'s strong electrical conductivity and mild H adsorption-free energy ($\Delta G_H$). These electrons transported to MXene can also be used in other photocatalytic processes to convert $CO_2$ into hydrocarbons (including methane) or formaldehyde, reduce sorbed nitrogen to $NH_3$, and form superoxide radical anions ($^{\bullet}O_2^-$) and hydroxyl radicals ($^{\bullet}OH$) for the degradation of organic pollutants [54,55].

II. ***Serving as strong support:*** Given MXene's exceptional physicochemical durability, it can be employed as a good support for other nanophotocatalysts [51,56] such as $TiO_2$ [57,58], ZnO [59,60], and $MoS_2$ [61] to prevent agglomeration and enhance its performance [50,62]. It is also important to note that MXene can act not only as a strong support [63,64] but also as a starting material for the in-situ development of associated metal oxide photocatalysts [65,66].

III. ***Limiting photocatalyst size:*** The dimensions of the MXene-based materials (MXBM) photocatalyst are important for photocatalytic operation; nevertheless, owing to their surface energy, they tend to aggregate into larger sizes, which reduces their contact area with pollutants [50]. Due to the MXBM's numerous surface functional groups, which are often formed using the wet chemical etching process, they may afford a better growth platform for the regulation of the morphological dimensions of the photocatalyst [67,68]. More specifically, the metal cations could be adsorbed on the negatively charged surface, subsequently enabling the uniform growth of photocatalysts [69]. As a result, the MXBM photocatalyst could reach a high SSA to afford a large number of surface-active sites to facilitate photocatalytic activity [50,51].

IV. ***Improving reactant adsorption:*** Another crucial stage in the modification of the MXBM is the enhanced reactant adsorption. Owing to the abundant surface functional groups on MXene, it can also enhance the photocatalyst's capacity to adsorb pollutants [70,71]. For instance, due to the negatively charged surface, MXBM can effectively sorb the positively charged molecules [72]. Besides, the hybrid photocatalyst's porous structure is advantageous for adsorption [50]. Specifically, numerous hydrophilic terminal groups (-OH, —O, and —F) on the $Ti_3C_2$ surface can improve its interaction with other nanosemiconductors as well as with $H_2O$ molecules or target pollutants, both of which are necessary for the migration of e– inside the hybrids and the chemical reaction in aqueous solution [73–75]. These unique properties and advantages play an important role in MXene degradation of dye pollutants.

## 5. Overview of the photocatalytic degradation mechanism for MXBM

When photocatalysts are exposed to light, photon energy higher than the bandgap energy is absorbed from the light source to generate $e^-$, and the photo-generated $e^-$ are captured and promoted to the upper band called the conduction band (CB), creating $h^+$ in the lower band called the valence band (VB) [76]. The active functional group present on the

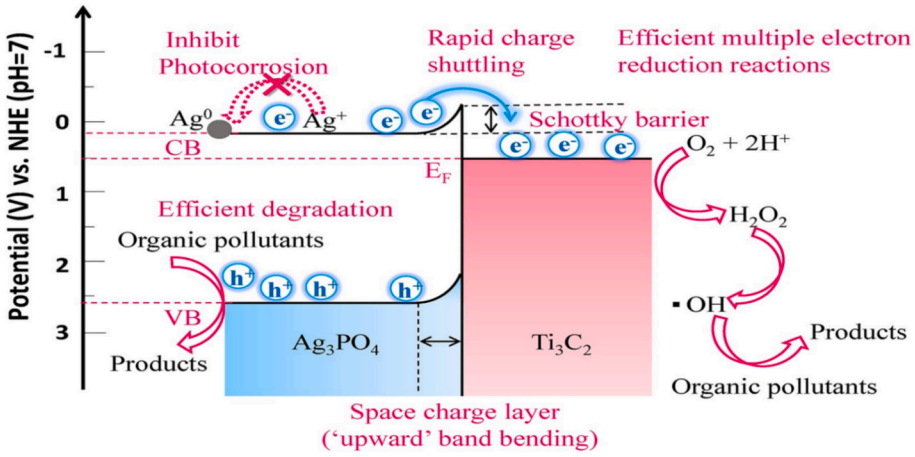


**Fig. 6.** Plausible MXBM photocatalytic degradation mechanism of dye pollutants using $Ag_3PO_4/Ti_3C_2$ [80]. Reused with approval from Elsevier (Copyright 2018).

surface of MXene can help to separate the electron-hole pair. Theoretically, hydroxyl radicals ($^{\bullet}OH$), $h^+$, and superoxide radicals ($^{\bullet}O_2^-$) are the three reactive species (RS) that account for the effective photocatalytic reactions [76,77]. In most of the photocatalysts containing MXenes, a transfer of charge from the photocatalyst to MXenes boosts the $e-/h^+$ pair separation and decreases its recombination, increasing the photocatalytic activity. Thus, photo-generated electrons are effectively utilized in the MXenes due to their outstanding electron-capture capabilities and efficient electron-hole separation. It has been suggested that MXene-based photocatalysts participate in photocatalytic activity by reacting with $H_2O$ and $O_2$ to produce $^{\bullet}OH$, $^{\bullet}O_2^-$, and $h^+$ [76,78], which are effective in several degradation reactions with organic pollutants, including attack on the aromatic ring, azo bond including the N═N bond, and C═N bond of pollutant molecules to degrade them into harmless molecules like $CO_2$ and $H_2O$ [79] as shown in Fig. 6. The Schottky barrier prevents the photo-charged electrons from returning from MXene to semiconductors. In the MXene, the photocatalytic degradation of water pollutants like dyes was enhanced by the Schottky connection as well as the excellent Fermi energy level of MXBM compared to the bare semiconductor photocatalytic materials, and this can be seen in their significantly improved degradation effectiveness discussed in the next section [76].

## 6. Performance evaluation of MXene-based material for dye photodegradation

This section discusses the degradation efficiency of various MXenes for the degradation of different dye pollutants. The treatment time and energy input are the most vital parameters that influence the process and thus control the degradation efficiency. These parameters were included in the comparison presented in Table 1. For example, the photocatalytic efficiency of the $Ti_3C_2/TiO_2$ nanocomposites was explored for the degradation of rhodamine blue under visible light illumination. In comparison to pure $TiO_2$ and commercial $TiO_2$, the composite of $TiO_2$ microspheres and multilayer $Ti_3C_2$ has comparatively high SSA, substantial photocurrent, and considerably less impedance. This material has offered a 94 % degradation in 60 min, which outperformed pure $TiO_2$ by a factor of two. The $Ti_3C_2$ addition successfully inhibited electron-hole pair recombination. The photo-generated $e^-$ in the MXBM moved from $TiO_2$ to $Ti_3C_2$. It was successfully blocked by the Schottky barrier at the $TiO_2$-$Ti_3C_2$ [81]. A high rhodamine B (RhB) photocatalytic degradation performance (97 %) was also observed for $TiO_2@Ti_3C_2$ in 40 min. Comparing the effectiveness of the $TiO_2@Ti_3C_2$ heterojunction to that of pristine and commercial $TiO_2$, with respect to RhB degradation, a significant improvement was confirmed for the hybrid material [82]. In another study [83], $Ti_3C_2$ MXenes were synthesized by employing several HF-based etching approaches and were then treated by alkalization to substitute O-containing terminal functional groups for —F to give multilayer $Ti_3C_2(OH)_2$. The performance of the multilayer $Ti_3C_2(OH)_2$ was assessed for photocatalytic degradation of methylene blue (MB), and about 81.2 % was degraded in 2 h under a 300-W Xe lamp [83]. In another work, Othman's group [84] investigated the degradation of RhB and MB utilizing $Ti_3C_2Tx$ MXene coated with Ag and Pd NPs. The authors studied the catalytic degradation properties of both pristine and fabricated MXBM under sunlight and UV irradiation. The $AgNPs/TiO_2/Ti_3C_2T_x$ demonstrated the highest degradation efficiency. The surface plasmon resonance effect for Ag played an important role in enhancing the absorption in the visible range of light to boost light harvesting and improve the charge separation step [84]. Improved efficiencies of such hybrids were also reported in other similar studies [85]. Another corresponding study reported the degradation of malachite green (MG) dye using $NiCo_2O_4$, doped Nd-$NiCo_2O_4$, and MXBM Nd-$NiCo_2O_4$/MXene [86]. It was found that the Nd-$NiCo_2O_4$/MXene nanocomposite showed the highest degrading activity of 98 % in 180 min compared to doped (61 %) and pure (52 %) forms. The synergy between Nd-doping and composite creation, which produces improved visible light absorption and effective $e^-/h^+$ decoupling, accounts for the Nd-$NiCo_2O_4$/MXene increased photocatalytic performance [86]. In another study, a $Ti_3C_2T_x$ nanosheet decorated with a metal organic framework (MOF) containing zinc for photocatalytic degradation of MB and DR31 was investigated. As presented in Table 1, for both the MB and Direct Red 31 (DR31) dyes, the MXene/MOF photocatalyst shows a degradation performance of 62 % and 35 %, respectively. Notably, the MXene/MOF was reported to exhibit better photocatalytic performance than the bare MOF and MXene. Furthermore, increased effectiveness takes place in the presence of $H_2O_2$ as it allows for maximizing the radical generation. Specifically, employing MXene/MOF, 74 % of MB and 51.6 % of DR31 dyes were photodegraded in the presence of $H_2O_2$ after 80 min. The authors stated that the excellent porosity of MXene/MOF nanocatalyst with an adjustable bandgap energy and high SSA facilitated fast charge transfer and prohibited the photo-generated $e^-$ and $h^+$ recombination [87]. In another photocatalytic study, $Ti_3C_2/BiFeO_3$ was employed to degrade Congo Red (CR) under visible light irradiation [88]. In just 42 min, 100 % CR was degraded. The authors pointed out that two variables contribute to CR's rapid and efficient degradation. Firstly, a greater SSA (147 $m^2/g$) and secondly, a decreased rate of $e^-/h^+$ recombination. Additionally, the control experiment performed under dark conditions only offered 21 % of the degradation, suggesting that $Ti_3C_2/BiFeO_3$ functions better as a photocatalyst, while exhibiting affinity (adsorption) to the pollutant. In parallel, an excellent photocatalytic degradation efficiency of 2D $Ti_3C_2T_x$ was reported by Bury [89]. Their work clarifies, for the first time, how the photocatalytic

**Table 1**
Summary of MXenes-based material performance for photocatalytic degradation of dyes.

| MXenes-based photocatalyst (MXBM) | Dye | Light input source | Dose (mg/L) | % Degradation | Time (Min.) | Ref. |
|---|---|---|---|---|---|---|
| ZIF-8@$Ti_3C_2$ MXene | Methylene blue | Xe lamp 160 W | 400 | 95 | 120 | [90] |
| Ag/$Ag_3PO_4$/MXene | Crystal violet | Xe lamp 300 W | | 84 | 90 | [91] |
| ZnO/$Ti_3C_2T_x$ | Methylene blue | Xe lamp | 500 | 97 | 45 | [92] |
| $Sm_2O_3$/MXene/g-$C_3N_4$ | Orange G | Tungsten halogen lamp 500 W | | ~100 | 300 | [93] |
| MXene@Cu/Tb/$MgFe_2O_4$ | Crystal violet | Tungsten bulb | 429 | 95 | 120 | [94] |
| MXene@carbon quantum dots | Malachite green | Halogen lamp 35 W | | 96 | 25 | [95] |
| $NiMoO_4$/MXene | Methylene blue | Visible light | 200 | 97 | 8 | [96] |
| MXene@V-CuO | Malachite green | Bulb 200 W | 429 | 88 | 100 | [97] |
| g-$C_3N_4$/MXene | Methylene blue | Halogen lamp 500 W | | ~99 | 150 | [98] |
| MXene@g-$C_3N_4$/$TiO_2$ | Rhodamine B | Xe lamp 300 W | | 99 | 120 | [99] |
| MXene@Cu/Tb/$MgFe_2O_4$ | Congo red | Xe lamp | 429 | 97 | 40 | [94] |
| MXene/CuO/B-g-$C_3N_4$ | Malachite green | Sunlight | | 98 | 120 | [100] |
| $MnWO_4$/MXene/carbon xerogel | Crystal violet | Xe lamp 500 W | | 95 | 60 | [101] |
| MXene/ZnO-tetrapod | Rhodamine B | Sunlight | | 78 | 120 | [102] |
| MXene/ZnO-tetrapod | Methyl orange | Sunlight | | 77 | 120 | [102] |
| ZnO/$NiWO_4$/$V_2C$ MXene | Rhodamine B | Xe lamp | | 92 | 120 | [103] |
| ZnO/$NiWO_4$/$V_2C$ MXene | Methylene blue | Xe lamp | | 93 | 120 | [103] |
| $Ti_3C_2$/$TiO_2$ | Rhodamine B | 300 W Xe lamp | 20 | 94 | 60 | [81] |
| ML-$Ti_3C_2(OH)_2$ | Methylene blue | 300-W Xe lamp | 6 | 83 | 120 | [83] |
| $TiO_2$@$Ti_3C_2$ | Rhodamine B | 300 W Xe lamp | 30 | 97 | 40 | [82] |
| MXene/g-$C_3N_4$ | Methylene blue | 500 W halogen lamp | 500 | ~70 | 180 | [104] |
| $Bi_{1-x}La_xFe_{1-y}Mn_yO_3$/$Ti_3C_2$ | Congo red | 300 W xenon lamp and 5 W light-emitting diode | 100 | ~100 | 30 | [105] |
| $Fe_2O_3$/$ZnFe_2O_4$@$Ti_3C_2$ | Rhodamine B | 300 W Xe lamp | 20 | 97 | 150 | [106] |
| AgNPs/$TiO_2$/$Ti_3C_2T_x$ | Methylene blue | 400 W Hg lamp | | 99 | 30 | [84] |
| $Ti_3C_2$–$TiO_2$ | Bromphenol blue | Solar | 35 | ~95 | 40 | [107] |
| AgNPs/$TiO_2$/$Ti_3C_2T_x$ | Rhodamine B | 400 W Hg lamp | | 99 | 40 | [84] |
| $TiO_2$/MXene | Methylene blue | 500 W mercury lamp | 10 | 99 | 60 | [85] |
| $TiO_2$/MXene | Methyl orange | 500 W Mercury lamp | 50 | 91 | 75 | [108] |
| Ag/$Ti_3C_2T_x$ | Safranin | Visible | 5 | 99 | 15 | [109] |
| MXene/Zn-MOF | Direct red 31 | 250 W mercury vapor lamp + $H_2O_2$ | 30 | 52 | 80 | [87] |
| AgNPs/$TiO_2$/$Ti_3C_2T_x$ | Methylene blue | Solar | | 96 | 120 | [84] |
| TMAOH-MXene | Bromocresol green | 128 W UV | 10 | 100 | 180 | [89] |
| $Ti_3C_2$–$TiO_2$ | Rhodamine B | Solar | 35 | ~95 | 40 | [107] |
| MXene/Zn-MOF | Methylene blue | 250 W mercury vapor lamp + $H_2O_2$ | 30 | 70 | 80 | [87] |
| $TiO_2$/$Ti_3C_2$ | Methyl orange | UV | 10 | 97 | 50 | [110] |
| AgNPs/$TiO_2$/$Ti_3C_2T_x$ | Rhodamine B | Solar light | | 96 | 80 | [84] |
| $TiO_2$/$Ti_3C2T_x$ | Methyl orange | 500 W Xenon lamp | | 92 | 50 | [111] |
| $Ti_3C_2T_x$/ $NH_2$-MIL-88B(Fe) | Methylene blue | 300 W Xenon lamp | 10 | 83 | 120 | [112] |
| $Ti_3C_2$–$TiO_2$ | Methyl orange | Solar | 35 | 99 | 40 | [107] |
| $Ti_3C_2$/$BiFeO_3$ | Congo red | 300 W xenon lamp | 100 | 100 | 42 | [88] |
| TMAOH-MXene | Methylene blue | 128 W UV | 10 | 100 | 180 | [89] |
| $Ti_3C_2T_x$/ $NH_2$-MIL-88B(Fe) | Methyl orange | 300 W Xenon lamp | 10 | 44 | 120 | [112] |
| ZnO/$Ti_3C_2$ | Methylene blue | 40-W UV lamp | 50 | 86 | 60 | [113] |
| ZnO@$Ti_3C_2$ | Methylene blue | 300 W Xe arc lamp | 20 | 95 | 180 | [114] |
| $TiO_2$/$Ti_3C_2$ | Methyl orange | 175 W mercury lamp | | 98 | 30 | [115] |
| $TiO_2$@$Ti_3C_2$/g-$C_3N_4$ | Rhodamine B | 300-W Xe lamp | 100 | 100 | 60 | [116] |
| $Ti_3C_2$/$TiO_2$/CuO | Methyl orange | 175 W mercury lamp | 100 | 99 | 80 | [117] |
| $Bi_2WO_6$/$Nb_2CT_x$ | Rhodamine B | 500 W Xenon lamp | 50 | 100 | 90 | [118] |
| $Ti_3C_2$/$MoS_2$ | Methyl orange | 400 W metal halide lamp | 50 | 97 | 30 | [119] |
| $Ti_3C_2$Tx | Methylene blue | 300 W visible | | 98 | 60 | [120] |
| $Ti_3C_2T_x$/ $NH_2$-MIL-88B(Fe) | Rhodamine B | 300 W Xenon lamp | 10 | 97 | 30 | [112] |
| ZnO@$Ti_3C_2T_x$ | Congo red | 300 W Xenon arc lamp | | 89 | 270 | [121] |
| $Bi_2WO_6$/$Nb_2CT_x$ | Methylene blue | 500 W Xenon lamp | 50 | 93 | 90 | [118] |
| $NiMnO_3$ / $NiMn_2O_4$ - $Ti_3C_2T_x$ | Methyl orange | LED lamp | | 100 | 180 | [122] |
| $Ti_3C_2$/ZnO | Rhodamine B | UV | 100 | 98 | 18 | [59] |
| $Ti_3C_2T_x$/$Ti_3AlC_2$@Ag | Methylene blue | 300 W UV lamp | | 100 | 55 | [78] |
| $Ti_2C$/$ZnCo_2O_4$ | Congo red | Visible | 50 | 78 | 270 | [123] |
| $Ti_3C_2$/ g-$C_3N_4$ | Rhodamine B | 270 W xenon lamp | 20 | 98 | 60 | [124] |
| $Bi_{0.90}Gd_{0.10}Fe_{0.80}Sn_{0.20}O_3$/MXene | Congo red | 300 W Xenon lamp | 100 | 100 | 120 | [125] |
| ZnO@$Ti_3C_2T_x$ | Rhodamine B | 300 W Xenon arc lamp | | 83 | 270 | [121] |
| $NiMnO_3$ / $NiMn_2O_4$ - $Ti_3C_2T_x$ | Methylene blue | LED lamp | | 100 | 20 | [122] |
| $Ti_3C_2T_x$/$Ti_3AlC_2$@Ag | Methyl orange | 300 W UV lamp | | 99 | 360 | [78] |
| $NiMnO_3$ / $NiMn_2O_4$ - $Ti_3C_2T_x$ | Rhodamine B | LED lamp | | 100 | 180 | [122] |
| $Mn_2O_3$-$Ti_3C_2T_x$ | Methyl orange | 250 W LED lamp | 20 | 93 | 35 | [126] |
| ZnO@$Ti_3C_2T_x$ | Methylene blue | 300 W Xenon arc lamp | | 92 | 270 | [121] |
| $Ti_3C_2T_x$/$Ti_3AlC_2$@Ag | Rhodamine B | 300 W UV lamp | | 99 | 20 | [78] |

(*continued on next page*)

**Table 1** (*continued*)

| MXenes-based photocatalyst (MXBM) | Dye | Light input source | Dose (mg/L) | % Degradation | Time (Min.) | Ref. |
|---|---|---|---|---|---|---|
| MXene/ZnS/chitosan-cellulose | Acid blue 80 | 1000 W deuterium lamp | 1 | >70 | – | [127] |
| $Nb_2C$/CdS | Rhodamine B | 300 W Xe lamp | 25 | 99 | 20 | [128] |
| Nd-$NiCo_2O_4$/MXene | Malachite green | solar | 40 | 98 | 180 | [86] |
| ZnO/$Ti_3C_2T_x$ | Methyl orange | 300 W xenon lamp | 30 | 100 | 50 | [129] |
| $Ti_3C_2$Tx@Chitosan@g–$C_3N_4$ | Orange G | 250 W Xe lamp | 100 | 89 | 60 | [130] |
| ZnO/$Ti_3C_2T_x$ | Rhodamine B | 300 W xenon lamp | 30 | 100 | 70 | [129] |
| $Mn_2O_3$-$Ti_3C_2T_x$ | Methylene blue | 250 W LED lamp | 20 | 100 | 25 | [126] |
| $Ti_3C_2$Tx@Chitosan@g–$C_3N_4$ | Rhodamine B | 250 W Xe lamp | 100 | ~99 | 40 | [130] |
| $Ti_3C_2$Tx@Chitosan@g–$C_3N_4$ | Methylene blue | 250 W Xe lamp | 100 | 99 | 60 | [130] |
| $Ti_3C_2$Tx@Chitosan@g–$C_3N_4$ | Methyl orange | 250 W Xe lamp | 100 | 60 | 60 | [130] |
| $Ti_3C_2$Tx@Chitosan@g–$C_3N_4$ | Malachite green | 250 W Xe lamp | 100 | 85 | 60 | [130] |
| CuO/$Ti_3C_2$ | Methylene blue | Sunlight | 50 | 100 | 80 | [131] |
| $NiCo_2S_4$/MXene | Rhodamine B | 250 W Xenon lamp | 5 | ~100 | 120 | [132] |
| ZnO/$V_2C$ | Methylene blue | 500 W Xe lamp | 50 | 100 | 120 | [60] |
| BiOBr/$TiO_2$/$Ti_3C_2T_x$ | Rhodamine B | 300 W Xe lamp | 20 | 100 | 30 | [133] |
| $Ag_3PO_4$/$Ti_3C_2$–$TiO_2$ | Methyl orange | 300 W Xe lamp | 50 | 98 | 120 | [134] |
| $CuFe_2O_4$/MXene | Methylene blue | Visible + $H_2O_2$ | 50 | 94 | 40 | [135] |
| $Ag_3PO_4$/$Ti_3C_2$–$TiO_2$ | Malachite green | 300 W Xe lamp | 50 | 99 | 120 | [134] |
| g-$C_3N_4$/$Ti_3C_2$ | Rhodamine B | 500 W metal halide lamp | 40 | 100 | 25 | [136] |
| $NiFe_2O_4$/MXene | Methylene blue | UV visible | | 74 | 70 | [137] |
| InSe/$TiO_2$/MXene | Methyl orange | 300 W Xe lamp | 60 | 92 | 60 | [138] |
| ZnO/$Nb_2C$ | Methylene blue | 500 W Xenon lamp | 50 | 63 | 120 | [60] |
| $Ti_3C_2$/$NiTiO_3$ | Methylene blue | Sunlight | 5 | 97 | 120 | [139] |
| Ag@ZnO@$Ti_3C_2$ | Methylene blue | 300 W Xenon lamp | 50 | 91 | 50 | [69] |
| $Ag_3PO_4$/$Ti_3C_2$–$TiO_2$ | Rhodamine B | 300 W Xenon lamp | 50 | 94 | 120 | [134] |
| $TiO_2$/$Ti_3C_2T_x$ | Methylene blue | 500 W mercury lamp | 50 | 98 | 30 | [140] |
| BPQDs/$Ti_3C_2$@$TiO_2$ | Methyl orange | 400 W metal halide lamp | 50 | 93 | 60 | [141] |
| I–$Ti_3C_2$@graphitic carbon-supported $TiO_2$ | Methylene blue | 500 W Hg lamps | 50 | 99 | 60 | [142] |
| CdS@$Ti_3C_2$@$TiO_2$ | Rhodamine B | Visible | 50 | 100 | 150 | [57] |
| $Ti_3C_2T_x$/$Bi_4Ti_3O_{12}$ | Methyl orange | 500 W Xe/Hg arc lamp | 35 | 100 | 60 | [143] |
| $Ag_3PO_4$/$Ti_3C_2$–$TiO_2$ | Methylene blue | 300 W Xenon lamp | 50 | 91 | 120 | [134] |
| BiOI/$TiO_2$/$Ti_3C_2$ | Rhodamine B | 500 W Xe lamp | | 100 | 80 | [144] |
| $TiO_2$/$Ti_3C_2T_x$ | Methyl orange | 500 W mercury lamp | 50 | 80 | 30 | [140] |
| CdS@$Ti_3C_2$@$TiO_2$ | Methylene blue | Visible | 50 | 100 | 150 | [57] |
| $TiO_2$@$Ti_3C_2$/g-$C_3N_4$ | Rhodamine B | 300 W Xe lamp | 100 | 100 | 60 | [116] |
| $BiVO_4$/$Ti_3C_2$ | Methyl orange | 300 W Xenon lamp | 100 | 99 | 130 | [145] |
| $WO_3$/MXene | Methylene blue | Sunlight | 5 | 99 | 80 | [146] |
| $Ti_3C_2T_x$/$Bi_4Ti_3O_{12}$ | Rhodamine B | 500 W Xe/Hg arc lamp | 35 | 100 | 50 | [143] |
| $Ti_3C_2$/$NiTiO_3$ | Malachite green | Sunlight | 5 | 98 | 120 | [139] |
| $Ti_3C_2$/$TiO_2$/g–$C_3N_4$ | Rhodamine B | 300 W Xenon lamp | 60 | 98 | 50 | [147] |
| $Ti_3C_2$/$NiTiO_3$ | Methyl orange | Sunlight | 5 | 87 | 120 | [139] |
| $BiVO_4$/$Ti_3C_2$ | Congo red | 300 W Xenon lamp | 100 | 100 | 60 | [145] |
| α-$Fe_2O_3$@$SnO_2$/MXene | Rhodamine B | 300 W Xe lamp | | 72 | 140 | [148] |
| ZnO/$Ti_2C$ | Methylene blue | 500 W Xe lamp | 50 | 99 | 120 | [149] |
| MXene/$PbCrO_4$ | Methylene blue | Sunlight | 20 | 93 | 120 | [150] |
| $Ti_3C_2(OH)_2$ | Methylene blue | 150 W Xe Arc Lamp | 20 | 97 | 80 | [151] |

characteristics of model 2D $Ti_3C_2T_x$ are affected by oxidation stabilization by enhancing efficiency. Two well-established methods are used to fabricate the delaminated MXene: minimum intensive layer delamination with hydrochloric acid/lithium fluoride (MILD-MXene) and hydrofluoric acid/tetramethylammonium hydroxide (TMAOH-MXene). L-ascorbic acid is then used to stabilize the product. In the 180 min under 128 W UV, 100 % degradation of methylene blue and bromocresol green was achieved. In addition, the process of industrial textile dye effluents treatment at 100 times higher concentration compared to the model dye solution must also ensure degradation effectiveness to attain industrial viability. These studies revealed that MILD-MXene exhibits superior efficiency over TMAOH-MXene because of its narrower optical band gap. To completely degrade the dye, the MILD-MXene only needed a few seconds of exposure to UV light. In another report, at around one hour, a 90 % MB degradation by CuO/$Ti_3C_2$ was achieved under sunlight irradiation. The enhanced rate of MB degradation by the MXBM can be attributed to the efficient intercalation of NPs between the $Ti_3C_2$ sheets, which enhances the photocatalyst's capacity to capture electrons.

Also, Liu et al. reported that a ZnO@$Ti_3C_2$ composite increases MB's photocatalytic degradation capacity and yields 94.84 % degradation in 180 min. The authors highlighted that the ZnO@$Ti_3C_2$ MXBM's photocatalytic activity is significantly enhanced by the Schottky junction, which inhibits photo-generated $e^-$ from returning to ZnO and encourages their separation from $h^+$ [114]. In another research, using a hydrothermal process, a unique 2D $Ti_3C_2$/$MoS_2$ nanosheets were effectively fabricated by Yao and co-workers [119]. It was found that the $Ti_3C_2$/$MoS_2$ has shown methyl orange (MO) degradation of 97.4 % in 30 min under irradiation by a 400 W metal halide lamp. It is attributed to its increased SSA and optical absorption capacity. Furthermore, $Ti_3C_2$ in conjunction with sheet-like $MoS_2$ NPs lowers the impedance, which brings an improved stimulated semiconductor $e^-$ transfer, inhibition of $e^-/h^+$ recombination, and then enhances photocatalytic degradation performance.

A summary of the research on the photocatalytic properties of MXenes for dye degradation is provided in Table 1. In most cases, the dye degradation efficiencies reached close to 100 %. This finding is noteworthy because it shows the possibility of using MXBM for pollutant elimination. However, it is important to highlight that most studies involving MXBM did not report the formation of intermediate products, the reaction mechanism, or the extent of mineralization. The fact of target pollutant removal confirmed by the analytical method does not ensure effective degradation of the formed by-products. Moreover, although the $^{\bullet}OH$ generation is suggested in most of the research articles to justify the photocatalytic degradation of dyes, the intermediate product formation and the mechanism were not clearly demonstrated. In addition, the dependency of degradation efficiency on operating conditions is critically discussed in the following sections to properly elucidate the potential of MXenes for dye photocatalytic degradation in

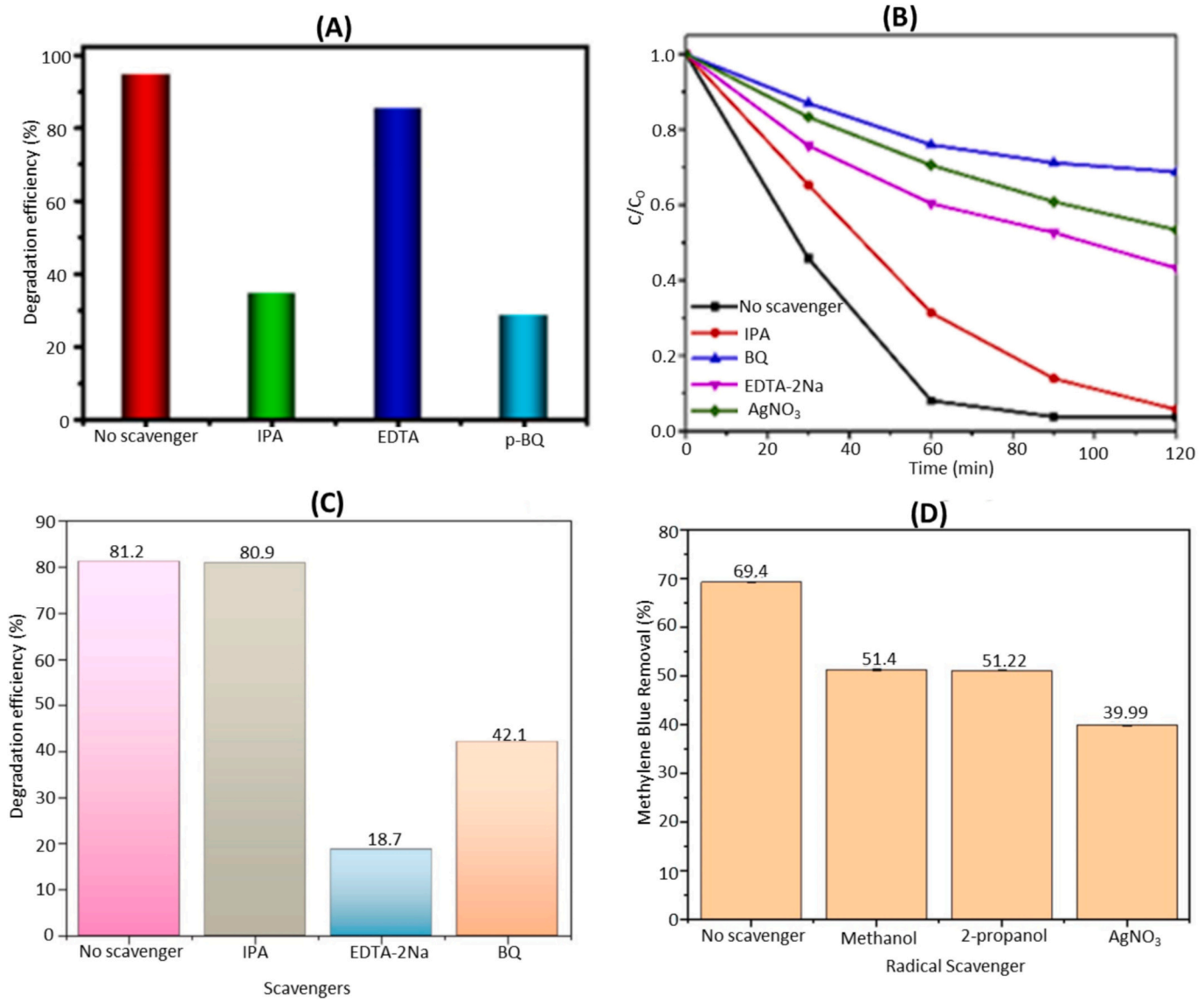


**Fig. 7.** Effect of radical scavenging on photocatalytic degradation of (a) RhB using $TiO_2$@$Ti_3C_2$ [82]. Reused with approval from Elsevier (Copyright 2020), (b) RhB using $Fe_2O_3$/$ZnFe_2O_4$@$Ti_3C_2$ [106]. Reused with approval from Elsevier (Copyright 2019), (c) MB using ML-$Ti_3C_2(OH)_2$ [83]. Reused with approval from Elsevier (Copyright 2022), (d) MB using MXene/g-$C_3N_4$ [104]. Reused with open access approval from MDPI (Copyright 2022).

industrial conditions.

## 7. Identification of dominant radical species

As given in the previous section, the major reactive species that could be evolved during dye photocatalytic degradation using MXBM as photocatalyst are $^{\bullet}OH$, $^{\bullet}O_2^-$, and $h^+$. In this context, scavenger tests could help to identify the reactive species [152–154]. The scavenger interferes with the pollutants' reactions with ROS, and some scavengers affect the catalytic activities [152]. Therefore, various studies have investigated the impact of radical scavengers on the photocatalytic degradation of dye pollutants to identify the contribution of ROS in MXBM. The major scavengers used in photocatalysis are methanol (MeOH) and isopropyl alcohol (IPA) (scavengers of $^{\bullet}OH$), p-benzoquinone (p-BQ) (as a scavenger of $^{\bullet}O_2^-$, triethanolamine (EDTA), (scavenger of $h^+$), and Furfuryl alcohol (FFA, scavenger for $^1O_2$). However, in general, scavengers are not specific for any reactive intermediate, as several RSs can react with the same scavenger with a bit different rate constant. Clarifying the relationship between quencher-induced inhibition and the contribution of reactive species is significant. The effectiveness of the quenching method is indisputable, and rather than simply disproving it, more research into its adequate use is needed [155]. Therefore, it is needed to take into account all their bimolecular rate constant values with all the reactive intermediates.

Numerous studies were carried out to identify the primary RSs that are responsible for the photocatalytic process and provide data about the RhB photodegradation mechanism in $TiO_2$@$Ti_3C_2$. Three different types of trapping agents were utilized in photocatalytic degradation: p-BQ, EDTA, and IPA. The addition of EDTA does not appear to have any discernible effect on RhB degradation using $TiO_2$@$Ti_3C_2$ photocatalyst, as seen in Fig. 7a. Thereby, it was suggested that $h^+$ is not the primary RS responsible for RhB degradation processes. Interestingly, it was observed that $^{\bullet}OH$ and $^{\bullet}O_2^-$ could have a weighty impact on photocatalytic processes because RhB degradation efficiencies sharply decline to around 50 % and 30 % by the introduction of IPA and p-BQ quenchers, respectively. Thus, $^{\bullet}OH$ and $^{\bullet}O_2^-$ radicals were involved in the photodegradation of RhB over $TiO_2$@$Ti_3C_2$ nanocomposite [82]. However, this study did not consider that it is not possible to discard the high influence of $h^+$ in RhB degradation processes. Because, although the three quenchers are at the same concentrations, IPA and p-BQ are at

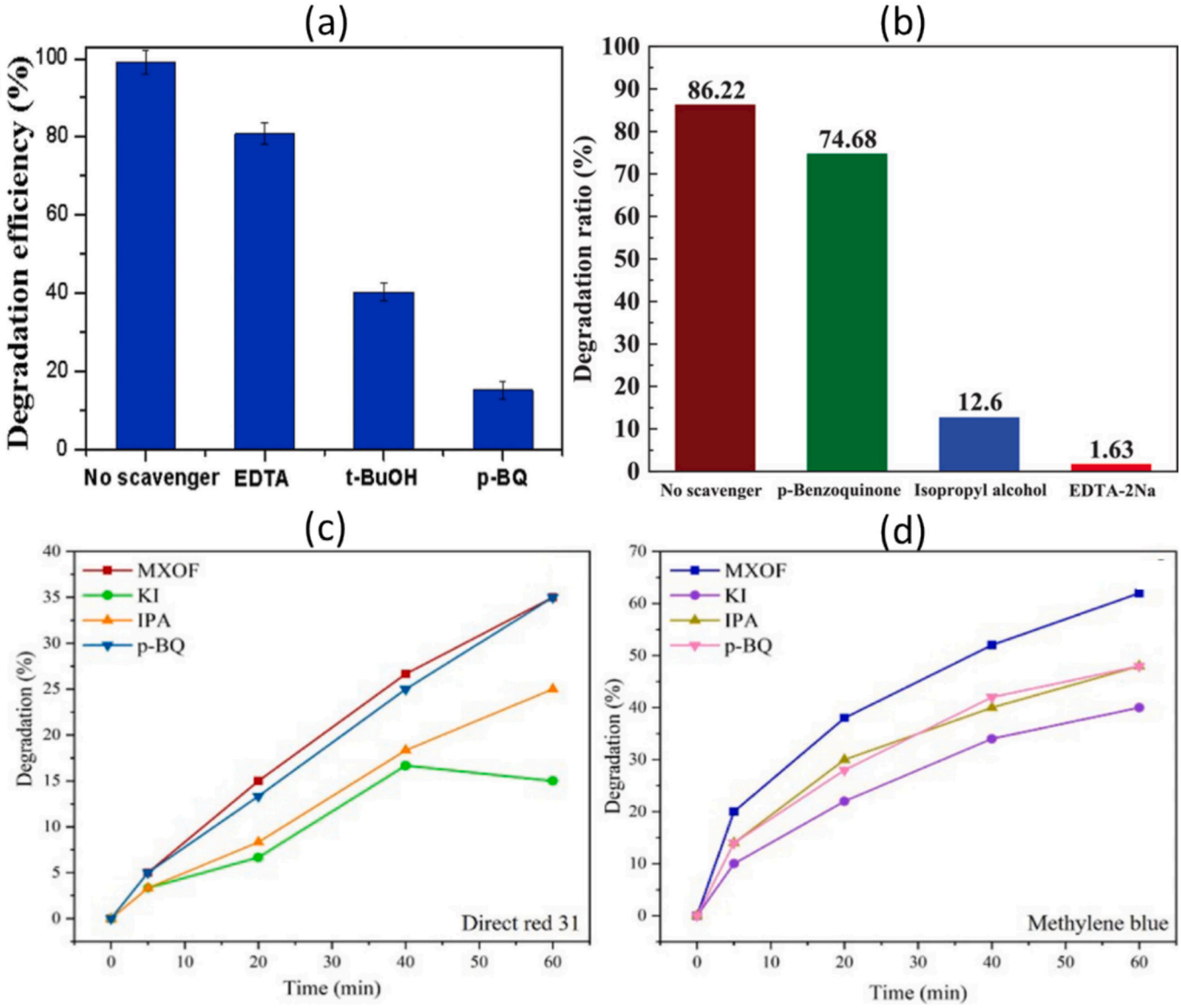


**Fig. 8.** Effect of radical scavenging on photocatalytic degradation of (a) MO using $Ti_3C_2/TiO_2$ [107]. Reused with approval from Elsevier (Copyright 2021), (b) MB using $ZnO/Ti_3C_2$ [87], (c) DR31 using MXene/Zn-MOF, (d) MB using MXene/Zn-MOF [113]. Reused with approval from Elsevier (Copyright 2023).

higher concentrations than RhB to react with the generated radicals, while the amount of EDTA is more than five times lower than that of $H_2O$ to reduce the $h^+$ of the VB.

In a similar study with $Fe_2O_3/ZnFe_2O_4@Ti_3C_2$, the evolution of reactive species was studied by adding 1 mM of BQ, $AgNO_3$, IPA, and EDTA-2Na to the RhB dye solution [106]. In this case, all the selected scavengers except IPA significantly reduced the degradation efficiency; it was suggested that the main RS were $^{\bullet}O_2^-$, $h^+$, and $e^-$. However, the result obtained with EDTA seems contradictory with respect to the other study. Thus, a plausible explanation for the result of this finding is that, as this material is not able to generate $^{\bullet}OH$ from the reaction of water with $h^+$. EDTA, as a good electron donor, could reduce $h^+$. In addition, the separation and transport efficiency of photo-generated electrons may be efficiently accelerated by the high conductivity of $Ti_3C_2$ MXene due to its distinctive lamellar nanostructure [106]. However, this work does not show any mineralization study, which, as commented above, is crucial for the process's understanding. Same conclusions were obtained when Qu and Co-workers identified the reactive species during the photocatalytic degradation of MB with multilayer $Ti_3C_2(OH)_2$'s as the catalyst [83]. This study showed that the major species were $h^+$ and $^{\bullet}O_2^-$, (Fig. 7c) with clear evidence from the scavenging study. It was further concluded that multilayer $Ti_3C_2(OH)_2$'s valence band electrons were excited by visible light, which resulted in the production of $h^+$. Following the passage of photo-generated $e^-$ to adsorbed $O_2$, $^{\bullet}O_2^-$ is formed, which attacks and degrades MB completely. [83]. $AgNO_3$ as the scavenger revealed the role of electrons during the photocatalytic degradation of MB by MXene/g-$C_3N_4$ (Fig. 7d) [104]. In this context, the activity of the MXene/g-$C_3N_4$ was only moderately affected by the addition of other scavengers such as MeOH and IPA because the band gap of the material is not able to generate hydroxyl radicals from $h^+$ of VB. The hydrated electron is expected to play a key function in the degradation of the MB dye pollutant by confirming the active sites contributing to the photocatalytic reaction; the degradation process is further supported by the $^{\bullet}O_2^-$, and slightly by $^{\bullet}OH$ [104]. This study again does not perform any mineralization study and suggests the hydroxyl radicals generation from the VB of g-$C_3N_4$. However, this cannot occur because the VB value is 1 eV above the needed level to generate hydroxyl radicals from water.

In general, the studies performed with MXene derivative materials containing $TiO_2$ propose plausible mechanisms to explain the oxidation

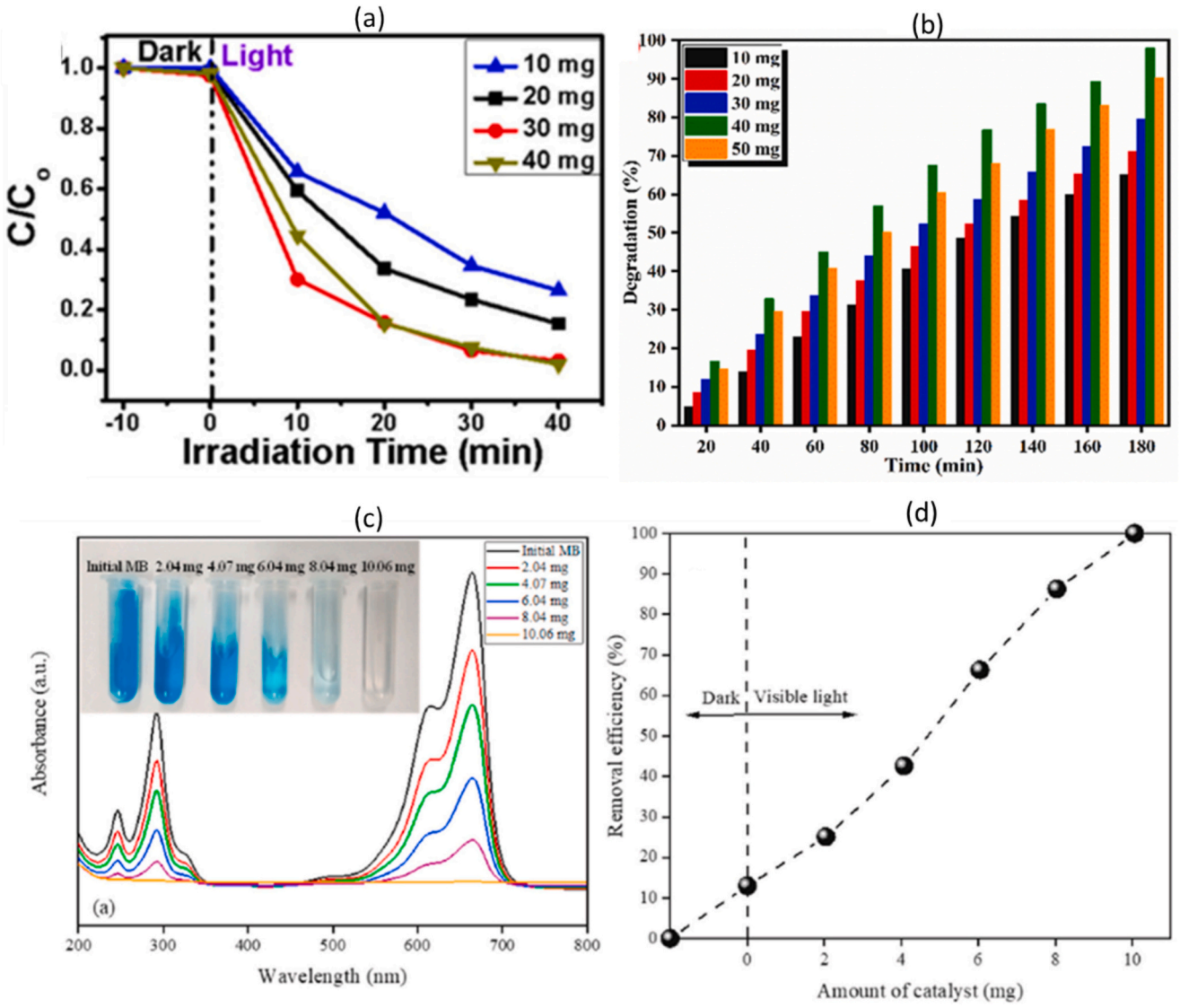


**Fig. 9.** (a) Impact of dose on photocatalytic degradation of RhB utilizing $TiO_2$@$Ti_3C_2$ [82]. Reused with approval from Elsevier (Copyright 2020). (b) Effect of Nd-$NiCo_2O_4$/MXene dose on the degradation of MG [86]. Reused with approval from Elsevier (Copyright 2024). Effect of ML-$Ti_3C_2(OH)_2$ dose on the degradation of MB (c) UV–visible absorption spectra (d) % degradation efficiency [83]. Reused with approval from Elsevier (Copyright 2022).

of the dyes. In this context, the major species involved during the photoirradiation of $Ti_3C_2$–$TiO_2$ for the degradation of MO were $^{\bullet}O_2^-$ and $^{\bullet}OH$. Their contribution to the degradation mechanism was confirmed by scavenging experiments with EDTA, p-BQ, and *tert*-butanol. In this case, EDTA had only a little effect on the MO degradation efficiency. On the other hand, as shown in Fig. 8a, the MO photocatalytic performances drop sharply to around 15 % and 40 %, respectively, in the presence of p-BQ and t-BuOH, suggesting the significant role of corresponding radicals in the degradation [107]. Scavengers such as p-BQ, IPA, and EDTA-2Na were employed to scavenge $^{\bullet}O_2^-$, $^{\bullet}OH$, and $h^+$, respectively, in ZnO/$Ti_3C_2$ for the degradation of the MB solution. Fig. 8b shows that the inclusion of IPA and EDTA considerably inhibits the photodegradation of MB, although the presence of p-BQ somewhat reduces the process. These findings show that while $^{\bullet}O_2^-$ is not the major radical in this photocatalytic process, $^{\bullet}OH$ and $h^+$ could be the primary active species [113]. Likewise, the major species in MXene/Zn-MOF for the photocatalytic degradation of DR31 dye was $^{\bullet}O_2^-$ as clear from the scavenging experiment with KI, IPA, and p-BQ, respectively, as shown in Fig. 8c. However, the major species involved in the degradation of MB with the same photocatalyst were $h^+$, $^{\bullet}OH$, and $^{\bullet}O_2^-$ as shown in Fig. 8d [87]. Conversely, in the case of photocatalytic degradation of RhB performed by Ding et al. [116] using $TiO_2$@$Ti_3C_2$/g-$C_3N_4$, it was reported that $^{\bullet}O_2^-$ could be the major RS in this photocatalytic process as BQ inhibited the photocatalytic degradation of RhB dye compare to IPA ($^{\bullet}OH$ scavenger) and ammonium oxalate ($h^+$ scavenger) and this is consistent with what was reported by [118]. In the same way, the degradation efficiency of MG using Nd-$NiCo_2O_4$/MXene was compared in the presence of scavengers like IPA, EDTA, BQ, and $AgNO_3$. The degradation efficiency was inhibited mainly with the addition of IPA, indicating the evolution of $^{\bullet}OH$ as the major RSs [86]. Many other studies identified the major RSs based on the scavengers and carried out the same protocols [122,126,127]. In general, it can be inferred that, depending on the targeted dye pollutants and the MXene material used, either of the RS ($h^+$, $e^-$, $^{\bullet}OH$, $^{\bullet}O_2^-$) can play a major role in the photocatalytic degradation operation. However, as commented before, to fully analyze the process effectiveness, it will be necessary to perform mineralization studies. Besides, for using the quenchers, one must take into account their concentrations, the reaction rate constant values between them and the reactive intermediates, and also the concentration of the dye.

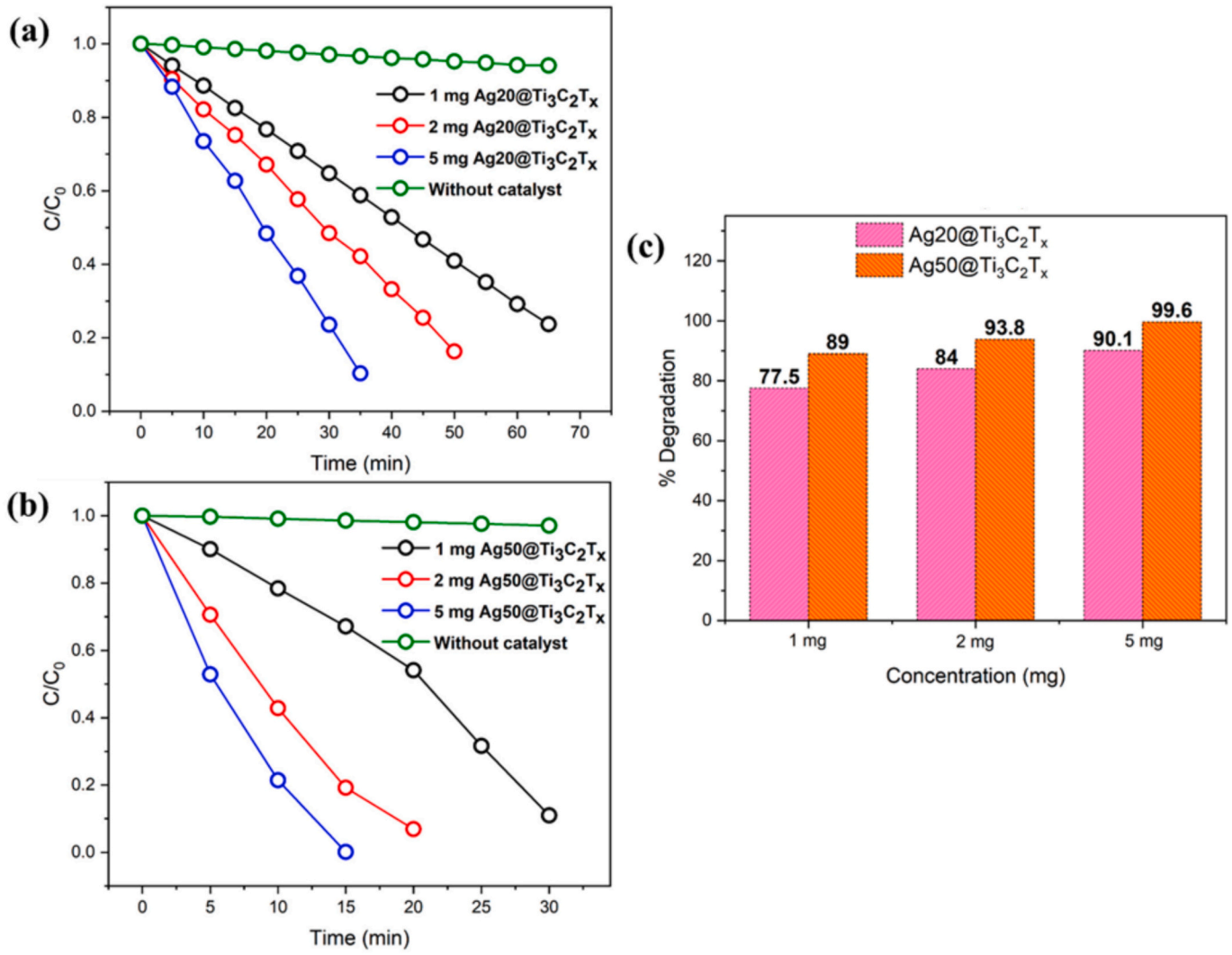


**Fig. 10.** Effect of dose on photocatalytic action of (a) Ag20@$Ti_3C_2T_x$ and (b) Ag50@$Ti_3C_2T_x$; (c) % degradation efficiency [109]. Reused with open access approval from MDPI (Copyright 2024).

## 8. Effect of MXene-based photocatalyst dose

In terms of economic value, using the right amounts of photocatalyst in a photodegradation reaction can save treatment costs [82,86]. Thus, another crucial factor to be considered in the degradation of dye contaminants under the influence of irradiation is the quantity of the MXene employed, as this dictates the numerical strength of the active site available for interaction. For instance, Quyen's research team [82] investigated the impact of the dose of $TiO_2$@$Ti_3C_2$ heterojunction on RhB (10 mg/L) photocatalytic degradation efficiency. As expected, the RhB degradation efficiency for $TiO_2$@$Ti_3C_2$ quantity was increasing in a reasonable range of 143 to 429 mg/L (Fig. 9**a**). This rise in the rate of photocatalytic degradation results in an increased amount of active sites and increased exposure to RhB molecules. However, the photodegradation efficiency did not show any additional improvement with 571 mg/L of photocatalyst. This fact might be because of active surface overlapping at high doses, but it also could be attributed to the full absorption of the dose of light using 429 mg/L of $TiO_2$@$Ti_3C_2$ photocatalyst. On the other hand, while some positive effect of increased amount of catalysts, a negative effect of increased turbidity of the solution could "compensate" for it, thus not revealing an overall increase in the effectiveness. However, this point of view was not considered in this study (and also in the next), and they concluded that the ideal dosage may be thought of as 429 mg/L [82]. A similar trend was also reported by Othman's team [84]. The MB and RhB photocatalytic degradation efficiency increased up to a certain catalyst dose, and beyond this dose, the dyes' photocatalytic degradation efficiency remained constant. In this case, the authors pointed out that this is because MXene materials have a shielding effect that can influence light penetration. This impact becomes more noticeable when catalyst loadings are large. However, the degradation productivity at larger MXBM loading remained the highest due to the increase in photocatalyst active sites. Furthermore, it was suggested that the SSA will be reduced due to the agglomeration of the material at higher doses [84]. Similar results were also observed with different doses of Nd-$NiCo_2O_4$/MXene for the degradation of MG (Fig. 9b) [86].

In another study, the MB (10 mg/L) photocatalytic degradation efficiency progressively increased from 0 % to 100 % with an increase in ML-$Ti_3C_2(OH)_2$ dose, as shown in Fig. 9c-d. The color of the reaction system may be used to visually measure the efficacy of MB degradation. The largest degradation rate (the slope of the tangent at each point) was observed at an ML-$Ti_3C_2(OH)_2$ dosage of 604 mg/L, even though MB was degraded fully at a dose of 1006 mg/L [83]. Doses of catalysts exceeding 100 mg/L seem to be impractical. Much lower optimal dose of MXBM was reported for Ag/$Ti_3C_2T_x$ on the photocatalytic degradation of safranin (30 mg/L). As seen in Fig. 10a–c, an increase in the Ag/$Ti_3C_2T_x$ mass to 5 mg/L yielded 99 % safranin degradation in 15 min, whereas 1 mg/L and 2 mg/L Ag/$Ti_3C_2T_x$ loading demonstrated 90 % and 93 %

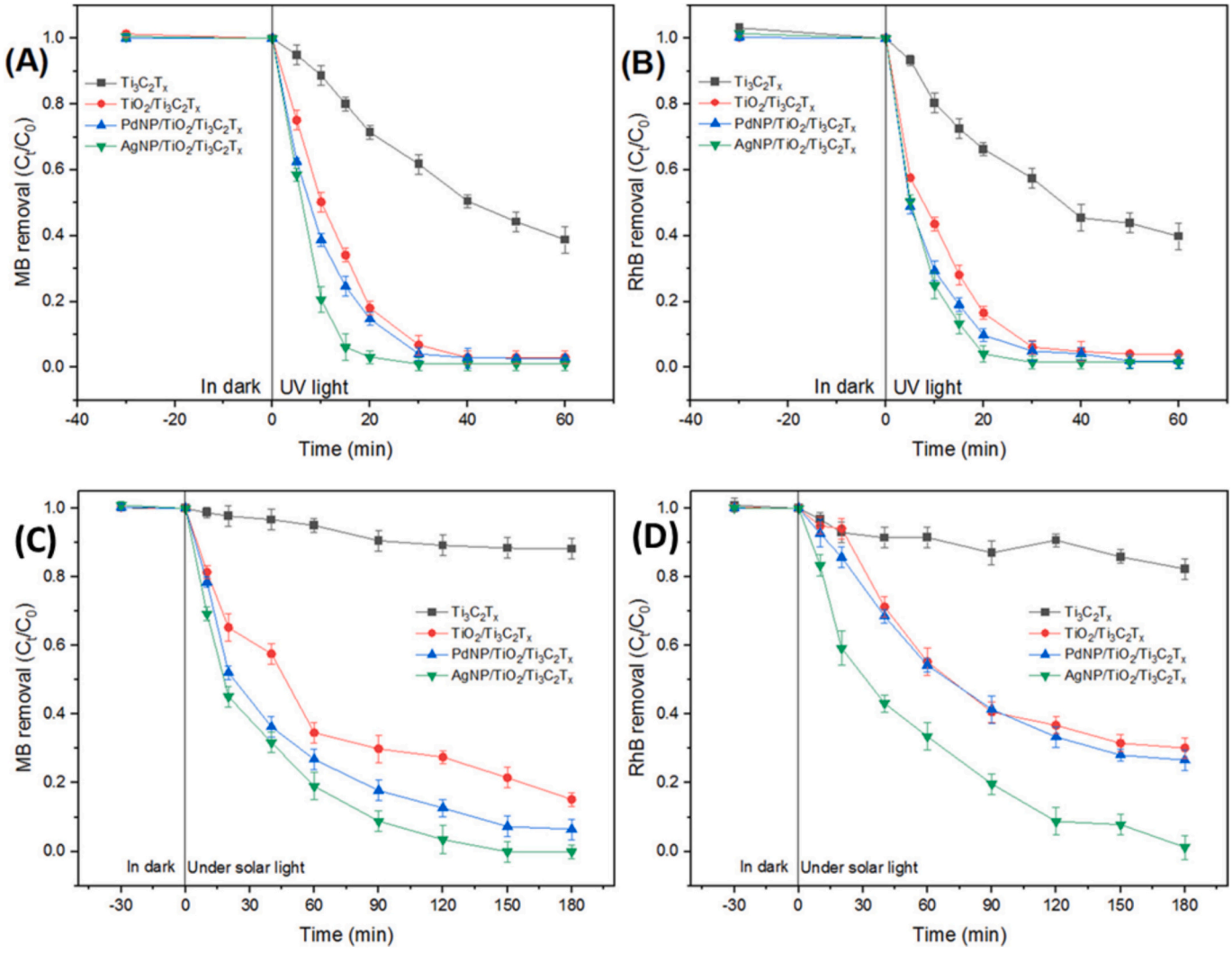


**Fig. 11.** Influence of irradiation time on the degradation of dyes by $Ti_3C_2Tx$-based nanocatalysts for (A) MB using UV, (B) RhB using UV, (C) MB using solar light, (D) RhB using solar light [84]. Reused with open access approval from the American Chemical Society (Copyright 2021).

photocatalytic degradation in 0.33 and 0.5 h, respectively [109]. A similar result was reported for the degradation efficiency of MO and CR with different doses of $BiVO_4$/MXene. Specifically, it was found that when the amount of $BiVO_4$/MXene is high, a much higher amount of $^{\bullet}OH$ and $^{\bullet}O_2^-$ radicals are produced, which leads to better photocatalytic activity, while the amount of catalyst is low, fewer oxidizing agents are present and this accounted for the increase in degradation efficiency with the increase in photocatalyst dose until optimum [145].

In short, most dye photocatalytic degradation operations were favored when the MXene dose was increased since more active sites for degradation were created, and there was an expansion of a large SSA for light harvesting. However, an excessively high dose may have negative effects due to the possibility of active surface overlapping, agglomeration, and shielding effects at high doses, which reduce the photocatalytic degradation efficiency. Depending on the characteristics of the MXene composite, there are variations in the dose level at which this happens. Typically, a dose in the range of 5–600 mg/L was reported as optimal, with 50 and 100 mg/L being the frequent optimal values. However, in these types of studies, light intensity is a key point that must be taken into account to determine the optimum photocatalyst dose. Too high a catalyst concentration can cause high turbidity and a significant drop in the photocatalytic process effectiveness.

## 9. Effect of irradiation time

The irradiation time greatly impacts the process effectiveness. Most degradation operations are completed at extended residence time. Additionally, residence time affects the kinetics of degradation [156]. The dye degradation with the irradiation time can also be observed based on the color change, as reported in many studies [83]. In a particular irradiation time study [84], AgNPs/$TiO_2$/$Ti_3C_2Tx$ was discovered to have a fast kinetic response, and its photocatalytic degradation efficacy against MB and RhB rose very high in the first 60 min when exposed to solar irradiation and the first 15 min (Fig. 11). The reaction patterns with PdNPs/$TiO_2$/$Ti_3C_2Tx$ and $TiO_2$/$Ti_3C_2Tx$ were likewise comparable. According to the authors, it seems logical to assume that the dye molecule's interaction with photocatalysts will decline along with a drop in MB or RhB concentration. Additionally, according to the authors, when these dyes degrade, by-products like benzoic acid, 1,2-benzenedicarboxylic acid, thionin, and ethanediotic acid compete with the primary pollutant for the active sites on the MXBM's surface [84]. A similar trend was reported for the photocatalytic degradation of different dyes using ZnO/$Ti_3C_2T_x$ (Fig. 12) [129] and other types of MXene-based materials [126,150,151].

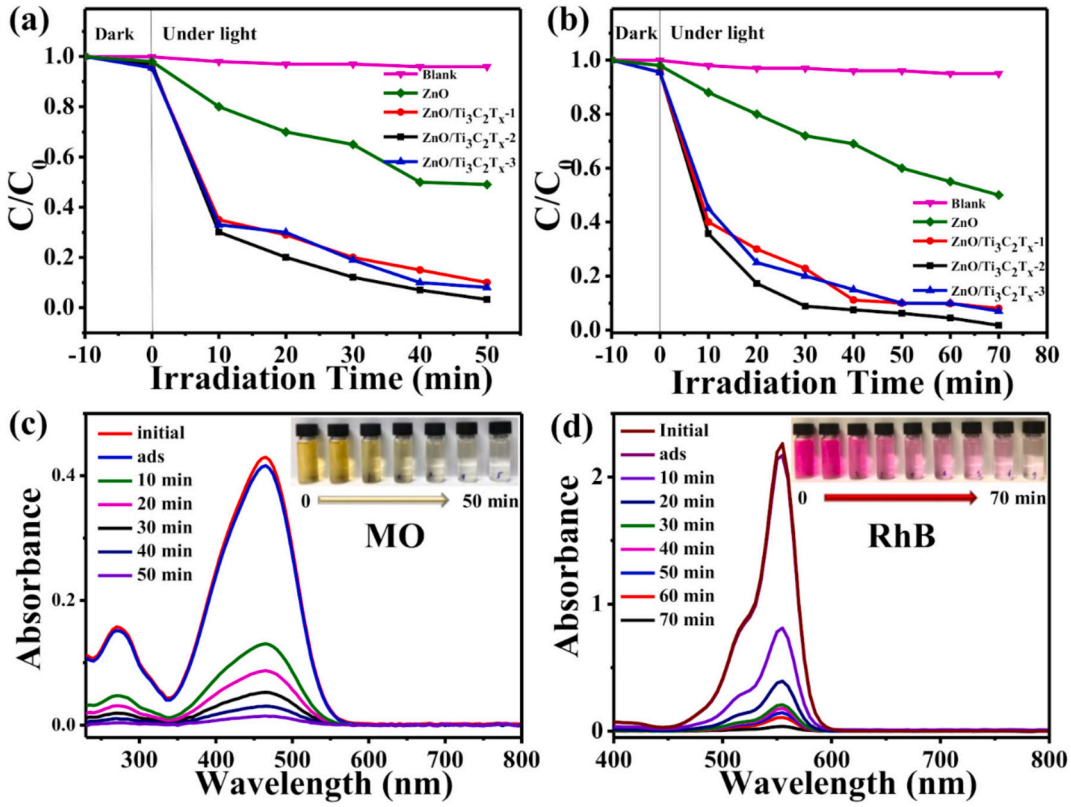


**Fig. 12.** Influence of irradiation resident time on ZnO/$Ti_3C_2T_x$ for the degradation of rhodamine blue and methyl orange and their corresponding UV–Visible absorption spectra [129]. Reused with open access approval from MDPI (Copyright 2020).

## 10. Effect of initial dye concentration

Another important parameter that affects photocatalytic degradation is the initial pollutant concentration. In this context, many studies have been performed from a low to a higher concentration to observe the effect. It is reported that higher dye concentrations diminished the degradation output due to the oversaturation of the employed nanomaterial [157]. There are a large number of studies that analyze the efficiency of a process by comparing the results of the percentage of degraded dye at different dye concentrations vs the irradiation time. However, this is not the correct way to evaluate this parameter because it must be compared to the amount of degraded dye vs irradiation time. For instance, in a particular study, the effect of the initial concentration of MO dye on the photocatalytic activity of $Ti_3C_2$–$TiO_2$ was explored by comparing the efficiency of MO degradation at varying concentrations using the percentage of degraded dye vs irradiation times, as it is shown in Fig. 13a. Thus, the MO degradation efficiencies decreased to 99 %, 98.5 %, and 70 %, respectively, when the starting concentrations were increased from 30 mg/L to 40 mg/L and 50 mg/L. However, calculating the amount of degraded dye from these data, it can be observed that close efficiencies are obtained at the three dye concentrations.

Thus, as in the study commented, most MO molecules interface and are exposed completely to the MXBM nanocatalyst at MO concentrations of 30 mg/L and 40 mg/L, which results in a full reaction and achieves optimal efficiency. Hence, it was suggested that the ideal MO concentration was 40 mg/L [107]. In this context, the degradation rate of RhB gradually decreases with increasing the initial concentration of RhB in their photocatalytic degradation by g-$C_3N_4$/$Ti_3C_2$ [136]. However, although this is true, the efficiency of the dye photodegradation was similar. In this case, it was represented as $C/C_0$ vs irradiation time, but the amount of degraded dye was very similar. It is clear that in photocatalyzed dye degradation at a fixed intensity of light and amount of photocatalyst, the efficiency of the process increases by adding more amount of dye to reach a limit where all the surface of the activated photocatalyst is fully occupied by interactions with the dye, and this with be the optimum, higher amount of dye or do not change the efficiency of the reaction or decreases it, if other phenomena affecting the photocatalytic process are occurring such as light absorption of the dye.

In another research, Yao's group [119] investigated the effect of initial MO concentration on the photocatalytic degradation effectiveness of $Ti_3C_2$/$MoS_2$. As displayed in Fig. 13b, as the concentration of the MO solution rises from 20 to 30 to 50 mg/L, the MXene's degrading efficiency generally falls. It is evident that after 25 min, almost 90 % of the MO solution at lower concentrations degrades. The variations in the UV absorption spectra of the 30 and 50 mg/L MO solutions are displayed in Fig. 13c and d, respectively. The photodegradation impact of MXene causes the high absorption spike of the MO solution at 554 nm to progressively decline. Additionally, the MXene sample shows a high ability to degrade MO (50 mg/L) in 125 min, with a degradation efficiency of around 80 %. The aforementioned findings demonstrate the potential for MXene photocatalysts to degrade organic pollutants at high concentrations. Similar observation was reported for other MXBM such as $Ti_3C_2$/$TiO_2$/g–$C_3N_4$, Nd-$NiCo_2O_4$/MXene (Fig. 13e-f), and $Ti_3C_2$Tx@Chitosan@g–$C_3N_4$ [130,132,145,147,151].

This can be attributed to the following factors: (i) As the initial concentration of pollutants increases, the transmittance of the solution could be weakened, which extends the pathlength of photons to the increased surface and diminishes the number of photons absorbed by the photocatalyst; (ii) Higher initial pollutants concentrations, a larger number of pollutant molecules covered the active sites on photocatalyst surface, resulting in the reduction in radicals generation; (iii) at the fixed dosage of photocatalyst, the ability of photocatalytic system for radicals production is not increasing while increase of pollutant dose, thus the ratio between radical species and pollutant decreases. Finally, as the concentration of pollutants increases, more pollutants and degradation intermediates compete with the limited radicals [147].

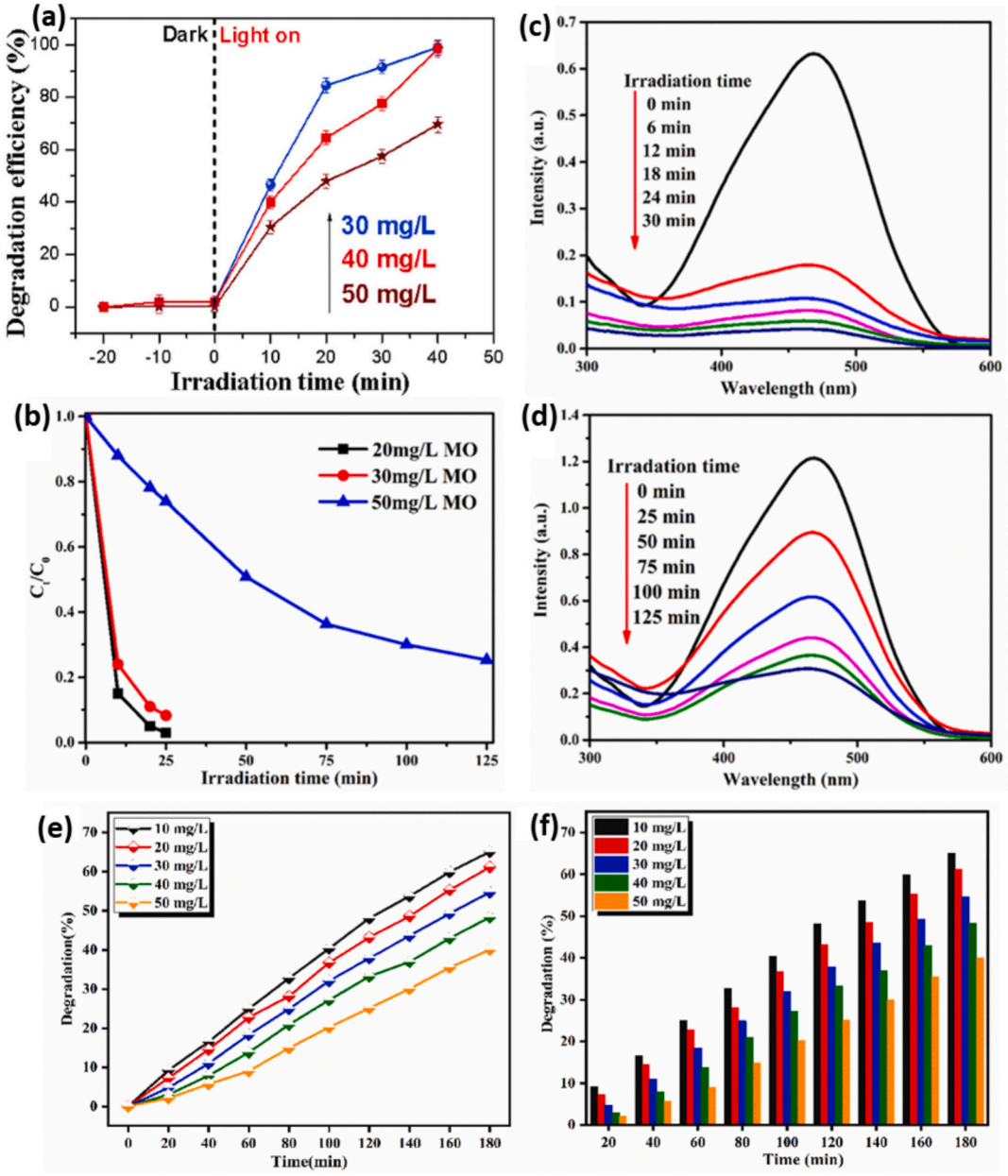


**Fig. 13.** Effect of different initial concentrations of dye pollutant in the matrix on photocatalytic degradation of MO (a) using $Ti_3C_2$–$TiO_2$ [107]. Reused with approval from Elsevier (Copyright 2021), (b) using $Ti_3C_2$/$MoS_2$ (c) UV–Vis absorption bands for 30 mg/L and (d) for 50 mg/L of MO solutions following irradiation by a 400 W metal halide lamp, respectively [119]. Reused with open access approval from Springer (Copyright 2020) (e-f). Effect of different initial concentrations of dye pollutant in the matrix on photocatalytic degradation of MG using Nd-$NiCo_2O_4$/MXene [86]. Reused with approval from Elsevier (Copyright 2024).

## 11. Effect of ionic species/co-existing ions

It has been established that the presence of ionic species like NaCl and KCl, which are often found in industrial runoffs and are often used in some stages of dyeing processes, affects their degradation [134,158,159]. In photocatalysis, the existence and increase of ionic species can either enhance or reduce the degradation of dye pollutants or have no discernible effect [134]. The influence of the ionic strength of the solution on the photocatalytic elimination of RhB on $Ti_3C_2$/ g-$C_3N_4$ MXBM was studied by Tu et al. [124]. The outcome demonstrated that the NaCl greatly decreased the photocatalytic degradation of RhB, equivalent to the k values spanning from 0.0483 $min^{-1}$ to 0.0139 $min^{-1}$ with NaCl concentration between 0 and 0.08 M. Here, as shown in Fig. 14, the inorganic ions inhibited both the photocatalytic and adsorption processes. This may have been caused by the removal of free radicals and photo-excited holes.

There are two possibilities in the presence of inorganic salt during the photocatalytic oxidation. One is the competitive reaction between the ions and reactive species. The second possibility is the adsorption on the reaction site. The electrostatic interaction relationship caused the negatively charged $Ti_3C_2$/ g-$C_3N_4$ MXBM to attract the $Na^+$, eventually exhausting its active sites. The reaction between $^{\bullet}OH$ and $Cl^-$ formed the $HOCl^{\bullet-}$ and next the $Cl^{\bullet}$, i.e., served as an $^{\bullet}OH$ scavenger to inhibit the entire degradation process. So, to maintain higher photocatalytic capabilities in future applications, it is imperative to lower the salt content [124].

Tan's research group [134] achieved a different result on the effect of ionic species on the photocatalytic degradation of dye pollutants by $Ag_3PO_4$/$Ti_3C_2$–$TiO_2$ MXBM. Notably, the addition of potassium chromate significantly decreased the photocatalytic effectiveness of $Ag_3PO_4$/

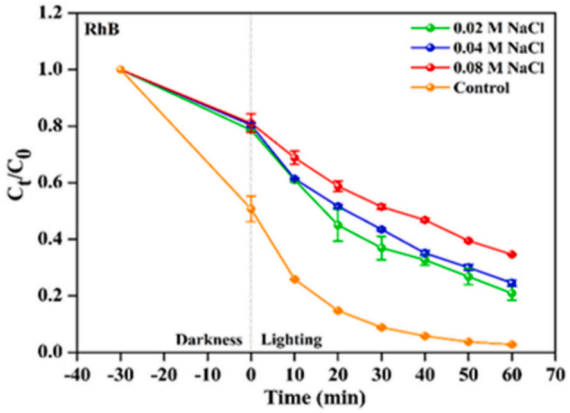


**Fig. 14.** Influence of ionic species on degradation of RhB using $Ti_3C_2$/ g-$C_3N_4$ under light illumination [124]. Reused with approval from Elsevier (Copyright 2022).

$Ti_3C_2$–$TiO_2$, as seen in Fig. 15. This is because the strong oxidizing ability of potassium dichromate and the strong activity of loaded $Ag_3PO_4$ impact the photocatalytic performance. The fact that $Ag_3PO_4$ has high oxidation and will reduce to elemental Ag when exposed to irradiation, but the introduction of inorganic species suppresses this process, may be the reason why the introduction of supplementary inorganic ions accelerated the degradation of dye contaminants. Thus, enhancing the material's photocatalytic activity in the process. The aforementioned findings demonstrate that $Ag_3PO_4$/$Ti_3C_2$–$TiO_2$ composite has strong applicability and future application prospects. It can adjust/adapt to most inorganic salts and the humic acid-containing environment, with the exception of $Cr_2O_7^{2-}$ [134].

Overall, it can be concluded that degrading dye pollutants from effluent is more challenging than degrading a one-dye-containing solution, because wastewater comprises a variety of inorganic ions and heavy metals in addition to organic pollutants. Inorganic ions can change the ionic strength of the solution and impact its photocatalytic degradation capabilities [158,160]. These ions may directly interact with active sites on the MXBM surface [161]. In certain instances, though, the effect can be advantageous. Competitive tests are especially crucial for assessing the MXBM's capability for industrial wastewater treatment.

## 12. Effect of pH

The initial pH of the solution is critical in any of the water treatment processes [162,163]. In photocatalysis, pH can affect the degree of ionization of the dye pollutant as well as functional groups, thus the

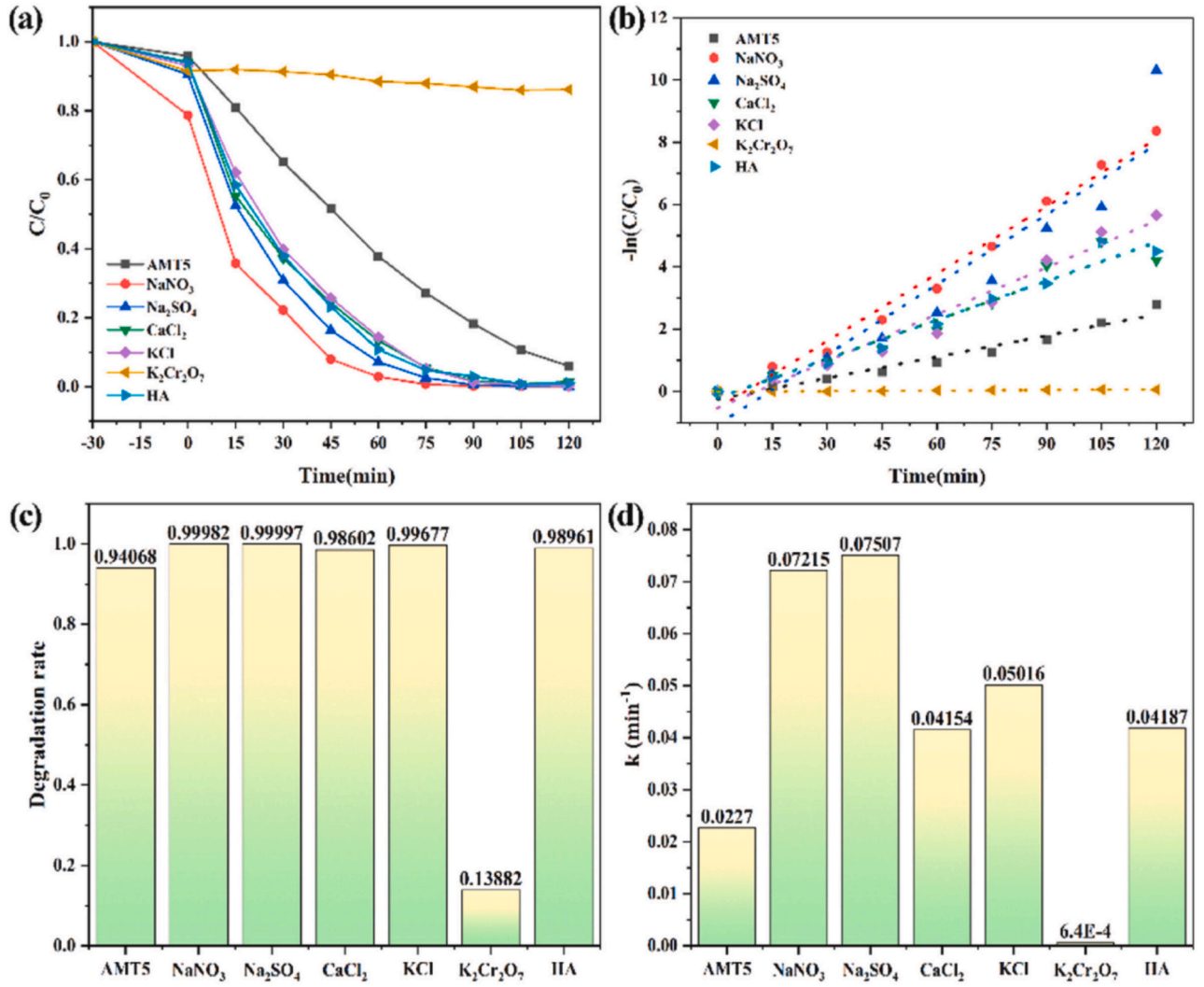


**Fig. 15.** Influence of diverse inorganic salts on the photocatalytic efficiency of $Ag_3PO_4$/$Ti_3C_2$–$TiO_2$ (a) the equivalent degradation output of dye contaminants; (b) Rate constant; (c) and (d) are histograms of equivalent values [134]. Reused with approval from Elsevier (Copyright 2022).

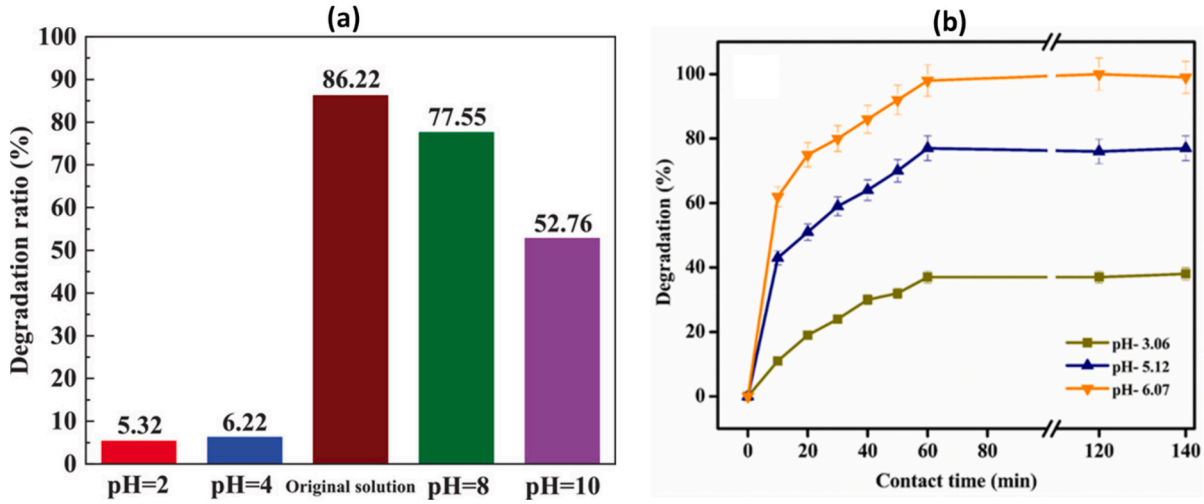


**Fig. 16.** Effect of different initial pH on photocatalytic degradation of (a) MB dye pollutant solution using ZnO/$Ti_3C_2$ [113]. Reused with approval from John Wiley and Sons (Copyright 2022), (b) RhB dye pollutant solution using $NiCo_2S_4$/MXene [132]. Reused with approval from Elsevier (Copyright 2020).

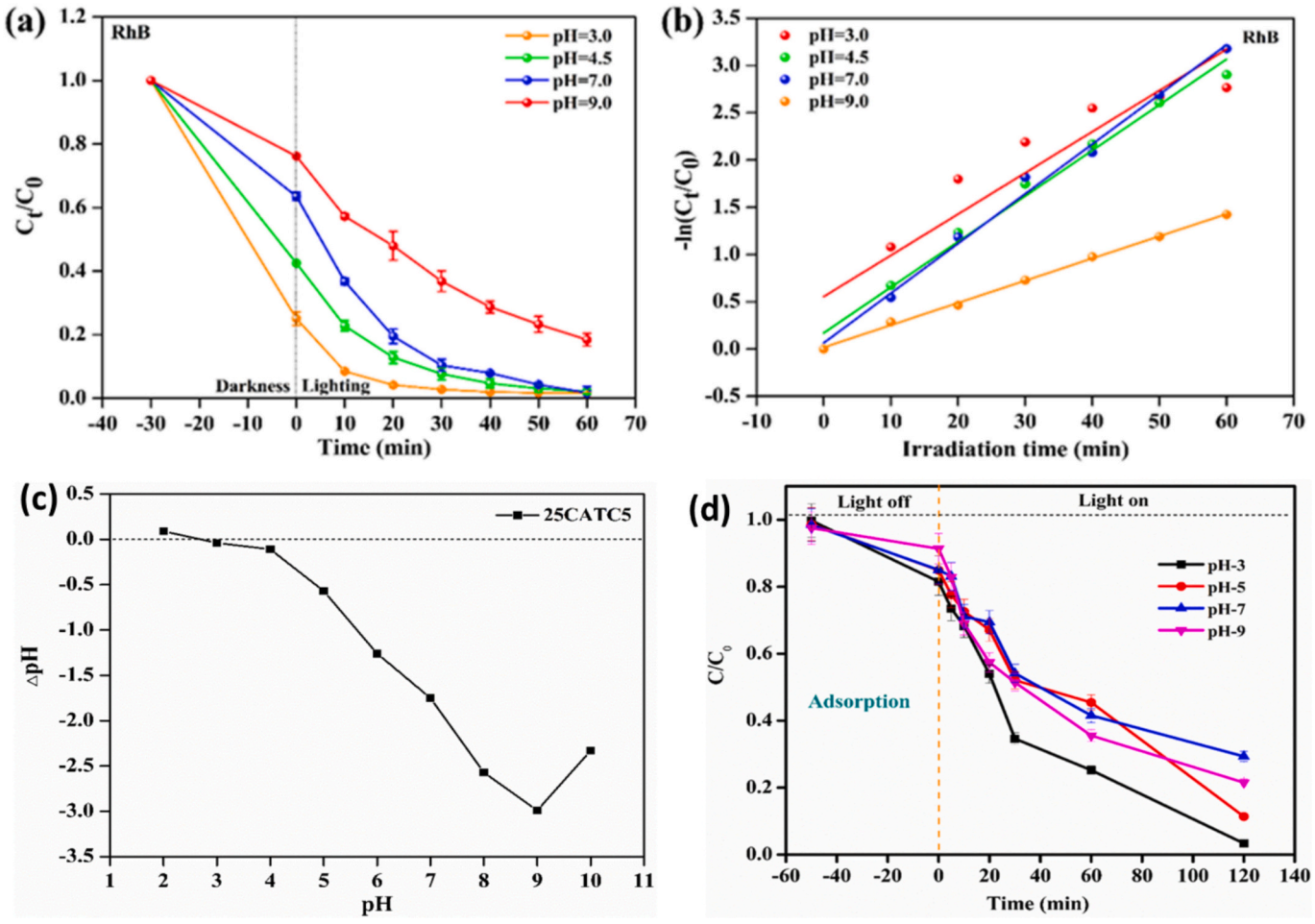


**Fig. 17.** (a) Effect of pH on RhB degradation using $Ti_3C_2$/ g-$C_3N_4$ when exposed to visible light illumination, (b) Pseudo-1st order rate constants of rhodamine blue when degraded by $Ti_3C_2$/ g-$C_3N_4$ at different initial pH, (c) Dependence of pH on △pH during the equilibration of $Ti_3C_2$/ g-$C_3N_4$ [124]. Reused with approval from Elsevier (Copyright 2022), (d) Effect of pH on MB and RhB degradation using $Ti_3C_2$Tx@Chitosan@g–$C_3N_4$ [130]. Reused with approval from Elsevier (Copyright 2020).

adsorption capacity of the photocatalyst, etc. [16,124,164,165]. Also, pH governs the photocatalytic mechanism process since the operation involves using radicals like $^{\bullet}$OH. However, only a few investigations are available on this effect. For example, Luo's research group investigated the influence of pH on the catalytic degradation of MB using ZnO/$Ti_3C_2$ under light illumination. Fig. 16a displays the degradation efficiency of

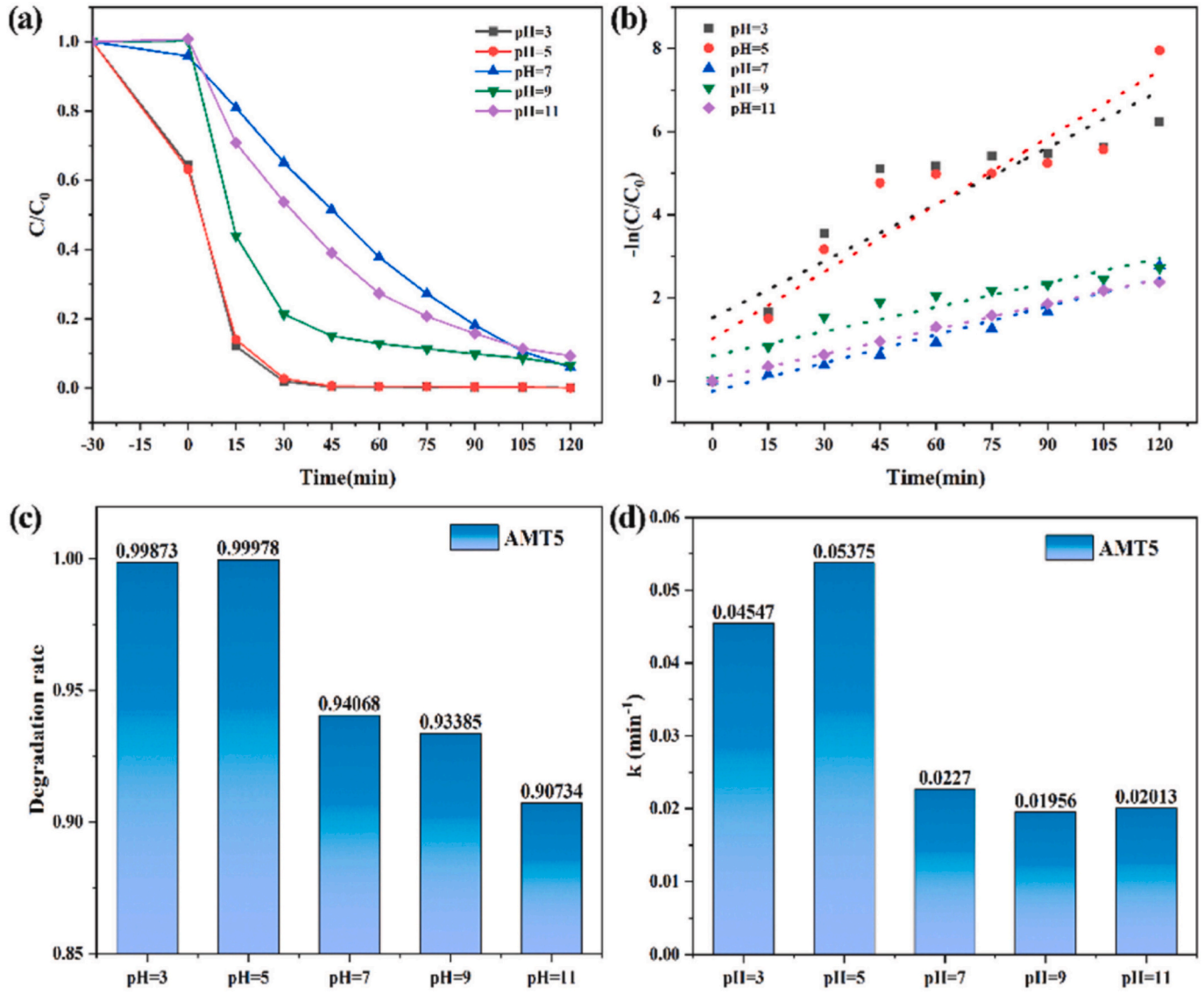


**Fig. 18.** Photocatalytic efficiency of $Ag_3PO_4/Ti_3C_2–TiO_2$ under various pH (a) the equivalent degradation rate of RhB; (b) Rate constant; (c) and (d) are histograms of equivalent values [134]. Reused with approval from Elsevier (Copyright 2022).

MB over $ZnO/Ti_3C_2$ in 60 min at various pH values. The dissolution of ZnO in acidic conditions causes the degradation efficiency of MB to drop drastically between pH 2 and 4. Moreover, for pH values of 8 and 10, the photocatalytic efficiencies also drop because the basic solution's $OH^-$ might lessen the generation of $^{\bullet}OH$ [113]. This claim about better photocatalytic degradation performance of MXene at a neutral pH region is consistent with what was reported by Vigneshwaran research group [132] and Khaneghahi's team [151] for the degradation of RhB using $NiCo_2S_4$/MXene under 250 W Xe lamp illumination for 140 min as shown in Fig. 16b and for the degradation of MB using $Ti_3C_2(OH)_2$ under 150 W Xenon Arc Lamp irradiation for 80 min respectively.

In another study [124], the photocatalytic degradation of 20 mg/L RhB employing 20 mg of $Ti_3C_2$/ g-$C_3N_4$ is explored at different pH levels. As shown in Fig. 17a, RhB's degradation process showed a distinct trend, with a clear decline in RhB's degradation efficiency at pH 9. At pH levels of 3, 4.5, 7, and 9, the k values were 0.044 $min^{-1}$, 0.048, 0.052, and 0.023 $min^{-1}$, respectively, as shown in Fig. 17b. Specifically, the data shown in Fig. 17 indicate that RhB degradation favored an acidic and neutral reaction environment. The charge characteristics for $Ti_3C_2$/g-$C_3N_4$ MXBM were found by dipping the material into 0.1 mol/L KCl solutions and stirring it for 24 h. The △pH values were related to these surface charge characteristics. Fig. 17c illustrates that the △pH was negative from pH 3 to 11, and below this pH range, it was positive. These findings suggested that the surface of $Ti_3C_2$/g-$C_3N_4$ is negatively charged. This explains why the degradation of the targeted contaminant, cationic RhB dye (which is positively charged), is very high between pH 3–11 but very poor below this pH range. Nonetheless, the outcome of the experiment showed that the effectiveness of photocatalysis and adsorption in an acidic environment was greater than in an alkaline one. Therefore, the adsorption and degradation of the RhB were not primarily driven by the electrostatic attraction relationship. However, the H-bond that forms between the protonated Ti—O, the unprotonated Ti-OH, and the rhodamine blue present in aqueous solution may improve $Ti_3C_2$/ g-$C_3N_4$'s adsorption ability. Through the noncovalent surface-π attraction, the aromatic groups on RhB and the peroxy groups on $Ti_3C_2$/g-$C_3N_4$ material interacted. Because of the attack of photoexcited $h^+$, the acidic aqueous solution further speeds up the reaction process. Conversely, the reduction in photodegradation efficiency at higher pH values is caused by the generation of less active free radicals ($HO_2^{\bullet}$). As shown in Fig. 17d, a similar acidic pH positive effect for the photocatalytic degradation of MB and RhB using $Ti_3C_2Tx$@Chitosan@g–$C_3N_4$ was observed [130]. Tan and co-workers also found a similar observation when exploring the

**Table 2**
Regeneration and recyclability of MXene towards photocatalytic degradation of various dye pollutants in brief.

| MXenes-based photocatalyst | Dye degraded | Eluent/Regenerant | % effectiveness at $n = 1$ | Number of cycles(n) | % effectiveness after n-th cycle | References |
|---|---|---|---|---|---|---|
| $Sm_2O_3$/MXene/g-$C_3N_4$ | Orange G | Washed and dried | ~100 | 5 | ~95 | [93] |
| MXene@Cu/Tb/$MgFe_2O_4$ | Crystal violet | DI $H_2O$ | 95 | 5 | 79 | [94] |
| $NiMoO_4$/MXene | Methylene blue | 99.5 % pure EtOH | 97 | 5 | 91 | [96] |
| MXene@V-CuO | Malachite green | Washed and dried | ~88 | 5 | 78 | [97] |
| g-$C_3N_4$/MXene | Methylene blue | Washed and dried | 100 | 4 | ~85 | [98] |
| MXene@g-$C_3N_4$/$TiO_2$ | Rhodamine B | Washed | ~99 | 4 | >90 | [99] |
| MXene/CuO/B-g-$C_3N_4$ | Malachite green | Washed | >90 | 5 | >90 | [100] |
| $MnWO_4$/MXene/carbon xerogel | Crystal violet | Washed | 95 | 5 | 86 | [101] |
| MXene/ZnO-tetrapod | Rhodamine B | Washed | ~78 | 4 | >62 | [102] |
| ZnO/$NiWO_4$/$V_2C$ MXene | Rhodamine B | Washed | ~92 | 4 | 86 | [103] |
| ZnO/$NiWO_4$/$V_2C$ MXene | Methylene blue | – | ~93 | 4 | 89 | [103] |
| $Ti_3C_2$/$TiO_2$ | Rhodamine B | – | ~94 | 4 | 90 | [81] |
| $TiO_2$-$Ti_3C_2$ | Rhodamine B | Washed | 97 | 5 | 97 | [82] |
| MXene-COOH@$(PEI/PAA)_{10}$ | Methylene blue | EtOH | 85 | 8 | 65 | [173] |
| MXene@$Fe_3O_4$ | Methylene blue | EtOH | >80 | 5 | 77 | [174] |
| $TiO_2$/$Ti_3C_2$ | Methyl orange | deionized $H_2O$ | ~97 | 4 | ~93 | [110] |
| $Fe_2O_3$/$ZnFe_2O_4$@$Ti_3C_2$ | Rhodamine B | – | 97 | 4 | >90 | [106] |
| TMAOH-MXene | Bromocresol green | Deionized $H_2O$ | 100 | 2 | 70 | [89] |
| $TiO_2$/$Ti_3C2T_x$ | Methyl orange | – | 92 | 5 | ~88 | [111] |
| p-MXene/SWCNTs | Methylene blue | $H_2O$ and EtOH | 95 | 5 | ~95 | [175] |
| $V_2CT_x$ | Methylene blue | EtOH | ~76 | 4 | >50 | [176] |
| $NiCo_2S_4$/MXene | Rhodamine B | 0.1 M HCl | 99 | 5 | ~98 | [132] |
| $Ti_3C_2$Tx@Chitosan@g–$C_3N_4$ | Methylene blue | Double-distilled $H_2O$ and 99.9 % pure EtOH | 99 | 5 | ~93 | [130] |
| Sodium alginate aerogel/$Ti_3C_2T_x$ | Congo red | Pure EtOH and deionized $H_2O$ | ~96 | 5 | 70 | [177] |
| $Ti_3C_2(OH)_2$ | Methylene blue | Double-distilled $H_2O$ | ~97 | 3 | ~89 | [151] |
| Sodium alginate aerogel/d-$Ti_3C_2T_x$ | Methylene blue | 5 % EtOH and deionized $H_2O$ | 88 | 10 | 84 | [178] |
| $Ti_3C_2$–$TiO_2$ | Methyl orange | – | 99 | 5 | ~97 | [107] |
| g-$C_3N_4$/$Ti_3C_2$/$TiO_2$ | Rhodamine B | EtOH and deionized $H_2O$ | >95 | 5 | ~95 | [179] |
| $TiO_2$/MXene | Methylene blue | – | ~99 | 5 | ~84 | [85] |
| MXene/Zn-MOF | Direct red 31 | EtOH and acetone (50:50) | 35 | 5 | ~35 | [87] |
| $TiO_2$/MXene | Methyl orange | – | ~91 | 5 | ~87 | [108] |
| MXene/Zn-MOF | Methylene blue | EtOH and acetone (50:50) | 62 | 5 | ~62 | [87] |
| $Ti_3C_2$/$BiFeO_3$ | Congo red | – | 100 | 4 | ~100 | [88] |
| TMAOH-MXene | Methylene blue | Deionized $H_2O$ | 100 | 2 | 70 | [89] |
| ZnO/$Ti_3C_2$ | Methylene blue | Deionized $H_2O$ | ~86 | 5 | ~70 | [113] |
| ZnO/$Ti_3C_2$ | Methylene blue | – | ~95 | 3 | >90 | [114] |
| $Ti_3C_2$/$MoS_2$ | Methyl orange | Centrifugation | ~97 | 3 | >75 | [119] |
| $Ti_3C_2$/ZnO | Rhodamine B | – | ~98 | 7 | >90 | [59] |
| $Ti_3C_2T_x$/$Ti_3AlC_2$@Ag | Methyl orange | – | ~99 | 5 | >90 | [78] |
| ZnO@$Ti_3C_2T_x$ | Rhodamine B | Without treatment | ~93 | 6 | ~89 | [121] |
| ZnO/$V_2C$ | Methylene blue | Centrifugation | ~100 | 4 | ~97 | [60] |
| $Ti_3C_2T_x$/$Ti_3AlC_2$@Ag | Methylene blue | – | ~100 | 5 | >95 | [78] |
| $Ag_3PO_4$/$Ti_3C_2$–$TiO_2$ | Rhodamine B | Centrifugation | ~94 | 8 | 80 | [134] |
| ZnO/$Ti_3C_2T_x$ | Methyl orange | – | ~100 | 5 | >95 | [129] |
| $Ti_3C_2T_x$/$Ti_3AlC_2$@Ag | Rhodamine B | – | ~99 | 5 | >95 | [78] |
| $Nb_2C$/CdS | Rhodamine B | – | 99 | 3 | ~80 | [128] |
| Nd-$NiCo_2O_4$/MXene | Malachite green | DI $H_2O$ and EtOH | 98 | 5 | >80 | [86] |
| ZnO/$Ti_3C_2T_x$ | Rhodamine B | Washed with deionized $H_2O$ | ~100 | 5 | >95 | [129] |
| ZnO/$Ti_2C$ | Methylene blue | Centrifugation | ~99 | 4 | >97 | [149] |
| $Ti_3C_2$Tx@Chitosan@g–$C_3N_4$ | Rhodamine B | DD $H_2O$ and EtOH | ~99 | 5 | ~92 | [130] |
| CuO/$Ti_3C_2$ | Methylene blue | – | ~100 | 3 | >80 | [131] |
| $NiFe_2O_4$/MXene | Methylene blue | – | 74 | 3 | >70 | [137] |
| MXene/$PbCrO_4$ | Methylene blue | DI $H_2O$ and EtOH | ~93 | 3 | 90 | [150] |

effect of different pH conditions on the photocatalytic efficacy of $Ag_3PO_4$/$Ti_3C_2$–$TiO_2$ for the degradation of RhB [134]. In this study, the solution pH was adjusted to 3, 5, 9, and 11. Fig. 18 demonstrates that the photocatalytic degradation and adsorption capacity are substantially higher in acidic conditions as opposed to neutral and alkaline conditions. This could be due to the increased incidence of hydrogen ions in acidic solutions, which react with $^{\bullet}O_2^-$ in the CB to form $H_2O_2$. This $H_2O_2$ then reacts with $^{\bullet}O_2^-$ to yield $^{\bullet}$OH radicals, boosting the efficiency of the photocatalytic process. $Ag_3PO_4$'s strong oxidizing ability allowed dyes to oxidize more readily in the presence of $H^+$. Nevertheless, the photocatalytic performance will not significantly improve with additional pH lowering. Since the $Ag_3PO_4$/$Ti_3C_2$–$TiO_2$ reaction mechanism has a restricted rate of $H^+$ consumption, too much $H^+$ will cause the reaction to be restricted. In comparison to neutral conditions, the degradation rate was marginally lower under basic conditions during the first hour of photocatalytic degradation. This might be the result of higher $OH^-$ concentration, which increased $Ag_3PO_4$/$Ti_3C_2$–$TiO_2$ oxidation potential, and an interaction between the $h^+$ in the VB and $OH^-$ in the solution that produces $^{\bullet}$OH, which facilitates the photocatalytic operation [134]. Many other researchers [145,147] also established the ability of MXene and its composite to provide high effectiveness in an acidic medium rather than an alkaline medium, and this proves the chemical stability of this emerging photocatalyst in difficult environmental conditions.

## 13. Regenerability and recyclability

From an economic, ecological, and sustainability perspective, the reusability of MXenes should be ultimately considered for an all-around

environmental application as per pollutant elimination, especially in real wastewater treatment scenarios and industrial/commercial scale level [166–168]. Regeneration-recyclability is an adsorption-desorption process of recovering the expended photocatalytic material (MXene) from the reaction mixture, restoring the photocatalyst integrity/capacity by removing pre-adsorbed pollutant (adsorbate) from the surface with the aid of eluent and then reusing the nanocatalyst in the next photocatalytic degradation operation [167,169–172]. This is the desired way; however, in many cases, additional operations to recover full catalytic properties can also be needed (for example, heating in high temperatures, calcination, or treatment with specific chemicals).

Various research works on the reusability of MXenes for the degradation of dye contaminants are analyzed and summarized in Table 2. For example, in a regeneration-reusability experiment, Luo's research group [113] used deionized $H_2O$ to wash the photocatalyst (desorption of remaining pollutants) of ZnO/$Ti_3C_2$ MXene that had degraded MB during five consecutive cycles. As presented in Table 2, the MB photocatalytic degradation effectiveness of MXenes declined a little after the 5th regeneration-reusability round. The authors highlighted that this may be due to slight structural deterioration and a decrease in functional groups on the surface of the MXenes [113]. These findings resonate with the conclusion drawn by Yao's team [103]and Zhang's group [85], which reported a minor drop in the degradation effectiveness after several regeneration cycles of spent MXenes. It may be ascribed to the loss of the number of functional groups on the surface of the spent MXenes as a result of reactions occurring during their usage. In such cases, additional regeneration steps should be developed to ensure recovery of photocatalyst properties for long-term applications.

In another stability study [87], expended MXene/Zn-MOF after recovery was regenerated using EtOH and acetone (50:50 *v*/v). It was discovered that the photocatalytic degradation efficiency of the MB pollutant was around 62 % in the 1st round, and there was no slight drop in effectiveness trend until the 5th round [87]. This excellent reusability and stability performance is consistent with that reported for g-$C_3N_4$/$Ti_3C_2$/$TiO_2$ by Diao's research group [179] towards photocatalytic degradation of RhB. The authors concluded that the catalyst amount lowered only minimally, which might be affected by the MXBM cleaning step with EtOH and $H_2O$ during the reusability test.

Vigneshwaran and co-workers also reported regeneration-reusability experiments. In this experiment, $H_2O$ and EtOH were used to achieve desorption of MB degradation by-products from the surface of $Ti_3C_2Tx$@Chitosan@g–$C_3N_4$ and to restore the photocatalytic activity. The regeneration experiment was performed for 5 rounds, and there was no significant drop in the photocatalytic degradation capacity towards MB removal, indicating that $Ti_3C_2Tx$@Chitosan@g–$C_3N_4$ has outstanding stability [130]. This is comparable to the reusability study of Nd-$NiCo_2O_4$/MXene towards the degradation of MG. In this study, the spent Nd-$NiCo_2O_4$/MXene nanocomposites were easily regenerated upon contact with DI $H_2O$ and EtOH. The regenerated Nd-$NiCo_2O_4$/MXene was then subjected to the next round of MG degradation. Notably, the photocatalytic degradation efficiency did not exhibit any significant loss until the third recycle, but a very slight decrease (about 12 %) in the photocatalytic degradation efficiency was found in the fifth cycle, and this was suggested to be due to incomplete desorption. However, the fifth time regenerated spent Nd-$NiCo_2O_4$/MXene still had >80 % photocatalytic degradation efficiency [86].

In another work [175], to assess the practical applicability, the reusability of the porous MXene/SWCNTs film for adsorbing MB was investigated. Using the same material, the adsorption and desorption procedures were carried out five times. The outcome implies that the p-MXene/SWCNTs film in its current state may find application as a stable and reusable electro-sorption film. Washing many times with $H_2O$ and EtOH allowed the MB to desorb. The authors [175] affirmed that, from the theoretical point of view, because of the incomplete desorption of the organic dye or partial oxidation of the film during recycling, the removal effectiveness would gradually decline. On the other hand, MB's degradation effectiveness starts at 95 % and rises to 97.8 % in the third cycle. The intercalation of MB during the electro-sorption process may have been the cause of this event. This might encourage the MXenes to further delaminate, exposing more active sites and functional groups and enhancing the SSA, hence improving the degradation performance of MB. However, the fifth cycle yielded a degradation effectiveness of up to 95.2 %, suggesting that the developed MXene-based film might serve as a cost-effective and recyclable adsorbent for the removal of MB [175]. The above-mentioned reason is consistent with what was suggested by [150] in the recyclability study of MXene/$PbCrO_4$ towards the photocatalytic degradation of MB using DI $H_2O$ and EtOH as the eluent.

Notably, it can be seen from the regenerability and reusability data collected in Table 2 that the least number of times that MXene can be reused was 3, the highest number of times was 8, the average MXene pollutant degradation efficiency after n-th round of application is >70 %, and different eluents/regeneration agents that have been explored for regeneration of the MXene photocatalyst and desorbing dye pollutants from expended MXene include EtOH, and deionized/distilled $H_2O$.

It is worth highlighting that real-case scenario applications would demand a 1–4 year constant stability over continuous operation of the catalyst, which still is not confirmed for MXene-based materials.

## 14. Challenges and areas for future work

The review has identified main strategies for enhancing the photocatalytic effectiveness of MXBM for dye pollutant degradation in aqueous conditions. Notably, MXBM has proven to offer several advantages and become a real game-changer in environmental remediation. Nevertheless, based on the review of the literature, some problematic issues must be resolved before its pilot-scale implementation. The following are some of these issues and possible improvements that would be necessary to promote MXBM applicability in the research area, especially in the context of dye pollutant degradation.

Firstly, much of the research that is currently accessible on MXBM for dye pollutant photocatalytic degradation is conducted on a laboratory scale for model pollutant solutions. As a result, it is recommended that attempts on the industrial scale application level be considered in future studies. Secondly, the safe disposal of spent MXBM even after multiple reusability is another up-to-date topic that is worth looking into because the spent MXBM will still retain traces of dyes along with their degradation products and thus might still be potentially harmful. The presence of adsorbed degradation by-products also poses risks for the environment. Therefore, it is important to develop a method for the management of the spent MXBM.

Secondly, to significantly reduce MXenes' stability disadvantage, especially under humid and oxidative conditions, which is key for long-term potential use as well as pilot-scale implementation, we suggest that future researchers should look into surface modification or coating MXene with stabilizing materials like biopolymers, as this can create protective layers that inhibit oxidation and structural degradation. Additionally, elemental doping with N or Fe, and constructing heterostructures with stable semiconductors like g-$C_3N_4$ can reinforce the MXene lattice, boost the stability, and modulate its band structure, thus enhancing durability as well as photocatalytic efficiency.

Thirdly, in the future, researchers may examine the circular economy potential of spent MXBM, as they may be recycled as raw materials for supercapacitors. Moreover, it is essential to perform a thorough life cycle analysis and ecotoxicological evaluation of MXBM [180].

Also, the relationship between the MXene structure and its photocatalytic activity can take many different forms, and many of the underlying processes are still unknown. Its photocatalytic properties and electrical activity, for instance, will also be influenced by surface alteration and quantum dot doping. There hasn't been much related study done yet on these aspects. Moreover, computational and density functional theory simulation studies can also be employed to predict the photocatalytic degradation mechanism of dye pollutants. Therefore,

**Table 3**
MXenes vs other common materials with respect to toxicity, cost-effectiveness, and sustainability as gathered from open literature [185–189].

| Characteristics | MXenes | Graphene | Carbon nanotubes | Metal and metal oxide nanomaterial | Activated carbon |
|---|---|---|---|---|---|
| Toxicity | Moderate to low; depends on surface termination and metal core. In particular, MXenes produced using the HF etching method are considered to have a toxic effect because of HF involvement. However, there are now better synthesis methods with low toxicity been developed | Generally low; however, reduced graphene oxide can exhibit longer toxicity because of oxidative stress | Moderate; long carbon nanotubes may cause lung toxicity | Low to moderate; e.g., ZnO, $TiO_2$ may induce oxidative stress, phototoxicity, and genotoxicity. Moreover, heavy metal leaching is still a problem | Low; generally considered safe and non-toxic. Although, depending on the source |
| Cost-effectiveness | Moderate. Although still perceived as expensive, depending on the synthesis method. For example, the CVD method is considered costly | Moderate to high; depends on type. For instance, CVD graphene and graphene oxides are somewhat expensive | High production is complex and energy-intensive | Moderate; bulk synthesis is cheap and scalable | Moderate to high; Those made from biomass waste widely available are considered cheaper |
| Sustainability | Medium; relies on MAX phase precursors and HF or safer alternatives | Medium; synthetic routes use chemicals and high energy | Low; petroleum-based, difficult to recycle | Medium to high; depending on source and lifecycle | High; derived from renewable sources, recyclable |

MXBM photocatalytic study in the future should include computational chemistry approaches. Also, future research projects can further explore the possibility of combining MXBM with different adsorbents of semiconductors. We believe this can deliver better degradation performance synergistically. We also identify a need for more studies on the effect of temperature and ionic species as part of technical operating parameters. On the other hand, each study on the application of MXBM for environmental remediation should include aspects of metal leaching into the treated environment.

Right now, large-scale production strategies are still far from ideal. Producing MXene in large amounts that are both of constant size and good quality will become essential in the coming years. Also, the use of hybrid technology like tribo-photocatalytic degradation can enhance the generation of radicals, which can, in turn, improve dye degradation and thus should be explored in the future. In addition, future researchers should look into the financial analysis aspect of this subject, from the production of MXBM to their usage in pollution remediation, as this is a crucial topic for engineers, investors, industries, and other stakeholders. Notably, for many materials, a size-dependent toxicity was found. Particles at nano- or sub-nano-scale can show higher toxicity compared to micro-scale particles of the same material [181–184]. The same studies on size-dependent toxicity should be performed in the future on different types of photocatalytic MXene-based materials. Finally, as summarized in Table 3, future research work will need to take note of the comparison of MXenes with other commonly used materials in terms of toxicity, cost-effectiveness, and sustainability for scalability advancement.

## 15. Conclusion

This review has critically explored the recent innovations and advances in the application of MXene-based materials (MXBM) for photocatalytic degradation of dye pollutants in wastewater and the experimentally confirmed effect of process parameters. A key innovation is the evaluation of photocatalytic degradation performance of MXenes integrated with other functional materials, resulting in hybrid materials with improved surface activity, efficient charge separation, and reduced recombination of electron-hole pairs. These properties significantly enhance photocatalytic efficiency, reusability, and ability to work under various operating conditions, crucial for sustainable water remediation. The findings show that MXBM typically achieves degradation efficiencies greater than 90 % within a treatment time of 60–80 min under optimal operating conditions of 10–100 mg/L photocatalyst dose and solution pH 2–7.5. The major reactive species in the photocatalytic reaction of MXBM were hydroxyl radicals ($^{\bullet}OH$) and superoxide radical anions ($^{\bullet}O_2^-$), which are accountable for the degradation of the dye contaminants. The reusability of the materials is an important advantage of MXBM, as it can be reused up to 3–8 cycles while still maintaining degradation efficiency of >75 %, demonstrating both environmental friendliness and practical applicability. In conclusion, MXene-based photocatalysts represent a transformative class of emerging materials in photocatalytic water treatment, combining efficiency, tunability, and reusability. However, to fast-track their practical applications like for other existing materials that have been reviewed, future research should focus on intermediate products (by-products) formation, long-term toxicity assessments, cost analysis, sustainable scale-up strategies under real-case scenario conditions, and perform studies on particle size-dependent toxicity of different types of photocatalytic MXene-based materials. Bridging these gaps will help translate MXene from a promising laboratory remediation system to an impactful environmental material.

A still overlooked potential of MXBMs relates to their application in Advanced Reduction Processes (ARPs). Due to utilisation of hydrated electrons in specific conditions MXBMs could find applicability also in ARPs, which provide high effectiveness towards pollutants persistent to degradation via AOPs. Future research should include experiments in anoxic conditions (to favour hydrated electron driven reduction reactions), activation of reductants like sulphite or dithionate. MXBNs containing metals having affinity to hydrogen ($H_2$), could catalyse reduction reactions by molecular hydrogen as well as hydrogen radical.

## CRediT authorship contribution statement

**Stephen Sunday Emmanuel:** Writing – review & editing, Writing – original draft, Project administration, Conceptualization. **Ademidun Adeola Adesibikan:** Writing – original draft, Visualization, Data curation. **Shepherd M. Tichapondwa:** Writing – original draft, Visualization, Data curation. **Manoj P. Rayaroth:** Writing – review & editing, Validation. **Francisco Bosca:** Writing – review & editing, Writing – original draft, Validation. **Maria Luisa Marin:** Writing – review & editing. **Bakhtiar Ali Samejo:** Writing – review & editing, Writing – original draft, Visualization. **Grzegorz Boczkaj:** Writing – review & editing, Writing – original draft, Validation, Supervision, Project administration, Conceptualization.

## Declaration of competing interest

The authors declare that they have no known competing financial interests or personal relationships that could have appeared to influence the work reported in this paper.

## Acknowledgements

The authors gratefully acknowledge financial support from the National Science Centre, Warsaw, Poland for project OPUS nr UMO-2021/41/B/ST8/01575. Emmannuel S. S. appreciates the University of Pretoria doctoral scholarship body.

## Data availability

No primary research results, software, or code have been included, and no new data were generated or analyzed as part of this review.

## References

[1] A.V. Mohod, M. Momotko, N.S. Shah, M. Marchel, M. Imran, L. Kong, G. Boczkaj, Degradation of rhodamine dyes by advanced oxidation processes (AOPs)–focus on caviatation and photocatalysis-a critical review, Water Resour. Ind. 30 (2023) 100220, https://doi.org/10.1016/j.wri.2023.100220.

[2] F. Sagita, C.L. Radiman, M. Ledyastuti, M. Khalil, G.T.M. Kadja, Salt-modified MXene membrane for ultrafast and efficient cationic and anionic dyes removal, J Water Process Eng 49 (2022) 103133, https://doi.org/10.1016/j.jwpe.2022.103133.

[3] S. Dutta, S. Adhikary, S. Bhattacharya, D. Roy, S. Chatterjee, A. Chakraborty, D. Banerjee, A. Ganguly, S. Nanda, P. Rajak, Contamination of textile dyes in aquatic environment: adverse impacts on aquatic ecosystem and human health, and its management using bioremediation, J. Environ. Manag. 353 (2024) 120103, https://doi.org/10.1016/j.jenvman.2024.120103.

[4] R.A. Akboura, J. El Gaaydaa, F.E. Titchoua, A. Khenifib, H. Afangaa, A. Farahic, P.-S. Yapd, M.B.S. Fortee, M. Hamdania, Adsorption of anionic dyes from aqueous solution using polyelectrolyte PDAD-PDADMAC-modified-montmorillonite clay, Desalin. Water Treat. 208 (2020) 407–422, https://doi.org/10.5004/dwt.2020.26446.

[5] P. Najibikhah, H. Shayesteh, A. Rahbar-Kelishami, Two-dimensional Ti3C2Tx MXene/MOF composite for enhanced methylene blue adsorption, J. Mol. Liq. 127627 (2025), https://doi.org/10.1016/j.molliq.2025.127627.

[6] N. Damayanti, D. Prasetyoko, S. Suprapto, R. Tamim, R. Subagyo, L. Kusnawati, N. Asikin-Mijan, R. Yusop, H. Holilah, A.A. Jalil, Pluronic P123 modified MXene as an efficient adsorbent for aqueous dye Removal: Optimization using CCD-RSM, J. Ind. Eng. Chem. (2025), https://doi.org/10.1016/j.jiec.2025.07.022 in press.

[7] F.E. Titchou, H. Afanga, H. Zazou, R.A. Akbour, M. Hamdani, Batch elimination of cationic dye from aqueous solution by electrocoagulation process, Mediterr. J. Chem. 10 (2020) 1–12, https://doi.org/10.13171/mjc10102001201163mh.

[8] K. Saravanakumar, S. De Silva, S.S. Santosh, A. Sathiyaseelan, A. Ganeshalingam, M. Jamla, A. Sankaranarayanan, V.P. Veeraraghavan, D. MubarakAli, J. Lee, Impact of industrial effluents on the environment and human health and their remediation using MOFs-based hybrid membrane filtration techniques, Chemosphere 307 (2022) 135593, https://doi.org/10.1016/j.chemosphere.2022.135593.

[9] C. Xing, L. Liu, X. Guo, M. Zhang, M. Zhou, S. Zhang, C. Liu, Efficient water purification using stabilized MXene nanofiltration membrane with controlled interlayer spacings, Sep. Purif. Technol. 317 (2023) 123774, https://doi.org/10.1016/j.seppur.2023.123774.

[10] S. Singh, V.C. Srivastava, I.D. Mall, Mechanism of dye degradation during electrochemical treatment, J. Phys. Chem. C 117 (2013) 15229–15240, https://doi.org/10.1021/jp405289f.

[11] Y.A. Bustos-Terrones, J.J. Hermosillo-Nevárez, B. Ramírez-Pereda, M. Vaca, J. G. Rangel-Peraza, V. Bustos-Terrones, M.N. Rojas-Valencia, Removal of BB9 textile dye by biological, physical, chemical, and electrochemical treatments, J. Taiwan Inst. Chem. Eng. 121 (2021) 29–37, https://doi.org/10.1016/j.jtice.2021.03.041.

[12] S.S. Emmanuel, A.A. Adesibikan, O.D. Saliu, Phytogenically bioengineered metal nanoarchitecture for degradation of refractory dye water pollutants: a pragmatic minireview, Appl. Organomet. Chem. 37 (2023) e6946, https://doi.org/10.1016/j.molliq.2021.115468.

[13] S.S. Emmanuel, A.A. Adesibikan, C. Olusola Olawoyin, A.A. Bayode, A review of Antithrombolytic, anticoagulant, and antiplatelet activities of biosynthesized metallic nanostructured multifunctional materials, ChemistrySelect 8 (2023) e202302712, https://doi.org/10.1002/slct.202302712.

[14] M.P. Rayaroth, M. Marchel, G. Boczkaj, Advanced oxidation processes for the removal of mono and polycyclic aromatic hydrocarbons–a review, Sci. Total Environ. 857 (2023) 159043, https://doi.org/10.1016/j.scitotenv.2022.159043.

[15] L. Wang, D. Luo, O. Hamdaoui, Y. Vasseghian, M. Momotko, G. Boczkaj, G. Z. Kyzas, C. Wang, Bibliometric analysis and literature review of ultrasound-assisted degradation of organic pollutants, Sci. Total Environ. 876 (2023) 162551, https://doi.org/10.1016/j.scitotenv.2023.162551.

[16] B.A. Samejo, M.P. Rayaroth, C. Wang, X. Sun, G. Boczkaj, Hydrated electrons and other reductive species - properties, formation and applications in advanced reduction processes for degradation of emerging organic pollutants – a review, Water Resour. Ind. (2025) 100311, https://doi.org/10.1016/j.wri.2025.100311.

[17] A. Fernandes, M. Gągol, P. Makoś, J.A. Khan, G. Boczkaj, Integrated photocatalytic advanced oxidation system (TiO2/UV/O3/H2O2) for degradation of volatile organic compounds, Sep. Purif. Technol. 224 (2019) 1–14, https://doi.org/10.1016/j.seppur.2019.05.012.

[18] Y. Li, C. Gao, R. Long, Y. Xiong, Photocatalyst design based on two-dimensional materials, Mater. Today Chem. 11 (2019) 197–216, https://doi.org/10.1016/j.mtchem.2018.11.002.

[19] B. Luo, G. Liu, L. Wang, Recent advances in 2D materials for photocatalysis, Nanoscale 8 (2016) 6904–6920, https://doi.org/10.1039/C6NR00546B.

[20] Y. Gogotsi, Q. Huang, MXenes: two-dimensional building blocks for future materials and devices, ACS Nano 15 (2021) 5775–5780, https://doi.org/10.1021/acsnano.1c03161.

[21] B. Wang, S. Zhong, P. Xu, H. Zhang, Booming development and present advances of two dimensional MXenes for photodetectors, Chem. Eng. J. 403 (2021) 126336, https://doi.org/10.1016/j.cej.2020.126336.

[22] Q. Zhong, J. Liu, Z. Wang, J.B. Ghasemi, G. Zhang, Ti3C2 MXene/Ag2ZnGeO4 Schottky heterojunctions with enhanced photocatalytic performances: efficient charge separation and mechanism studies, Sep. Purif. Technol. 278 (2021) 119560, https://doi.org/10.1016/j.seppur.2021.119560.

[23] Z. Guo, L. Gao, Z. Xu, S. Teo, C. Zhang, Y. Kamata, S. Hayase, T. Ma, High electrical conductivity 2D MXene serves as additive of perovskite for efficient solar cells, Small 14 (2018) 1802738, https://doi.org/10.1002/smll.201802738.

[24] S. Lyu, H. Chang, L. Zhang, S. Wang, S. Li, Y. Lu, S. Li, High specific surface area MXene/SWCNT/cellulose nanofiber aerogel film as an electrode for flexible supercapacitors, Compos. Part B Eng. 264 (2023) 110888, https://doi.org/10.1016/j.compositesb.2023.110888.

[25] T.R. Dmytriv, V.I. Lushchak, Potential biosafety of Mxenes: stability, biodegradability, toxicity and biocompatibility, Chem. Rec. 24 (2024) e202300338, https://doi.org/10.1002/tcr.202300338.

[26] A. Sudhaik, P. Raizada, T. Ahamad, S.M. Alshehri, V.-H. Nguyen, Q. Van Le, S. Thakur, V.K. Thakur, R. Selvasembian, P. Singh, Recent advances in cellulose supported photocatalysis for pollutant mitigation: A review, Int. J. Biol. Macromol.226 (2022) 1284, https://doi.org/10.1016/j.ijbiomac.2022.11.241.

[27] F.A. Janjhi, I. Ihsanullah, M. Bilal, R. Castro-Muñoz, G. Boczkaj, F. Gallucci, MXene-based materials for removal of antibiotics and heavy metals from wastewater–a review, Water Resour. Ind. 29 (2023) 100202, https://doi.org/10.1016/j.wri.2023.100202.

[28] M. Bilal, A.K. Singh, H.M.N. Iqbal, G. Boczkaj, Enzyme-conjugated MXene nanocomposites for biosensing and biocatalysis acuities, Chem. Eng. J. 145020 (2023), https://doi.org/10.1016/j.cej.2023.145020.

[29] C. Illahi, W.E.F. Hutabarat, N. Nurdini, F. Failamani, G.T.M. Kadja, Photocatalytic degradation of azo dyes over MXene-based catalyst: recent developments and future prospects, Next Nanotechnol. 6 (2024) 100055, https://doi.org/10.1016/j.nxnano.2024.100055.

[30] S. Mathew, M. Ramachandra, S. Devi, D. Pinheiro, S. Manickam, C.H. Pang, S. H. Sonawane, Synthesis, mechanisms, challenges, and future prospects of Ti3C2 MXene and its heterojunctions for photocatalytic dye degradation efficiency: a comprehensive review, Mater Today Sustain 24 (2023) 100568, https://doi.org/10.1016/j.mtsust.2023.100568.

[31] T.R. Seling, M. Songsart-Power, A.K. Shringi, J. Paudyal, F. Yan, T.B. Limbu, Ti3C2Tx MXene-based hybrid photocatalysts in organic dye degradation: a review, Molecules 30 (2025), https://doi.org/10.3390/molecules30071463.

[32] G.S. Gopika, P.M.H. Prasad, A.G. Lekshmi, S. Lekshmypriya, S. Sreesaila, C. Arunima, M.S. Kumar, A. Anil, A. Sreekumar, Z.S. Pillai, Chemistry of cyanine dyes-a review, Mater Today Proc 46 (2021) 3102–3108, https://doi.org/10.1016/j.matpr.2021.02.622.

[33] N. Chandel, B.B. Singh, C. Dureja, Y.-H. Yang, S.K. Bhatia, Indigo production goes green: a review on opportunities and challenges of fermentative production, World J. Microbiol. Biotechnol. 40 (2024) 62, https://doi.org/10.1007/s11274-023-03871-2.

[34] A. Ayele, D. Getachew, M. Kamaraj, A. Suresh, Phycoremediation of synthetic dyes: an effective and eco-friendly algal technology for the dye abatement, J. Chemother. 2021 (2021), https://doi.org/10.1155/2021/9923643.

[35] S. Velusamy, A. Roy, S. Sundaram, T. Kumar Mallick, A review on heavy metal ions and containing dyes removal through graphene oxide-based adsorption strategies for textile wastewater treatment, Chem. Rec. 21 (2021) 1570–1610, https://doi.org/10.1002/tcr.202000153.

[36] A.P. Periyasamy, Textile dyes in wastewater and its impact on human and environment: focus on bioremediation, Water Air Soil Pollut. 236 (2025) 562, https://doi.org/10.1007/s11270-025-08204-7.

[37] R. Al-Tohamy, S.S. Ali, F. Li, K.M. Okasha, Y.A.-G. Mahmoud, T. Elsamahy, H. Jiao, Y. Fu, J. Sun, A critical review on the treatment of dye-containing wastewater: Ecotoxicological and health concerns of textile dyes and possible remediation approaches for environmental safety, Ecotoxicol. Environ. Saf. 231 (2022) 113160, https://doi.org/10.1016/j.ecoenv.2021.113160.

[38] A. Tkaczyk, K. Mitrowska, A. Posyniak, Synthetic organic dyes as contaminants of the aquatic environment and their implications for ecosystems: a review, Sci. Total Environ. 717 (2020) 137222, https://doi.org/10.1016/j.scitotenv.2020.137222.

[39] K.H. Hama Aziz, N.M. Fatah, K.T. Muhammad, Advancements in application of modified biochar as a green and low-cost adsorbent for wastewater remediation from organic dyes, R, Soc. Open Sci. 11 (2024) 232033, https://doi.org/10.1098/rsos.232033.

[40] J. Lin, W. Ye, M. Xie, D.H. Seo, J. Luo, Y. Wan, B. Van der Bruggen, Environmental impacts and remediation of dye-containing wastewater, Nat. Rev. Earth Environ. 4 (2023) 785–803, https://doi.org/10.1038/s43017-023-00489-8.

[41] P.M. Kapanga, G.W.A. Nyakairu, C.I. Nkanga, S.N. Lusamba, R.M. Tshimanga, Z. Shehu, A review of dye effluents polluting African surface water: sources,

impacts, physicochemical properties, and treatment methods, Discov. Water 4 (2024) 85, https://doi.org/10.1007/s43832-024-00129-2.
[42] Q. Xiang, D. Fan, L. Zhu, T. Zhang, D. Shen, H. Wang, B. Dong, Weighted comprehensive risk assessment and pollution analysis of long-term printing and dyeing sludge landfills in an industrialized Chinese city, Environ. Pollut. 367 (2025) 125665, https://doi.org/10.1016/j.envpol.2025.125665.
[43] H. Arshad, M. Imran, M. Ashraf, Toxic effects of red-S3B dye on soil microbial activities, wheat yield, and their alleviation by pressmud application, Ecotoxicol. Environ. Saf. 204 (2020) 111030, https://doi.org/10.1016/j.ecoenv.2020.111030.
[44] M. Noman, M. Shahid, T. Ahmed, M.B.K. Niazi, S. Hussain, F. Song, I. Manzoor, Use of biogenic copper nanoparticles synthesized from a native Escherichia sp. as photocatalysts for azo dye degradation and treatment of textile effluents, Environ. Pollut. 257 (2020) 113514, https://doi.org/10.1016/j.envpol.2019.113514.
[45] H.M. Munjur, M.N. Hasan, M.R. Awual, M.M. Islam, M.A. Shenashen, J. Iqbal, Biodegradable natural carbohydrate polymeric sustainable adsorbents for efficient toxic dye removal from wastewater, J. Mol. Liq. 319 (2020) 114356, https://doi.org/10.1016/j.molliq.2020.114356.
[46] D. Markandeya, S.P. Mohan, Shukla, hazardous consequences of textile mill effluents on soil and their remediation approaches, Clean. Eng. Technol. 7 (2022) 100434, https://doi.org/10.1016/j.clet.2022.100434.
[47] N.M. Hosny, I. Gomaa, M.G. Elmahgary, Adsorption of polluted dyes from water by transition metal oxides: a review, Appl Surf Sci Adv 15 (2023) 100395, https://doi.org/10.1016/j.apsadv.2023.100395.
[48] T.N. Lotha, V. Sorhie, P. Bharali, L. Jamir, Advancement in sustainable wastewater treatment: a multifaceted approach to textile dye removal through physical, Biol. Chem. Tech. Chem. Sel. 9 (2024) e202304093, https://doi.org/10.1002/slct.202304093.
[49] A.A. Bayode, S.S. Emmanuel, S.O. Sanni, O.A. Olalekan, O.T. Ore, K.D. Terlanga, M.O. Omorogie, Current status and performance evaluation of emerging advanced remediation techniques for the removal of steroidal hormones in water, Environ. Chem. Ecotoxicol. 6 (2024) 315–337, https://doi.org/10.1016/j.enceco.2024.07.006.
[50] P. Kuang, J. Low, B. Cheng, J. Yu, J. Fan, MXene-based photocatalysts, J. Mater. Sci. Technol. 56 (2020) 18–44, https://doi.org/10.1016/j.jmst.2020.02.037.
[51] K. Huang, C. Li, H. Li, G. Ren, L. Wang, W. Wang, X. Meng, Photocatalytic applications of two-dimensional Ti3C2 MXenes: a review, ACS Appl. Nano Mater. 3 (2020) 9581–9603, https://doi.org/10.1021/acsanm.0c02481.
[52] M. Bagheri, R. Ibragimova, H.-P. Komsa, Fermiology of two-dimensional titanium carbide and nitride MXenes, Phys. Rev. B 104 (2021) 35408, https://doi.org/10.1103/PhysRevB.104.035408.
[53] B. Liu, X. Zhang, J. Chu, F. Li, C. Jin, J. Fan, 2D/2D BiOIO3/Ti3C2 MXene nanocomposite with efficient charge separation for degradation of multiple pollutants, Appl. Surf. Sci. 618 (2023) 156565, https://doi.org/10.1016/j.apsusc.2023.156565.
[54] Y. Wu, Y. Zang, L. Xu, J. Wang, H. Jia, F. Miao, Synthesis of functional conjugated microporous polymer/TiO 2 nanocomposites and the mechanism of the photocatalytic degradation of organic pollutants, J. Mater. Sci. 56 (2021) 7936–7950, https://doi.org/10.1007/s10853-021-05790-9.
[55] H. Gu, H. Zhang, X. Wang, Q. Li, S. Chang, Y. Huang, L. Gao, Y. Cui, R. Liu, W.-L. Dai, Robust construction of CdSe nanorods@ Ti3C2 MXene nanosheet for superior photocatalytic H2 evolution, Appl. Catal. B Environ. 328 (2023) 122537, https://doi.org/10.1016/j.apcatb.2023.122537.
[56] S.M. George, B. Kandasubramanian, Advancements in MXene-polymer composites for various biomedical applications, Ceram. Int. 46 (2020) 8522–8535, https://doi.org/10.1016/j.ceramint.2019.12.257.
[57] Q. Liu, X. Tan, S. Wang, F. Ma, H. Znad, Z. Shen, L. Liu, S. Liu, MXene as a non-metal charge mediator in 2D layered CdS@ Ti 3 C 2@ TiO 2 composites with superior Z-scheme visible light-driven photocatalytic activity, Environ. Sci. Nano 6 (2019) 3158–3169, https://doi.org/10.1039/C9EN00567F.
[58] C. Peng, H. Wang, H. Yu, F. Peng, (111) TiO2-x/Ti3C2: synergy of active facets, interfacial charge transfer and Ti3+ doping for enhance photocatalytic activity, Mater. Res. Bull. 89 (2017) 16–25, https://doi.org/10.1016/j.materresbull.2016.12.049.
[59] M.F. Khadidja, J. Fan, S. Li, S. Li, K. Cui, J. Wu, W. Zeng, H. Wei, H.-G. Jin, N. Naik, Hierarchical ZnO/MXene composites and their photocatalytic performances, Colloids Surf. A Physicochem. Eng. Asp. 628 (2021) 127230, https://doi.org/10.1016/j.colsurfa.2021.127230.
[60] W. Zhou, B. Yu, J. Zhu, K. Li, S. Tian, Hierarchical ZnO/MXene (Nb2C and V2C) heterostructure with efficient electron transfer for enhanced photocatalytic activity, Appl. Surf. Sci. 590 (2022) 153095, https://doi.org/10.1016/j.apsusc.2022.153095.
[61] S. Jiao, L. Liu, Friction-induced enhancements for photocatalytic degradation of MoS2@ Ti3C2 nanohybrid, Ind. Eng. Chem. Res. 58 (2019) 18141–18148, https://doi.org/10.1021/acs.iecr.9b03680.
[62] Q. Zhong, Y. Li, G. Zhang, Two-dimensional MXene-based and MXene-derived photocatalysts: recent developments and perspectives, Chem. Eng. J. 409 (2021) 128099, https://doi.org/10.1016/j.cej.2020.128099.
[63] L. Biswal, S. Nayak, K. Parida, Recent progress on strategies for the preparation of 2D/2D MXene/gC 3 N 4 nanocomposites for photocatalytic energy and environmental applications, Catal, Sci. Technol. 11 (2021) 1222–1248, https://doi.org/10.1039/D0CY02156C.
[64] Y. Huang, S. Jiang, R. Liang, P. Sun, Y. Hai, L. Zhang, Thermal-triggered insulating fireproof layers: a novel fire-extinguishing MXene composites coating, Chem. Eng. J. 391 (2020) 123621, https://doi.org/10.1016/j.cej.2019.123621.
[65] Y. Peng, J. Xu, J. Xu, J. Ma, Y. Bai, S. Cao, S. Zhang, H. Pang, Metal-organic framework (MOF) composites as promising materials for energy storage applications, Adv. Colloid Interf. Sci. 307 (2022) 102732, https://doi.org/10.1016/j.cis.2022.102732.
[66] Y.-J. Hsu, A. Nain, Y.-F. Lin, Y.-T. Tseng, Y.-J. Li, A. Sangili, P. Srivastava, H.-L. Yu, Y.-F. Huang, C.-C. Huang, Self-redox reaction driven in situ formation of Cu2O/Ti3C2Tx nanosheets boost the photocatalytic eradication of multi-drug resistant bacteria from infected wound, J. Nanobiotechnol. 20 (2022) 235, https://doi.org/10.1186/s12951-022-01428-3.
[67] M. Ding, C. Han, Y. Yuan, J. Xu, X. Yang, Advances and promises of 2D MXenes as cocatalysts for artificial photosynthesis, Sol. RRL 5 (2021) 2100603, https://doi.org/10.1002/solr.202100603.
[68] V. Soni, P. Singh, H.H.P. Quang, A.A.P. Khan, A. Bajpai, Q. Van Le, V.K. Thakur, S. Thakur, V.-H. Nguyen, P. Raizada, Emerging architecture titanium carbide (Ti3C2Tx) MXene based photocatalyst toward degradation of hazardous pollutants: recent progress and perspectives, Chemosphere 293 (2022) 133541, https://doi.org/10.1016/j.chemosphere.2022.133541.
[69] W. Liu, M. Zhou, H. Fu, Design of Ag@ ZnO@ Ti3C2 MXene heterojunction photocatalyst for enhanced photocatalytic degradation activity of methylene blue and levofloxacin under visible light irradiation, J. Environ. Chem. Eng. 11 (2023) 110926, https://doi.org/10.1016/j.jece.2023.110926.
[70] Y. Wu, G. Feng, R. Huang, B. Liang, T. Gan, H. Hu, Y. Zhang, Z. Feng, Z. Huang, Simultaneous growth strategy for constructing a Cu–Fe/carboxylate-decorated carbon composite with improved interface compatibility and charge transfer to boost the visible photocatalytic degradation of tetracycline, Chem. Eng. J. 448 (2022) 137608, https://doi.org/10.1016/j.cej.2022.137608.
[71] N. Li, J. Ma, Y. Zhang, L. Zhang, T. Jiao, Recent developments in functional nanocomposite photocatalysts for wastewater treatment: a review, Adv. Sustain. Syst. 6 (2022) 2200106, https://doi.org/10.1002/adsu.202200106.
[72] X. Liu, T. Chen, Y. Xue, J. Fan, S. Shen, M.S.A. Hossain, M.A. Amin, L. Pan, X. Xu, Y. Yamauchi, Nanoarchitectonics of MXene/semiconductor heterojunctions toward artificial photosynthesis via photocatalytic CO2 reduction, Coord. Chem. Rev. 459 (2022) 214440, https://doi.org/10.1016/j.ccr.2022.214440.
[73] S. Yang, J. Yin, Q. Li, C. Wang, D. Hua, N. Wu, Covalent organic frameworks functionalized electrodes for simultaneous removal of UO22+ and ReO4-with fast kinetics and high capacities by electro-adsorption, J. Hazard. Mater. 429 (2022) 128315, https://doi.org/10.1016/j.jhazmat.2022.128315.
[74] Z. Jiang, X. Zhang, S. Guo, Y. Zheng, J. Wang, T. Wen, X. Wang, Recent advances and perspectives of emerging two-dimensional transition metal carbide/nitride-based materials for organic pollutant photocatalysis, Mater. Chem. Front. 7 (2023) 4658, https://doi.org/10.1039/D3QM00288H.
[75] S. Suragtkhuu, S. Sunderiya, S. Purevdorj, M. Bat-Erdene, B. Sainbileg, M. Hayashi, A.S.R. Bati, J.G. Shapter, S. Davaasambuu, M. Batmunkh, Rhenium anchored Ti 3 C 2 T x (MXene) nanosheets for electrocatalytic hydrogen production, Nanoscale Adv. 5 (2023) 349–355, https://doi.org/10.1039/D2NA00782G.
[76] N.H. Solangi, R.R. Karri, S.A. Mazari, N.M. Mubarak, A.S. Jatoi, G. Malafaia, A. K. Azad, MXene as emerging material for photocatalytic degradation of environmental pollutants, Coord. Chem. Rev. 477 (2023) 214965, https://doi.org/10.1016/j.ccr.2022.214965.
[77] S.S. Emmanuel, A.O. Esan, F.S.O. Afigo, A.A. Adesibikan, M.O. Idris, A review on eco-sustainable photocatalytic degradation of pharmaceutical pollutants using biosynthesized nanoparticles, J. Chin. Chem. Soc. 71 (2024) 1332–1357, https://doi.org/10.1002/jccs.202400250.
[78] Y. Lv, K. Wang, D. Li, P. Li, X. Chen, W. Han, Rare ag nanoparticles loading induced surface-enhanced pollutant adsorption and photocatalytic degradation on Ti3C2Tx MXene-based nanosheets, Chem. Phys. 560 (2022) 111591, https://doi.org/10.1016/j.chemphys.2022.111591.
[79] S.S. Emmanuel, A.A. Adesibikan, E.A. Opatola, C.O. Olawoyin, A pragmatic review on photocatalytic degradation of methyl orange dye pollutant using greenly biofunctionalized nanometallic materials: a focus on aquatic body, Appl. Organomet. Chem. 3 (2023) e7108, https://doi.org/10.1002/aoc.7108.
[80] T. Cai, L. Wang, Y. Liu, S. Zhang, W. Dong, H. Chen, X. Yi, J. Yuan, X. Xia, C. Liu, S. Luo, Ag3PO4/Ti3C2 MXene interface materials as a Schottky catalyst with enhanced photocatalytic activities and anti-photocorrosion performance, Appl. Catal. B Environ. 239 (2018) 545–554, https://doi.org/10.1016/j.apcatb.2018.08.053.
[81] L. Chen, X. Ye, S. Chen, L. Ma, Z. Wang, Q. Wang, N. Hua, X. Xiao, S. Cai, X. Liu, Ti3C2 MXene nanosheet/TiO2 composites for efficient visible light photocatalytic activity, Ceram. Int. 46 (2020) 25895–25904, https://doi.org/10.1016/j.ceramint.2020.07.074.
[82] V.T. Quyen, L.T.T. Ha, D.M. Thanh, Q. Van Le, N.M. Viet, N.T. Nham, P.Q. Thang, Advanced synthesis of MXene-derived nanoflower-shaped TiO2@Ti3C2 heterojunction to enhance photocatalytic degradation of rhodamine B, Environ. Technol. Innov. 21 (2021) 101286, https://doi.org/10.1016/j.eti.2020.101286.
[83] J. Qu, D. Teng, X. Zhang, Q. Yang, P. Li, Y. Cao, Preparation and regulation of two-dimensional Ti3C2Tx MXene for enhanced adsorption–photocatalytic degradation of organic dyes in wastewater, Ceram. Int. 48 (2022) 14451–14459, https://doi.org/10.1016/j.ceramint.2022.01.338.
[84] Z. Othman, A. Sinopoli, H.R. Mackey, K.A. Mahmoud, Efficient photocatalytic degradation of organic dyes by AgNPs/TiO2/Ti3C2Tx MXene composites under UV and solar light, ACS Omega 6 (2021) 33325–33338, https://doi.org/10.1021/acsomega.1c03189.
[85] S. Zhang, M. Cai, J. Wu, Z. Wang, X. Lu, K. Li, J.-M. Lee, Y. Min, Photocatalytic degradation of TiO2 via incorporating Ti3C2 MXene for methylene blue removal

from water, Catal. Commun. 174 (2023) 106594, https://doi.org/10.1016/j.catcom.2022.106594.
[86] K. MohammedSaleh Katubi, A. Rasheed, A. Ihsan, B. Shaheen, Z.A. Alrowaili, M. S. Al-Buriahi, M.I. Din, I. Shakir, S. Munir, Neodymium-doped nickel cobaltite reinforced with 2D MXene nanocomposite (Nd-NiCo2O4/MXene) for enhanced photocatalytic degradation of the organic pollutants, Opt. Mater. (Amst.) 152 (2024) 115390, https://doi.org/10.1016/j.optmat.2024.115390.
[87] H. Shahriyari Far, M. Najafi, M. Hasanzadeh, R. Rahimi, Synthesis of MXene/metal-organic framework (MXOF) composite as an efficient photocatalyst for dye contaminant degradation, Inorg. Chem. Commun. 152 (2023) 110680, https://doi.org/10.1016/j.inoche.2023.110680.
[88] M.A. Iqbal, A. Tariq, A. Zaheer, S. Gul, S.I. Ali, M.Z. Iqbal, D. Akinwande, S. Rizwan, Ti3C2-MXene/bismuth ferrite Nanohybrids for efficient degradation of organic dyes and colorless pollutants, ACS Omega 4 (2019) 20530–20539, https://doi.org/10.1021/acsomega.9b02359.
[89] D. Bury, M. Jakubczak, M.A.K. Purbayanto, A. Wojciechowska, D. Moszczyńska, A.M. Jastrzębska, Photocatalytic activity of the oxidation stabilized Ti3C2Tx MXene in decomposing methylene blue, bromocresol green and commercial textile dye, Small Methods 7 (2023) 2201252, https://doi.org/10.1002/smtd.202201252.
[90] F. Ashamary, P.C. Neba, S. Harivarsha, A. Raji, P. Annamalai, M.G. Mohamed, P. Kalambate, P. Muthirulan, S.-W. Kuo, D. Manoj, In situ synthesis of 3D ZIF-8 on 2D MXene nanosheets for efficient photocatalytic degradation of methylene blue (MB), Mater. Adv. 6 (2025) 4660, https://doi.org/10.1039/D5MA00340G.
[91] Q. Zhang, X. Ma, L. Zhang, H. Wang, Y. Chen, L. Fu, J. Zhou, Z. Xing, J. Xia, Dual-function reusable SERS substrate based on Ag/Ag3PO4/MXene heterojunction: efficient detection and photocatalytic degradation of organic pollutants, J. Colloid Interface Sci. 685 (2025) 826–842, https://doi.org/10.1016/j.jcis.2025.01.160.
[92] H.T. Mathew, K. Greeshma, K. Abhisek, S.S. Vhatkar, K.M. Nissamudeen, R. Oraon, Expeditious photocatalytic degradation of methylene blue using ZnO decorated Ti3C2Tx matrix, Ionics (Kiel) (2025) 1–14, https://doi.org/10.1007/s11581-025-06389-9.
[93] D. Vasvini Mary, S. Rubesh Ashok Kumar, G.A. Suganya Josephine, An efficient rare earth metal oxide-supported MXene/g-C3N4 photocatalyst for removing organic dye from wastewater, J. Indian Chem. Soc. 102 (2025) 101750, https://doi.org/10.1016/j.jics.2025.101750.
[94] S. Tul Shafa, M.A. Habila, I. Shakir, M.F. Warsi, A. Irshad, M. Imran, Enhanced photocatalytic activity of copper, terbium co-doped magnesium ferrite@ MXene for degradation of organic compounds, J. Inorg. Organomet. Polym. Mater. (2025) 1–18, https://doi.org/10.1007/s10904-025-03600-2.
[95] M.M. Zahedi, S.K. Samarin, S.D. Abkenar, A.B. Pebdeni, M. Hosseini, S. Kalikeri, H. Karimi-Maleh, Efficient visible light-driven Photodegradation of malachite green dye using carbon quantum dots-MXene nanocomposite: synthesis, characterization, and performance evaluation, J. Taiwan Inst. Chem. Eng. 166 (2025) 105521, https://doi.org/10.1016/j.jtice.2024.105521.
[96] T.J. Jenila, P.A. Vinosha, B. Xavier, A. Dinesh, R.P. Patil, L. Gnanasekaran, M. Ayyar, Y. Slimani, M.A. Almessiere, A. Baykal, M. Iqbal, Exploring the synergistic photocatalytic performance and optical properties of NiMoO4 decorated Ti3C2Tx (NiMoO4/MXene) nanocomposite via hydrothermal technique, Inorg. Chem. Commun. 172 (2025) 113679, https://doi.org/10.1016/j.inoche.2024.113679.
[97] K.M. Katubi, S. Siddique, T.R. Aldhafeeri, Z.A. Alrowaili, M.S. Al-Buriahi, I. Shakir, A. Irshad, M.F. Warsi, Vanadium doped copper oxide and its composite with MXene for effective degradation of organic pollutants, J. Alloys Compd. 1026 (2025) 180431, https://doi.org/10.1016/j.jallcom.2025.180431.
[98] N. Saafie, S. Sufian, N. Mufti, M.F.R. Samsudin, The role of g-C3N4 loadings in MXene for photocatalytic degradation of methylene blue, J. Mater. Sci. Mater. Electron. 36 (2025) 1–15, https://doi.org/10.1007/s10854-025-14395-w.
[99] Z. Asghar, H. Habib, M. Bilal, Z.U. Rehman, F.K. Butt, K. Zheng, Y. Liu, H. Lin, Y. Zhang, X. Wang, J. Hou, Enhancing electron-hole pair generation by Ti3C2 MXene-derived TiO2 integrated with g-C3N4 heterojunction for excellent photocatalytic H2 production and CO2 reduction, Int. J. Hydrog. Energy 149 (2025) 150052, https://doi.org/10.1016/j.ijhydene.2025.150052.
[100] S. Mutahir, M.A. Khan, W. Liu, R. Butt, M. Humayun, L. Meng, I. Shaheen, Engineering a dual Z-scheme copper oxide/boron carbon nitride/MXene heterojunction with tailored band alignment for high-efficiency photocatalytic degradation of refractory organic pollutants, J. Colloid Interface Sci. 691 (2025) 137442, https://doi.org/10.1016/j.jcis.2025.137442.
[101] Y. Verma, M. Naushad, A. García-Peñas, A. Kumar, P. Dhiman, G. Sharma, Exploring the potential of MnWO4/MXene/carbon xerogel photocatalyst for photo efficient degradation of crystal violet, Chem. Eng. Res. Des. 219 (2025) 235–248, https://doi.org/10.1016/j.cherd.2025.05.053.
[102] S. Jangra, A. Raza, B. Kumar, J. Sharma, S. Das, K. Pandey, Y.K. Mishra, M. S. Goyat, MXene decorated ZnO-tetrapod for efficient degradation of methyl orange, methylene blue, and rhodamine B dyes, Mater. Sci. Eng. B 311 (2025) 117832, https://doi.org/10.1016/j.mseb.2024.117832.
[103] W. Zhou, L. Sun, S. Xiang, S. Tian, Enhanced photocatalytic degradation of organic dyes by dual heterojunction of ZnO/NiWO4/V2C MXene, Appl. Surf. Sci. 679 (2025) 161260, https://doi.org/10.1016/j.apsusc.2024.161260.
[104] M.S.I. Nasri, M.F.R. Samsudin, A.A. Tahir, S. Sufian, Effect of MXene loaded on g-C3N4 photocatalyst for the photocatalytic degradation of methylene blue, Energies 15 (2022) 955, https://doi.org/10.3390/en15030955.
[105] M.A. Iqbal, S.I. Ali, F. Amin, A. Tariq, M.Z. Iqbal, S. Rizwan, La- and Mn-codoped bismuth ferrite/Ti3C2 MXene composites for efficient photocatalytic degradation of Congo red dye, ACS Omega 4 (2019) 8661–8668, https://doi.org/10.1021/acsomega.9b00493.
[106] H. Zhang, M. Li, C. Zhu, Q. Tang, P. Kang, J. Cao, Preparation of magnetic α-Fe2O3/ZnFe2O4@ Ti3C2 MXene with excellent photocatalytic performance, Ceram. Int. 46 (2020) 81–88, https://doi.org/10.1016/j.ceramint.2019.08.236.
[107] V.Q. Hieu, T.K. Phung, T.-Q. Nguyen, A. Khan, V.D. Doan, V.A. Tran, V.T. Le, Photocatalytic degradation of methyl orange dye by Ti3C2–TiO2 heterojunction under solar light, Chemosphere 276 (2021) 130154, https://doi.org/10.1016/j.chemosphere.2021.130154.
[108] J. Chen, H. Zheng, Y. Zhao, M. Que, W. Wang, X. Lei, Morphology and photocatalytic activity of TiO2/MXene composites by in-situ solvothermal method, Ceram. Int. 46 (2020) 20088–20096, https://doi.org/10.1016/j.ceramint.2020.05.083.
[109] M. Faheem, A. Riaz, M. Alam, F. Wahad, M. Sohail, M. Altaf, S.M. Abbas, 2D nanostructured MXene-based silver nanoparticles for photocatalytic degradation of safranin dye, Catalysts 14 (2024), https://doi.org/10.3390/catal14030201.
[110] C. Peng, X. Yang, Y. Li, H. Yu, H. Wang, F. Peng, Hybrids of two-dimensional Ti3C2 and TiO2 exposing {001} facets toward enhanced photocatalytic activity, ACS Appl. Mater. Interfaces 8 (2016) 6051–6060, https://doi.org/10.1021/acsami.5b11973.
[111] J. Chen, H. Zheng, Y. Zhao, M. Que, X. Lei, K. Zhang, Y. Luo, Preparation of facet exposed TiO2/Ti3C2Tx composites with enhanced photocatalytic activity, J. Phys. Chem. Solids 145 (2020) 109565, https://doi.org/10.1016/j.jpcs.2020.109565.
[112] R. Long, Z. Yu, Q. Tan, X. Feng, X. Zhu, X. Li, P. Wang, Ti3C2 MXene/NH2-MIL-88B(Fe): research on the adsorption kinetics and photocatalytic performance of an efficient integrated photocatalytic adsorbent, Appl. Surf. Sci. 570 (2021) 151244, https://doi.org/10.1016/j.apsusc.2021.151244.
[113] Q. Luo, Y. Wu, J. Chen, Q. Cai, Hydrothermal growth of ZnO nanoparticles on the surface of two kinds of Ti3C2 co-catalysts with different interlayer spacing towards enhanced photocatalytic activity, Micro, Nano Lett. 17 (2022) 337–348, https://doi.org/10.1049/mna2.12141.
[114] M. Liu, J. Li, R. Bian, X. Wang, Y. Ji, X. Zhang, J. Tian, F. Shi, H. Cui, ZnO@Ti3C2 MXene interfacial Schottky junction for boosting spatial charge separation in photocatalytic degradation, J. Alloys Compd. 905 (2022) 164025, https://doi.org/10.1016/j.jallcom.2022.164025.
[115] Y. Gao, L. Wang, A. Zhou, Z. Li, J. Chen, H. Bala, Q. Hu, X. Cao, Hydrothermal synthesis of TiO2/Ti3C2 nanocomposites with enhanced photocatalytic activity, Mater. Lett. 150 (2015) 62–64, https://doi.org/10.1016/j.matlet.2015.02.135.
[116] X. Ding, Y. Li, C. Li, W. Wang, L. Wang, L. Feng, D. Han, 2D visible-light-driven TiO2@Ti3C2/g-C3N4 ternary heterostructure for high photocatalytic activity, J. Mater. Sci. 54 (2019) 9385–9396, https://doi.org/10.1007/s10853-018-03289-4.
[117] Y. Lu, M. Yao, A. Zhou, Q. Hu, L. Wang, Preparation and photocatalytic performance of Ti 3 C 2/TiO 2/CuO ternary nanocomposites, J. Nanomater. 2017 (2017), https://doi.org/10.1155/2017/1978764.
[118] C. Cui, R. Guo, H. Xiao, E. Ren, Q. Song, C. Xiang, X. Lai, J. Lan, S. Jiang, Bi2WO6/Nb2CTx MXene hybrid nanosheets with enhanced visible-light-driven photocatalytic activity for organic pollutants degradation, Appl. Surf. Sci. 505 (2020) 144595, https://doi.org/10.1016/j.apsusc.2019.144595.
[119] Z. Yao, H. Sun, H. Sui, X. Liu, 2D/2D heterojunction of R-scheme Ti3C2 MXene/MoS2 Nanosheets for enhanced photocatalytic performance, Nanoscale Res. Lett. 15 (2020) 78, https://doi.org/10.1186/s11671-020-03314-z.
[120] V. Thirumal, R. Yuvakkumar, P.S. Kumar, S.P. Keerthana, G. Ravi, D. Velauthapillai, B. Saravanakumar, Efficient photocatalytic degradation of hazardous pollutants by homemade kitchen blender novel technique via 2D-material of few-layer MXene nanosheets, Chemosphere 281 (2021) 130984, https://doi.org/10.1016/j.chemosphere.2021.130984.
[121] Y. Li, H. Luo, W. Ji, S. Li, P. Nian, N. Xu, N. Ye, Y. Wei, Visible-light-driven photocatalytic ZnO@Ti3C2Tx MXene nanofiltration membranes for enhanced organic dyes removal, Sep. Purif. Technol. 323 (2023) 124420, https://doi.org/10.1016/j.seppur.2023.124420.
[122] K. Chandiran, M.S. Pandian, S. Balakrishnan, S. Pitchaimuthu, Y.-S. Chen, K. C. Nagamuthu Raja, Ti3C2Tx MXene decorated with NiMnO3 / NiMn2O4 nanoparticles for simultaneous photocatalytic degradation of mixed cationic and anionic dyes, Colloids Surf. A Physicochem. Eng. Asp. 692 (2024) 133888, https://doi.org/10.1016/j.colsurfa.2024.133888.
[123] J. Fatima, M.B. Tahir, M.S. Tahir, M. Sagir, Solar driven photocatalytic dye degradation through the novel Ti2C– ZnCo2O4MXenes nanocomposite, Opt. Mater. (Amst.) 133 (2022) 113034, https://doi.org/10.1016/j.optmat.2022.113034.
[124] W. Tu, Y. Liu, M. Chen, Y. Zhou, Z. Xie, L. Ma, L. Li, B. Yang, Carbon nitride coupled with Ti3C2-Mxene derived amorphous Ti-peroxo heterojunction for photocatalytic degradation of rhodamine B and tetracycline, Colloids Surf. A Physicochem. Eng. Asp. 640 (2022) 128448, https://doi.org/10.1016/j.colsurfa.2022.128448.
[125] A. Tariq, S.I. Ali, D. Akinwande, S. Rizwan, Efficient visible-light Photocatalysis of 2D-MXene Nanohybrids with Gd3+− and Sn4+-codoped bismuth ferrite, ACS Omega 3 (2018) 13828–13836, https://doi.org/10.1021/acsomega.8b01951.
[126] C. Kalaiselvi, N. Krishna Chandar, Accordion-like multilayer Ti3C2Tx MXene sheets decorated 1D Mn2O3 nanorods-based nanocomposites: an efficient catalyst for swift removal of single and mixed dyes, J. Phys. Chem. Solids 182 (2023) 111591, https://doi.org/10.1016/j.jpcs.2023.111591.
[127] J. Lin, D. Gao, J. Zeng, Z. Li, Z. Wen, F. Ke, Z. Xia, D. Wang, MXene/ZnS/chitosan-cellulose composite with Schottky heterostructure for efficient removal of anionic dyes by synergistic effect of adsorption and photocatalytic degradation, Int. J.

Biol. Macromol. 131994 (2024), https://doi.org/10.1016/j.ijbiomac.2024.131994.
[128] M. Tayyab, U.E. Kulsoom, Y. Liu, S. Mansoor, M. Khan, Z. Akmal, A. Mushtaq, M. Arif, U. Shamriaz, L. Zhou, J. Lei, J. Zhang, Visible light-driven photocatalytic H2 evolution and dye degradation by electrostatic self-assembly of CdS nanowires on Nb2C MXene, Int. J. Hydrog. Energy 51 (2024) 1400–1413, https://doi.org/10.1016/j.ijhydene.2023.09.199.
[129] Q.T. Ta, N.M. Tran, J.-S. Noh, Rice crust-like ZnO/Ti3C2Tx MXene hybrid structures for improved photocatalytic activity, Catalysts 10 (2020), https://doi.org/10.3390/catal10101140.
[130] S. Vigneshwaran, P. Karthikeyan, C.M. Park, S. Meenakshi, Boosted insights of novel accordion-like (2D/2D) hybrid photocatalyst for the removal of cationic dyes: mechanistic and degradation pathways, J. Environ. Manag. 273 (2020) 111125, https://doi.org/10.1016/j.jenvman.2020.111125.
[131] I.A. Alsafari, Synthesis of CuO/MXene nanocomposite to study its photocatalytic and antibacterial properties, Ceram. Int. 48 (2022) 10960–10968, https://doi.org/10.1016/j.ceramint.2021.12.315.
[132] S. Vigneshwaran, C.M. Park, S. Meenakshi, Designed fabrication of sulfide-rich bi-metallic-assembled MXene layered sheets with dramatically enhanced photocatalytic performance for rhodamine B removal, Sep. Purif. Technol. 258 (2021) 118003, https://doi.org/10.1016/j.seppur.2020.118003.
[133] T. Xu, J. Wang, Y. Cong, S. Jiang, Q. Zhang, H. Zhu, Y. Li, X. Li, Ternary BiOBr/TiO2/Ti3C2Tx MXene nanocomposites with heterojunction structure and improved photocatalysis performance, Chin. Chem. Lett. 31 (2020) 1022–1025, https://doi.org/10.1016/j.cclet.2019.11.038.
[134] Q. Tan, Z. Yu, R. Long, N. He, Y. Huang, Y. Liu, Ag3PO4/MXene-TiO2-T: as an all-solid Z-type photocatalytic system with stable and enhanced photocatalytic performance, Opt. Mater. (Amst.) 131 (2022) 112685, https://doi.org/10.1016/j.optmat.2022.112685.
[135] I.A. Alsafari, S. Munir, S. Zulfiqar, M.S. Saif, M.F. Warsi, M. Shahid, Synthesis, characterization, photocatalytic and antibacterial properties of copper ferrite/MXene (CuFe2O4/Ti3C2) nanohybrids, Ceram. Int. 47 (2021) 28874–28883, https://doi.org/10.1016/j.ceramint.2021.07.048.
[136] D. Liu, C. Li, J. Ge, C. Zhao, Q. Zhao, F. Zhang, T. Ni, W. Wu, 3D interconnected g-C3N4 hybridized with 2D Ti3C2 MXene nanosheets for enhancing visible light photocatalytic hydrogen evolution and dye contaminant elimination, Appl. Surf. Sci. 579 (2022) 152180, https://doi.org/10.1016/j.apsusc.2021.152180.
[137] T. Rasheed, A. Rasheed, S. Munir, S. Ajmal, Z. Muhammad Shahzad, I.A. Alsafari, S.A. Ragab, P.O. Agboola, I. Shakir, A cost-effective approach to synthesize NiFe2O4/MXene heterostructures for enhanced photodegradation performance and anti-bacterial activity, Adv. Powder Technol. 32 (2021) 2248–2257, https://doi.org/10.1016/j.apt.2021.05.006.
[138] H. Wang, Y. Wu, T. Xiao, X. Yuan, G. Zeng, W. Tu, S. Wu, H.Y. Lee, Y.Z. Tan, J. W. Chew, Formation of quasi-core-shell In2S3/anatase TiO2@metallic Ti3C2Tx hybrids with favorable charge transfer channels for excellent visible-light-photocatalytic performance, Appl. Catal. B Environ. 233 (2018) 213–225, https://doi.org/10.1016/j.apcatb.2018.04.012.
[139] R. Nag, D. Das, S. Manna, S. Sasmal, A. Thander, A. Bera, Ti3C2 MXene modified porous NiTiO3 nanorod Schottky heterojunction towards enhanced photocatalytic dye degradation, Mater Today Commun 37 (2023) 107330, https://doi.org/10.1016/j.mtcomm.2023.107330.
[140] H. Zheng, X. Meng, J. Chen, M. Que, W. Wang, X. Liu, L. Yang, Y. Zhao, In situ phase evolution of TiO2/Ti3C2Tx heterojunction for enhancing adsorption and photocatalytic degradation, Appl. Surf. Sci. 545 (2021) 149031, https://doi.org/10.1016/j.apsusc.2021.149031.
[141] Z. Yao, H. Sun, H. Sui, X. Liu, Construction of BPQDs/Ti3C2@ TiO2 composites with favorable charge transfer channels for enhanced photocatalytic activity under visible light irradiation, Nanomaterials 10 (2020) 452, https://doi.org/10.3390/nano10030452.
[142] K. Rajavel, S. Shen, T. Ke, D. Lin, Photocatalytic and bactericidal properties of MXene-derived graphitic carbon-supported TiO2 nanoparticles, Appl. Surf. Sci. 538 (2021) 148083, https://doi.org/10.1016/j.apsusc.2020.148083.
[143] Y. Wang, J. Chen, M. Que, Q. Wu, X. Wang, Y. Zhou, Y. Ma, Y. Li, X. Yang, MXene-derived Ti3C2Tx/Bi4Ti3O12 heterojunction photocatalyst for enhanced degradation of tetracycline hydrochloride, rhodamine B, and methyl orange under visible-light irradiation, Appl. Surf. Sci. 639 (2023) 158270, https://doi.org/10.1016/j.apsusc.2023.158270.
[144] T. Ke, S. Shen, K. Yang, D. Lin, Construction and visible-light-photocatalysis of a novel ternary heterostructure BiOI/(001) TiO2/Ti3C2, Nanotechnology 31 (2020) 345603, https://doi.org/10.1088/1361-6528/ab90ba.
[145] M.M. Sajid, S.B. Khan, Y. Javed, N. Amin, Z. Zhang, N.A. Shad, H. Zhai, Bismuth vanadate/MXene (BiVO4/Ti3C2) heterojunction composite: enhanced interfacial control charge transfer for highly efficient visible light photocatalytic activity, Environ. Sci. Pollut. Res. 28 (2021) 35911–35923, https://doi.org/10.1007/s11356-021-13315-9.
[146] A.-Z. Warsi, F. Aziz, S. Zulfiqar, S. Haider, I. Shakir, P.O. Agboola, Synthesis, characterization, photocatalysis, and antibacterial study of WO3, MXene and WO3/MXene nanocomposite, Nanomaterials 12 (2022) 713, https://doi.org/10.3390/nano12040713.
[147] Z. Wu, Y. Liang, X. Yuan, D. Zou, J. Fang, L. Jiang, H. Yang, Z. Xiao, MXene Ti3C2 derived Z–scheme photocatalyst of graphene layers anchored TiO2/g–C3N4 for visible light photocatalytic degradation of refractory organic pollutants, Chem. Eng. J. 394 (2020) 124921, https://doi.org/10.1016/j.cej.2020.124921.
[148] X. Zhang, X. Jia, R. Xu, X. Lu, H. Liu, Y. Niu, Ellipsoidal α-Fe2O3@SnO2/Ti3C2 MXene core-shell nanoparticles for photodegradation of organic dyes, J. Alloys Compd. 923 (2022) 166315, https://doi.org/10.1016/j.jallcom.2022.166315.
[149] W. Zhou, B. Yu, J. Zhu, K. Li, Synthesis of ZnO/Ti 2 C composites by electrostatic self-assembly for the photocatalytic degradation of methylene blue, J. Mater. Sci. 1–17 (2022), https://doi.org/10.1007/s10853-021-06798-x.
[150] M. Akram, M. Rani, K. Batool, M.A. Habila, M. Sillanpää, A.A. Shah, R. Shafique, Lead integrated two-dimensional (MXene/PbCrO4) nanocomposite designed for energy storage and photocatalytic degradation applications, Phys Scr 99 (2023) 15902, https://doi.org/10.1088/1402-4896/ad0fcd.
[151] B.H. Khaneghahi, S.D. Abkenar, J. Gilnezhad, M.R. Ganjali, M. Hosseini, Application of Ti 3 C 2 (OH) 2 MXene nanosheets as a potential adsorbent and photocatalyst for degradation of organic dye in aqueous media, Pollution 9 (2023), https://doi.org/10.22059/poll.2022.351101.1684.
[152] A. Gaur, C. Porwal, V.S. Chauhan, R. Vaish, Synergic effect of photocatalysis and tribocatalysis for dye degradation by BaTiO3 ceramics, J. Am. Ceram. Soc. 107 (2024) 2393–2406, https://doi.org/10.1111/jace.19565.
[153] M. Akbari, J. Rasouli, K. Rasouli, S. Ghaedi, M. Mohammadi, H. Rajabi, S. Sabbaghi, MXene-based composite photocatalysts for efficient degradation of antibiotics in wastewater, Sci. Rep. 14 (2024) 31498, https://doi.org/10.1038/s41598-024-83333-3.
[154] Z. Yang, J. Wang, Highly efficient photocatalytic H2O2 production over a Zn0. 3Cd0. 7S/MXene photocatalyst for degradation of emerging pollutants under visible-light irradiation, Langmuir 40 (2024) 3168–3180, https://doi.org/10.1021/acs.langmuir.3c03607.
[155] L. Cai, Q. Yao, X. Du, J. Zhong, H. Lu, X. Tao, J. Zhou, Z. Dang, G. Lu, Validation of quenching effectiveness and pollutant degradation ability of singlet oxygen through model reaction system, J. Hazard. Mater. 460 (2023) 132488, https://doi.org/10.1016/j.jhazmat.2023.132488.
[156] S.S. Emmanuel, A.A. Adesibikan, C.O. Olawoyin, M.O. Idris, Photocatalytic degradation of Maxilon dye pollutants using Nano-architecture functional materials: a review, ChemistrySelect 9 (2024) e202400316, https://doi.org/10.1002/slct.202400316.
[157] S.S. Emmanuel, C.O. Olawoyin, A.A. Adesibikan, E.A. Opatola, A pragmatic review on bio-polymerized metallic nano-architecture for photocatalytic degradation of recalcitrant dye pollutants, J. Polym. Environ. 32 (2023) 1–30, https://doi.org/10.1007/s10924-023-02986-9.
[158] K.O. Iwuozor, K.G. Akpomie, J. Conradie, K.A. Adegoke, K.O. Oyedotun, J. O. Ighalo, J.F. Amaku, C. Olisah, A.O. Adeola, Aqueous phase adsorption of aromatic organoarsenic compounds: a review, J Water Process Eng 49 (2022) 103059, https://doi.org/10.1016/j.jwpe.2022.103059.
[159] M. Ding, W. Chen, H. Xu, Z. Shen, T. Lin, K. Hu, Q. Kong, G. Yang, Z. Xie, Heterogeneous Fe2CoTi3O10-MXene composite catalysts: synergistic effect of the ternary transition metals in the degradation of 2, 4-dichlorophenoxyacetic acid based on peroxymonosulfate activation, Chem. Eng. J. 378 (2019) 122177, https://doi.org/10.1016/j.cej.2019.122177.
[160] N. Yeddou Mezenner, H. Lagha, H. Kais, M. Trari, Biosorption of diazinon by a pre-treated alimentary industrial waste: equilibrium and kinetic modeling, Appl Water Sci 7 (2017) 4067–4076, https://doi.org/10.1007/s13201-017-0563-z.
[161] K.O. Iwuozor, I.P. Oyekunle, E.C. Emenike, S.M. Okoye-Anigbogu, E.M. Ibitogbe, O. Elemile, J.O. Ighalo, A.G. Adeniyi, An overview of equilibrium, kinetic and thermodynamic studies for the sequestration of Maxilon dyes, Clean Mater 6 (2022) 100148, https://doi.org/10.1016/j.clema.2022.100148.
[162] M. Kadhom, K. Kalash, M. Al-Furaiji, Performance of 2D MXene as an adsorbent for malachite green removal, Chemosphere 290 (2022) 133256, https://doi.org/10.1016/j.chemosphere.2021.133256.
[163] C. Hao, G. Li, G. Wang, W. Chen, S. Wang, Preparation of acrylic acid modified alkalized MXene adsorbent and study on its dye adsorption performance, Colloids Surf. A Physicochem. Eng. Asp. 632 (2022) 127730, https://doi.org/10.1016/j.colsurfa.2021.127730.
[164] Y. Xu, R. Yin, Y. Zhang, B. Zhou, P. Sun, X. Dong, Unveiling the mechanism of frictional catalysis in water by Bi12TiO20: a charge transfer and contaminant decomposition path study, Langmuir 38 (2022) 14153–14161, https://doi.org/10.1021/acs.langmuir.2c02093.
[165] L. Ruan, Y. Jia, J. Guan, B. Xue, S. Huang, Z. Wang, Y. Fu, Z. Wu, Tribo-electro-catalytic dye degradation driven by mechanical friction using MOF-derived NiCo2O4 double-shelled nanocages, J. Clean. Prod. 345 (2022) 131060, https://doi.org/10.1016/j.jclepro.2022.131060.
[166] S. Kim, F. Gholamirad, M. Yu, C.M. Park, A. Jang, M. Jang, N. Taheri-Qazvini, Y. Yoon, Enhanced adsorption performance for selected pharmaceutical compounds by sonicated Ti3C2TX MXene, Chem. Eng. J. 406 (2021) 126789, https://doi.org/10.1016/j.cej.2020.126789.
[167] A. Jain, S. Kumari, S. Agarwal, S. Khan, Water purification via novel nano-adsorbents and their regeneration strategies, Process. Saf. Environ. Prot. 152 (2021) 441–454, https://doi.org/10.1016/j.psep.2021.06.031.
[168] Y. Zhang, X. Zhang, S. Wang, Recent advances in the removal of emerging contaminants from water by novel molecularly imprinted materials in advanced oxidation processes—a review, Sci. Total Environ. 883 (2023) 163702, https://doi.org/10.1016/j.scitotenv.2023.163702.
[169] L. Hashemi, M.Y. Masoomi, H. Garcia, Regeneration and reconstruction of metal-organic frameworks: opportunities for industrial usage, Coord. Chem. Rev. 472 (2022) 214776, https://doi.org/10.1016/j.ccr.2022.214776.
[170] B.G. Fouda-Mbanga, E. Prabakaran, K. Pillay, Carbohydrate biopolymers, lignin based adsorbents for removal of heavy metals (Cd2+, Pb2+, Zn2+) from wastewater, regeneration and reuse for spent adsorbents including latent fingerprint detection: a review, Biotechnol. Reports 30 (2021) e00609, https://doi.org/10.1016/j.btre.2021.e00609.
[171] N. El Messaoudi, M. El Khomri, A. El Mouden, A. Bouich, A. Jada, A. Lacherai, H. M.N. Iqbal, S.I. Mulla, V. Kumar, J.H.P. Américo-Pinheiro, Regeneration and

reusability of non-conventional low-cost adsorbents to remove dyes from wastewaters in multiple consecutive adsorption–desorption cycles: a review, biomass convers, Biorefinery (2022) 1–18, https://doi.org/10.1007/s13399-022-03604-9.
[172] W.A.H. Altowayti, S. Shahir, N. Othman, T.A.E. Eisa, W.M.S. Yafooz, A. Al-Dhaqm, C.Y. Soon, I.B. Yahya, N.A.N. Binti Che Rahim, M. Abaker, The role of conventional methods and artificial intelligence in the wastewater treatment: a comprehensive review, Processes 10 (2022) 1832, https://doi.org/10.3390/pr10091832.
[173] K. Li, G. Zou, T. Jiao, R. Xing, L. Zhang, J. Zhou, Q. Zhang, Q. Peng, Self-assembled MXene-based nanocomposites via layer-by-layer strategy for elevated adsorption capacities, Colloids Surf. A Physicochem. Eng. Asp. 553 (2018) 105–113, https://doi.org/10.1016/j.colsurfa.2018.05.044.
[174] P. Zhang, M. Xiang, H. Liu, C. Yang, S. Deng, Novel two-dimensional magnetic titanium carbide for methylene blue removal over a wide pH range: insight into removal performance and mechanism, ACS Appl. Mater. Interfaces 11 (2019) 24027–24036, https://doi.org/10.1021/acsami.9b04222.
[175] C. Yao, W. Zhang, L. Xu, M. Cheng, Y. Su, J. Xue, J. Liu, S. Hou, A facile synthesis of porous MXene-based freestanding film and its spectacular electrosorption performance for organic dyes, Sep. Purif. Technol. 263 (2021) 118365, https://doi.org/10.1016/j.seppur.2021.118365.
[176] H. Lei, Z. Hao, K. Chen, Y. Chen, J. Zhang, Z. Hu, Y. Song, P. Rao, Q. Huang, Insight into adsorption performance and mechanism on efficient removal of methylene blue by accordion-like V2CT x MXene, J. Phys. Chem. Lett. 11 (2020) 4253–4260, https://doi.org/10.1021/acs.jpclett.0c00973.
[177] Y. Feng, H. Wang, J. Xu, X. Du, X. Cheng, Z. Du, H. Wang, Fabrication of MXene/PEI functionalized sodium alginate aerogel and its excellent adsorption behavior for Cr (VI) and Congo red from aqueous solution, J. Hazard. Mater. 416 (2021) 125777, https://doi.org/10.1016/j.jhazmat.2021.125777.
[178] M. Li, P. Zhang, Q. Wang, N. Yu, X. Zhang, S. Su, Electrospinning novel sodium alginate/MXene nanofiber membranes for effective adsorption of methylene blue, Polymers (Basel) 15 (2023) 2110, https://doi.org/10.3390/polym15092110.
[179] Y. Diao, M. Yan, X. Li, C. Zhou, B. Peng, H. Chen, H. Zhang, In-situ grown of g-C3N4/Ti3C2/TiO2 nanotube arrays on Ti meshes for efficient degradation of organic pollutants under visible light irradiation, Colloids Surf. A Physicochem. Eng. Asp. 594 (2020) 124511, https://doi.org/10.1016/j.colsurfa.2020.124511.
[180] X. Feng, Z. Yu, Y. Sun, R. Long, M. Shan, X. Li, Y. Liu, J. Liu, Review MXenes as a new type of nanomaterial for environmental applications in the photocatalytic degradation of water pollutants, Ceram. Int. 47 (2021) 7321–7343, https://doi.org/10.1016/j.ceramint.2020.11.151.
[181] C. Miao, P. Jia, C. Luo, J. Pang, L. Xiao, T. Zhang, J. Duan, Y. Li, Z. Sun, The size-dependent in vivo toxicity of amorphous silica nanoparticles: a systematic review, Ecotoxicol. Environ. Saf. 271 (2024) 115910, https://doi.org/10.1016/j.ecoenv.2023.115910.
[182] M. Senut, Y. Zhang, F. Liu, A. Sen, D.M. Ruden, G. Mao, Size-dependent toxicity of gold nanoparticles on human embryonic stem cells and their neural derivatives, Small 12 (2016) 631–646, https://doi.org/10.1002/smll.201502346.
[183] E. Byeon, P. Sanpradit, J.-S. Lee, H. Jeong, M.-S. Kim, M.-S. Hong, S. Peerakietkhajorn, A.E.-D.H. Sayed, J.-S. Lee, Size-dependent toxicity of nano- and microplastics with zinc oxide nanoparticles in the marine rotifer Brachionus koreanus, Mar. Pollut. Bull. 209 (2024) 117206, https://doi.org/10.1016/j.marpolbul.2024.117206.
[184] Q. Manzoor, A. Sajid, Z. Ali, A. Nazir, A. Sajid, F. Imtiaz, S. Iqbal, U. Younas, H. Arif, M. Iqbal, Toxicity spectrum and detrimental effects of titanium dioxide nanoparticles as an emerging pollutant: a review, Desalin. Water Treat. 317 (2024) 100025, https://doi.org/10.1016/j.dwt.2024.100025.
[185] Z.U.D. Babar, V. Iannotti, G. Rosati, A. Zaheer, R. Velotta, B. Della Ventura, R. Álvarez-Diduk, A. Merkoçi, MXenes in healthcare: synthesis, fundamentals and applications, Chem. Soc. Rev. 54 (2025) 3387, https://doi.org/10.1039/D3CS01024D.
[186] P. Javaherchi, A. Zarepour, A. Khosravi, P. Heydari, S. Iravani, A. Zarrabi, Innovative applications of MXenes in dialysis: enhancing filtration efficiency, Nanoscale 17 (2025) 4301, https://doi.org/10.1039/D4NR04329D.
[187] M. Mim, K. Habib, S.N. Farabi, S.A. Ali, M.A. Zaed, M. Younas, S. Rahman, MXene: a roadmap to sustainable energy management, synthesis routes, stabilization, and economic assessment, ACS Omega 9 (2024) 32350–32393, https://doi.org/10.1021/acsomega.4c04849.
[188] B. Uzair, A. Liaqat, H. Iqbal, B. Menaa, A. Razzaq, G. Thiripuranathar, N. Fatima Rana, F. Menaa, Green and cost-effective synthesis of metallic nanoparticles by algae: safe methods for translational medicine, Bioengineering 7 (2020) 129, https://doi.org/10.3390/bioengineering7040129.
[189] B. Senthil Rathi, L.S. Ewe, S. S, S. S, W.K. Yew, B. R, S.K. Tiong, Recent trends and advancement in metal oxide nanoparticles for the degradation of dyes: synthesis, mechanism, types and its application, Nanotoxicology 18 (2024) 272–298, https://doi.org/10.1080/17435390.2024.2349304.